

UNIVERSITÀ DEGLI STUDI DI PADOVA
DIPARTIMENTO DI INGEGNERIA INDUSTRIALE
CORSO DI LAUREA MAGISTRALE IN INGEGNERIA ENERGETICA

**Tesi di Laurea Magistrale in
Ingegneria Energetica**

**KINETIC MODELS IDENTIFICATION FOR THE
CATALYTIC SYNTHESIS OF FORMALDEHYDE
THROUGH THE PARTIAL OXIDATION OF METHANOL**

Relatore: Prof. Fabrizio Bezzo

Correlatore: Dr. Federico Galvanin

Laureando: MARCO QUAGLIO

ANNO ACCADEMICO 2015-2016

Abstract

The good management of numerous energy systems relies on the good capability of controlling chemical reactions. A good knowledge on the mechanisms of fuel oxidation, translated into kinetic models, can be fruitfully exploited for designing better energy systems, decreasing the primary energy demand and reducing the associated emission of pollutants. The conventional process of model identification involves the discrimination among a certain number of candidate models that might be based on different assumptions. One among the proposed models is typically selected on its better capability of fitting experimental data. The estimates of the kinetic parameters are then refined performing experiments designed to get the highest possible information from the trials. Advanced model-based design of experiments (MBD_{oE}) techniques have been developed for the quick identification, refinement, and statistical assessment of deterministic models. In this Thesis, MBD_{oE} methods are employed for the identification of a simplified kinetic model for the catalytic oxidation of methanol. The highly varying reactivity of the catalyst used in the given experimental data sets and the high variance associated to some of the measurements facilitated the development of a novel data-mining technique for the effective numerical quantification of the catalyst reactivity. The results obtained made possible further analysis on the key guidelines for the design of experiments in catalytic systems, especially whenever there is a high degree of uncertainty in the catalyst behaviour.

Abstract esteso

Le reazioni di combustione sono sfruttate in molti sistemi energetici. L'energia elettrica è ancora diffusamente generata in impianti termici, bruciando combustibile. Le caldaie domestiche sfruttano la combustione per riscaldare gli edifici e per produrre acqua calda sanitaria. Inoltre, quasi tutta la domanda energetica nell'ambito dei trasporti viene soddisfatta bruciando combustibili fossili. L'identificazione di modelli cinetici robusti per le reazioni di combustione è fondamentale per simulare e ottimizzare tutti quei sistemi di conversione energetica che coinvolgono l'energia chimica. La disponibilità di un modello cinetico consolidato per l'ossidazione del combustibile può essere sfruttata per progettare sistemi energetici migliori, riducendo la domanda di energia primaria e la correlata emissione di inquinanti [1]. Alla base dell'identificazione dei modelli cinetici è la conduzione di esperimenti ad elevato contenuto di informazione. Poiché gli esperimenti possono richiedere un considerevole impiego di tempo e risorse, pianificare accuratamente l'indagine è un aspetto fondamentale nel campo della moderna ingegneria di reazione. A partire dalla memoria scientifica lasciata da Box e Lucas [2], numerosi ricercatori si sono dedicati allo sviluppo di metodi avanzati di progettazione di esperimenti (MBDoe) [3, 4]. Queste tecniche permettono di individuare le condizioni sperimentali più ricche di informazione per l'identificazione del modello e la precisa stima dei suoi parametri non misurabili. In questa Tesi, strumenti sviluppati nell'ambito dell' MBDoe sono impiegati per l'identificazione di modelli cinetici per la sintesi catalitica di formaldeide attraverso l'ossidazione parziale del metanolo su argento [5]. Il caso di studio considerato permette l'applicazione di queste potenti teorie a una reazione di ossidazione analoga alle reazioni di combustione di interesse energetico.

Per il conseguimento dei risultati presentati in questa Tesi, 5 set di dati per l'ossidazione parziale del metanolo su catalizzatore argento sono stati resi disponibili. Questi set di dati erano stati ottenuti conducendo esperimenti su microreattori con differenti geometrie e differenti lunghezze del film di catalizzatore. Inoltre i catalizzatori utilizzati nei diversi reattori erano stati sintetizzati separatamente e potevano dunque presentare comportamenti diversi. I reattori utilizzati per investigare il meccanismo cinetico sono:

- due microreattori a canale largo C1 e C2;
- tre microreattori a serpentina R1, R2 e R3.

Un'analisi sulla qualità dei dati è stata eseguita evidenziando la presenza di significativi errori di misura nei set di dati raccolti sui reattori C2, R1, R2 e R3. Inoltre, è stata rilevata la scarsa ripetibilità dei risultati sperimentali ottenuti sul reattore R3, probabilmente a causa della disattivazione del catalizzatore nel corso dell'indagine [6]. I dati sperimentali raccolti su C1 sono invece caratterizzati da buona ripetibilità e da ridotto errore sperimentale.

I dati relativi a C1 sono stati utilizzati per definire un problema di stima parametrica mirato all'identificazione di un modello fenomenologico. Due modelli cinetici semplificati disponibili in letteratura [5, 7] sono stati considerati:

- un modello a due reazioni che comprende: *i*) una reazione di ossidazione parziale del metanolo in formaldeide; *ii*) una reazione di decomposizione della formaldeide in anidride carbonica;
- un modello a tre reazioni che include le stesse reazioni del modello precedente, ma considera anche una terza reazione: *iii*) ossidazione dell'idrogeno.

I limiti e le capacità descrittive dei due modelli sono stati confrontati dimostrando la necessità di includere la terza reazione di ossidazione dell'idrogeno nel meccanismo semplificato.

Il modello cinetico a tre reazioni, con i parametri stimati per C1 è stato successivamente utilizzato come modello di riferimento per quantificare la reattività dei catalizzatori presenti negli altri reattori. La quantificazione è stata eseguita applicando una tecnica innovativa di *model-based data mining* (MBDM) per l'identificazione degli esperimenti poco significativi per la stima (esperimenti affetti da grossolani errori di misura e/o eseguiti su un catalizzatore disattivato). Livelli di reattività più alti rispetto a quella del catalizzatore usato in C1 sono stati rilevati in tutti gli altri reattori.

La stima numerica della reattività ha permesso un'ulteriore analisi sull'identificazione delle migliori condizioni sperimentali da investigare per la stima dei parametri cinetici del modello a tre reazioni. La traccia della matrice di informazione di Fisher [8, 9] è stata calcolata al variare delle condizioni sperimentali e al variare della reattività. Le superfici di informazione ottenute dimostrano chiaramente la necessità di una scelta cosciente delle condizioni sperimentali, tenendo in considerazione la reattività del catalizzatore specifico analizzato. Regioni per la progettazione di esperimenti robusti (condizioni sperimentali per la stima parametrica quando l'incertezza sui parametri è elevata [10]), sono state identificate nello spazio delle condizioni sperimentali. Quando ancora non sono stati eseguiti esperimenti per quantificare la reattività, le condizioni sperimentali di *robust design* rappresentano il miglior compromesso per qualificare il comportamento del catalizzatore. Esperimenti successivi andranno progettati, tenendo in considerazione la reattività, attraverso tecniche note di MBDoE per la precisione parametrica.

Contents

Introduction.....	15
Chapter 1: Identification of phenomenological models.....	17
1.1 Objectives	18
1.2 Methodology	18
1.2.1 The parameter estimation problem.....	20
1.2.1.1 The maximum likelihood estimate.....	22
1.2.1.2 The covariance matrix.....	24
1.2.1.3 The correlation matrix.....	26
1.2.1.4 The <i>t</i> -test.....	27
1.2.1.5 Goodness of fit.....	28
1.2.2 Model-based design of experiments.....	29
1.2.2.1 Metric of information.....	30
1.2.2.2 MBDoE for parameter estimation.....	32
1.2.3 Alternative method for model identification.....	33
1.2.3.1 The Gaussian filter.....	34
1.3 gPROMS Model Builder.....	37
Chapter 2: Case study, experimental setup and available data sets	39
2.1 Kinetic mechanism.....	39
2.2 Experimental setup.....	40
2.2.1 Measurement system.....	42
2.3 Data sets and experimental conditions.....	43

2.3.1	Data quality	46
2.3.1.1	C1 wide-channel reactor	47
2.3.1.2	C2 wide-channel reactor	51
2.3.1.3	R1 serpentine reactor	52
2.3.1.4	R2 serpentine reactor	55
2.3.1.5	R3 serpentine reactor	56
2.3.1.6	Carbon balance.....	58
2.3.2	Assessment of catalyst reactivity	59
2.4	Summary of results	61
Chapter 3:	Identification of a simplified kinetic model.....	63
3.1	Assumptions.....	63
3.1.1	The plug flow reactor model.....	63
3.1.2	Kinetic models	66
3.2	Model identification.....	67
3.2.1	Preliminary discrimination.....	68
3.2.1.1	Parameter estimation results	69
3.2.1.2	Sensitivity analysis.....	72
3.2.1.3	Model comparison on goodness of fit.....	74
3.2.2	Parameter estimation with reduced set of experiments.....	78
3.2.2.1	Assessment of fitting.....	79
3.2.3	Definition of a reference model	81
3.3	Summary of results	83
Chapter 4:	Catalyst reactivity and information.....	85
4.1	Quantification of catalyst reactivity	85
4.1.1	Application of the filter.....	87
4.1.1.1	C2 wide-channel reactor	90
4.1.1.2	R1 serpentine reactor	91
4.1.1.3	R2 serpentine reactor	92
4.1.1.4	R3 serpentine reactor	93

4.1.2	Summary of results	94
4.2	Reactivity and information.....	96
4.2.1	Case 1: Temperature vs. Residence time	99
4.2.2	Case 2: Temperature vs. Inlet molar ratio methanol/oxygen	100
4.2.3	Case 3: Temperature vs. Inlet molar fraction of water.....	100
4.2.4	Case 4: Residence time vs. Inlet molar ratio methanol/oxygen	102
4.2.5	Case 5: Residence time vs. Inlet molar fraction of water.....	102
4.2.6	Case 6: Inlet molar ratio methanol/oxygen vs. Inlet molar fraction of water	103
4.3	Robust design of experiments.....	104
4.4	Summary of results	107
	Conclusions.....	109
	References.....	113
	Acknowledgements.....	115
	Appendix I	117
	Model identification through A-optimality criterion	117
	Appendix II	121
	Available experimental data	121
	Appendix III.....	125
	Pressure correction for serpentine reactors	125

Notation

Latin symbols

A	=	Cross-sectional area of the stage occupied by the catalyst film in the microchannel
A_j	=	Pre-exponential factor of the kinetic constant referring to the j -th reaction
C_i	=	Concentration of the i -th species
E_{aj}	=	Activation energy of the kinetic constant referring to the j -th reaction
F_{STC}^{IN}	=	Volumetric flowrate at the inlet expressed in standard conditions
F_{STC}^{OUT}	=	Volumetric flowrate at the outlet expressed in standard conditions
k_j	=	Kinetic constant of the j -th reaction
L_C	=	Catalyst film length
\dot{n}_i	=	Molar flowrate of the i -th component in the gas mixture
\dot{n}_{tot}	=	Total molar flowrate
N_C	=	Number of components considered in the gas mixture
N_{exp}	=	Number of experiments considered in a certain campaign
N_m	=	Number of dependent output variables in a given model
N_R	=	Number of reactions involved in a kinetic model
N_u	=	Number of independent control variables involved in a model
N_x	=	Number of state variables involved in a model
N_θ	=	Number of non-measurable parameters involved in a model
O_{ij}	=	Reaction order of the i -th species in the j -th reaction
P	=	Pressure
P^*	=	Pressure at standard conditions
p^{IN}	=	Pressure measured at the inlet
p^{OUT}	=	Pressure measured at the outlet
r_{ij}	=	Correlation coefficient between the i -th and the j -th parameter in a set of N_θ model parameters
r_j	=	Reaction rate of the j -th reaction
R_g	=	Ideal gas constant
S_j	=	Selectivity of the j -th product
T	=	Temperature
T^*	=	Temperature at standard conditions
t	=	Scalar variable representing time

t_k	=	t -value with cumulated probability k obtained from a Student distribution
u_i	=	i -th control variable appearing in the model
v^{IN}	=	Gas flow velocity at the inlet
v^{OUT}	=	Gas flow velocity at the outlet
$V_{\theta,ii}$	=	Variance associated to the i -th parameter in a set of N_θ model parameters
$V_{\theta,ij}$	=	Covariance between the i -th and the j -th parameter in a set of N_θ model parameters
V_{x_i}	=	Variance of the measurement error associated to variable x_i
x_i	=	i -th state variable appearing in the model
X_i	=	Conversion of the i -th reagent
\hat{y}_{ij}	=	Model prediction for the j -th output variable, out of N_m dependent variables involved in the model, in the i -th experiment of a campaign involving N_{exp} experiments
y_{ij}^*	=	True, real value of variable y_{ij}
y_{ij}	=	Measured value for variable \hat{y}_{ij}
$y_{CH_3OH}^{IN}$	=	Molar fraction of methanol measured at the inlet
$y_{O_2}^{IN}$	=	Molar fraction of oxygen measured at the inlet
$y_{H_2O}^{IN}$	=	Molar fraction of water measured at the inlet
$y_{CH_2O}^{OUT}$	=	Molar fraction of formaldehyde measured at the outlet
$y_{CH_3OH}^{OUT}$	=	Molar fraction of methanol measured at the outlet
y_{CO}^{OUT}	=	Molar fraction of carbon monoxide measured at the outlet
$y_{CO_2}^{OUT}$	=	Molar fraction of carbon dioxide measured at the outlet
$y_{H_2}^{OUT}$	=	Molar fraction of hydrogen measured at the outlet
$y_{H_2O}^{OUT}$	=	Molar fraction of water measured at the outlet
$y_{O_2}^{OUT}$	=	Molar fraction of oxygen measured at the outlet
z	=	Axial spatial coordinate of the microchannel
z_C	=	Axial coordinate at the beginning of the catalyst film
z_{IN}	=	Axial coordinate of the inlet
z_{MC}	=	Axial coordinate at the beginning of the main channel
z_{OC}	=	Axial coordinate at the beginning of the outlet channel
z_{OUT}	=	Axial coordinate at the outlet
z_R	=	Axial coordinate at the beginning of the retainer

Matrices and vectors

\mathbf{f}	=	Column array of functions [N_m]
\mathbf{H}	=	Hessian matrix evaluated with respect to the model parameters for a scalar objective function involving the measurements of N_m variables in N_{exp} experiments [$N_\theta \times N_\theta$]
\mathbf{H}_i	=	Matrix \mathbf{H} evaluated for an objective function involving only the N_m variables in the i -th experiment [$N_\theta \times N_\theta$]
\mathbf{u}	=	Column array of independent control variables [N_u]
\mathbf{u}_i	=	Column array of the control variables \mathbf{u} in the i -th experiment [N_u]
\mathbf{V}_θ	=	Covariance matrix of the parameter estimates [$N_\theta \times N_\theta$]

\mathbf{V}_{θ^0}	=	Covariance matrix associated to the initial parameter estimates [$N_{\theta} \times N_{\theta}$]
\mathbf{V}_z	=	Covariance matrix associated to all the variables measured in the experiment campaign [$N_{exp}N_m \times N_{exp}N_m$]
\mathbf{x}	=	Column array of state variables [N_x]
$\hat{\mathbf{y}}$	=	Column array of predicted output variables [N_m]
$\hat{\mathbf{y}}_i$	=	Column array of predicted values for the output variables in the i -th experiment [N_m]
\mathbf{y}_i^*	=	Column array of true values for the output variables in the i -th experiment [N_m]
\mathbf{y}_i	=	Column array of measured values for the output variables in the i -th experiment [N_m]
\mathbf{z}	=	Column array of output variables for the whole experiment campaign [$N_{exp}N_m$]
$\boldsymbol{\alpha}$	=	Array of binary variables [N_{exp}]
$\boldsymbol{\beta}$	=	Array of binary variables [N_m]
$\boldsymbol{\Gamma}$	=	Matrix of binary variables [$N_{exp} \times N_m$]
$\delta\hat{\boldsymbol{\theta}}$	=	Column array of random variables representing the deviation of the estimated parameters from the value $\hat{\boldsymbol{\theta}}$ derived from a variation in the measurements \mathbf{z} [N_{θ}]
$\delta\mathbf{z}$	=	Column array of random variables representing a small variation in the values of all the measured output variables used for estimating $\hat{\boldsymbol{\theta}}$ [$N_{exp}N_m$]
$\boldsymbol{\theta}$	=	Column array of model parameters [N_{θ}]
$\boldsymbol{\theta}^*$	=	Column array true values for model parameters [N_{θ}]
$\hat{\boldsymbol{\theta}}$	=	Column array of computed values for model parameters [N_{θ}]
$\boldsymbol{\theta}^0$	=	Column array of initial guesses for model parameters [N_{θ}]

Greek symbols

α_i	=	i -th binary element of array $\boldsymbol{\alpha}$
β_i	=	i -th binary element of array $\boldsymbol{\beta}$
γ_{ij}	=	ij -th binary element of matrix $\boldsymbol{\Gamma}$
χ_{ref}^2	=	Reference value for goodness of fit test obtained from a χ^2 -distribution
χ_{sample}^2	=	Sum of normalised squared residuals at the end of a parameter estimation problem
θ_i	=	i -th parameter in a set of model parameters
$\hat{\theta}_i$	=	Computed value for the i -th parameter in a set of model parameters
θ_{j1}	=	Natural logarithm of the pre-exponential factor A_j
θ_{j2}	=	Activation energy E_{aj} divided by a factor 10^4
κ_1	=	Dimensionless parameter scaling the pre-exponential factor A_1
κ_2	=	Dimensionless parameter scaling the pre-exponential factor A_2
ν_{ij}	=	Stoichiometric coefficient referring to the i -th species in the j -th reaction
ρ_{ij}	=	Difference between measured and predicted value for the j -th output variable in the i -th experiment
σ_{ij}	=	Standard deviation associated to measurement error for the j -th output variable measured in the i -th experiment
τ	=	Residence time

Acronyms

CHR	=	Catalyst with High Reactivity
CLR	=	Catalyst with Low Reactivity
DoE	=	Design of Experiments
GC	=	Gas Chromatograph
MBDM	=	Model-Based Data Mining
MBDoE	=	Model-Based Design of Experiments
MD	=	Model Discrimination
MLE	=	Maximum Likelihood Estimate
PDF	=	Probability Density Function
PE	=	Parameter Estimation
PFR	=	Plug Flow Reactor
PP	=	Parameter Precision
SDV	=	Standard Deviation
STC	=	Standard Conditions

Introduction

Combustion reactions are involved in numerous energy systems. In power plants, combustion is widely exploited to convert the chemical energy of a fuel into electricity. In domestic boilers, fuel is burned to produce hot water and warm up buildings. Furthermore, almost the entire transportation system relies heavily on the combustion of fossil fuels. The identification of reliable kinetic models is fundamental for simulating and improving the behaviour of the energy conversion processes involving these exothermic reactions. A better oxidation of the fuel, obtained through a model-based optimisation, can in fact lead to a significant reduction in the demand of primary energy and in the emission of pollutants [1]. The identification of a trustworthy model always relies on the conduction of highly informative experiments. Since experiments may require extensive amounts of time and resources, planning carefully the investigation is an aspect of great importance in modern reaction engineering. Following the seminal work by Box and Lucas [2] many researchers devoted their efforts to developing advanced model-based design of experiments techniques (MBDoE) for both model discrimination (MD) and parameter precision (PP) [3, 4]. These techniques allow for the identification of the most informative experimental conditions either for selecting the best model among a set of candidates (possibly based on different hypothesis), or for estimating precisely the kinetic parameters of an already selected model. In this Thesis, tools developed and implemented in model-based design of experiments theories have been employed for the aim of the identification of a simplified kinetic model for the catalytic synthesis of formaldehyde [5]. This case study gives the opportunity for applying the powerful theories of MBDoE to an oxidation reaction analogous to the combustion reactions, exploited for energetic purposes.

Formaldehyde is a fundamental basic block chemical in several industrial processes either as a final product or as a precursor to the production of numerous valuable chemicals. The versatility demonstrated by this organic compound led to its usage in numerous different production chains. In chemical industry, formaldehyde is mainly produced through the partial oxidation of methanol over silver catalyst. The process is usually carried out at atmospheric pressure and high temperature ($T = 850 - 923$ K) adding an opportune amount of steam for achieving high selectivity [11]. Despite the

great industrial importance of this process, however, a full comprehension of the reaction mechanism is yet to be established. One of the main issues making this system so complicated to be unravelled is related to the highly unstable nature of the catalyst whose reactivity can be influenced by a multitude of factors, from its production to the operating conditions it has to withstand. Many researchers in the years spent efforts in understanding the catalytic role of silver in the reaction and the possible mechanism occurring on the surface of the catalyst film. In 2003, a micro-kinetic model for methanol oxidation on silver was proposed by Anders Andreasen et al. [12] to explain the surface phenomena in experimental conditions of interest for industrial application and adopting physically meaningful parameters. However, the complexity of the proposed mechanism made its use for engineering purposes unrealistic and, for this reason, a simplified model derived from the micro-kinetic one was proposed by the same authors in 2005 [7]. The proposed model has been used in this work to fit 5 available experimental data sets (obtained on 5 different microreactor devices), which presented very contrasting results. The high inconsistency associated to some of the measurements advocated for the development of a novel data-mining technique allowing for an effective quantification of the reactivity of the catalysts in the different setups. The final aim of this work is to highlight the strong impact played by the specific catalyst on the information carried by the experiments and to define guidelines for identifying the best experimental conditions in both the conditions of known and completely unknown reactivity.

The work presented in this Thesis is organised in 4 chapters. The mathematical tools and the supporting software gPROMS Model Builder, used to perform the identification of the model and the following analysis on the information, is presented in detail in Chapter 1. Chapter 2 is dedicated to the description of the experimental apparatus and to the graphical assessment of the experimental data, highlighting both consistencies and inconsistencies of the measurements. In Chapter 3, a comparison between two candidate kinetic models available in the literature is proposed highlighting their strengths and weaknesses assessing their structural identifiability. A reference model is then defined using the best parameter estimates obtained fitting the most consistent data set. In Chapter 4, the reference model is used to filter unlikely experimental results quantifying the reactivity of the catalysts loaded in the different reactors. The quantification of the reactivity in the different setups allowed for plotting the trace of the Fisher information matrix [8, 9] in the experimental design space to quantify the impact of the reactivity on the information content of a trial. The resulting surfaces of information clearly show the importance of a conscious choice of the experimental conditions, keeping in mind the previous knowledge available on the specific catalyst analysed.

Chapter 1: Identification of phenomenological models

Typically, when a deterministic physical process needs to be analysed, the researcher is asked to identify regular patterns observing scattered measurements plotted on a graph. This identification can be performed simply fitting the data with known curves such as lines or parabolas. However, finding the best geometrical curve that fits the data does not increase much the knowledge on the key fundamental mechanisms occurring in the considered process. Furthermore, the extrapolation of the outcome of an experiment performed outside the range of investigated experimental conditions through a fitted curve would be only a guessed, speculated forecast. The availability of a well-established phenomenological model (i.e. a model founded on physically meaningful hypothesis), always represents a much more attractive alternative to the curve fitting for some reasons:

- the parameters involved in a phenomenological model carry information on physically meaningful quantities, thus, their evaluation brings to a better understanding of the physical reality that can be fruitfully exploited for a better process design;
- a validated, trustworthy phenomenological model can be reasonably used to predict the behaviour of the physical system in non-investigated experimental conditions, allowing for meaningful non-empirical process optimisation.

The development of reliable mathematical models, however, is not a direct and easy process, in particular in the presence of nonlinear dynamic phenomena as in the case of reaction kinetics. Further complexity in the establishment of deterministic models is also added when the system is affected by high uncertainty as in the case of catalytic reactions. In this work, the identification of a simplified phenomenological model for a catalytic kinetic reaction mechanism is carried out to recognise the best strategies for tackling the problem of model identification in conditions of uncertain, known or unknown catalyst behaviour. This introductory chapter is dedicated to presenting the objectives and the tools for model identification employed for the analysis presented throughout this thesis.

1.1 Objectives

Catalysts are synthetic chemicals added in the reactor to promote a desired chemical reaction offering active sites where the conversion of the reactants can occur with a lower activation energy (i.e. the desired reaction occurs at a higher rate and at lower temperature in the presence of an opportune catalyst). Catalytic systems are affected by uncertainty and instability in the sense that the number of active sites offered by the catalyst and the turnover frequency (i.e. the number of reactions occurring in a unit of time on a single site), depend on a multitude of factors, from the catalyst synthesis step to the particular experimental conditions the catalyst has to withstand. Furthermore, the reactivity can change over time or vanish because of different reasons, still tightly linked to the operating conditions. The dynamic behaviour of the catalyst can be detected through changes in the associated reaction mechanism, but because of the highly unstable nature of this system, the characterisation of its behaviour relies on the collection of valuable information from the trials.

Since experiments can require extensive amounts of time and resources, planning carefully the investigation is an aspect of key importance in modern reaction chemistry. Trials should always be planned considering the target of the analysis. Many researchers devoted their efforts to developing advanced design of experiments techniques [2-5, 13, 14] for the quick identification and refinement of phenomenological models through the conduction of thoughtful experiments. However, very little work has been done so far regarding the design of experiments under conditions of high system uncertainty and instability. The aim of the study presented in this thesis is to assess how the uncertainty intrinsically linked to these systems should be taken into account when planning the experimental campaign for characterising the catalyst behaviour through the identification of the associated kinetic mechanism. The analysis is conducted considering the specific case of the partial oxidation of methanol to formaldehyde over silver catalyst taking advantage on the availability of five rich data sets collected analysing catalysts showing very different levels of reactivity. The final target of this work is to define guidelines for the conduction of experiments in the situations of known and unknown or uncertain reactivity in order to gather the most valuable information for identifying the kinetic mechanism associated to the silver catalyst.

1.2 Methodology

The identification of a good deterministic phenomenological model is not straightforward. Frequently, the process of model identification requires dealing with the impossibility of measuring directly certain variables and parameters (coefficients), or the difficulty of identifying separately the key

mechanisms because of an overlap of their effects in the physical system. The conventional approach adopted for phenomenological model establishment is shown schematically in Figure 1.1.

The procedure always begins observing the physical reality of interest, which requires to be understood and unravelled, through the execution of preliminary experiments. In particular, in the presence of strongly nonlinear dynamic phenomena it happens that a number of different hypothesis may be proposed for describing the system. These hypotheses are translated mathematically in the form of candidate sets of equations (i.e. a certain number of candidate models), involving variables (i.e. quantities which generally vary in both space and time) and parameters that can be either directly measurable or require to be estimated.

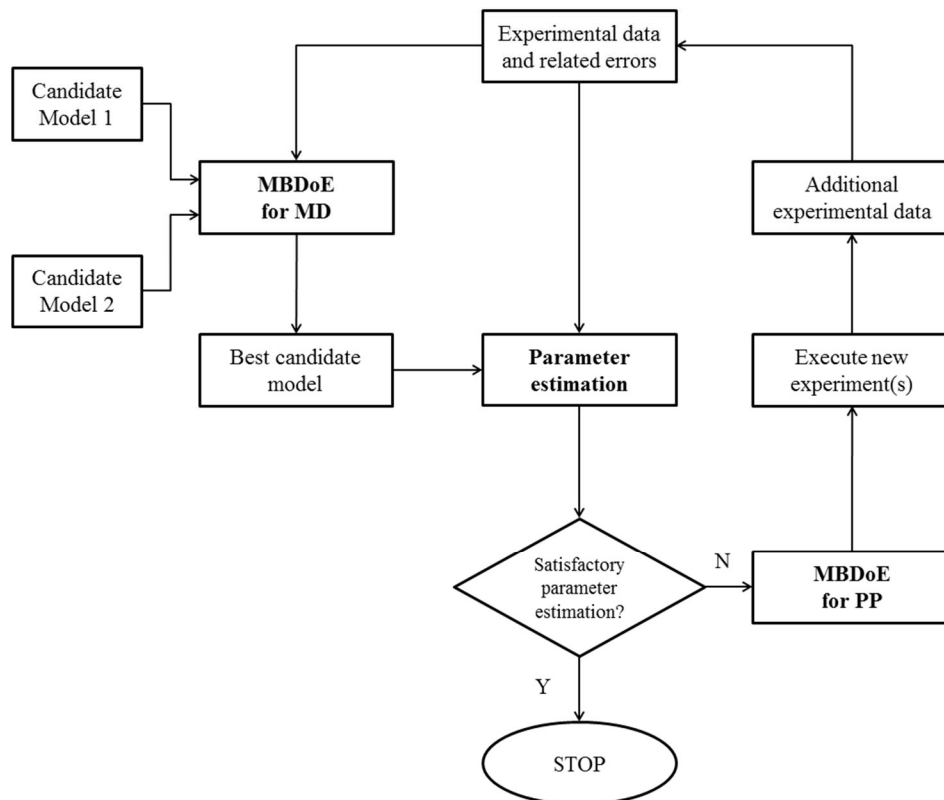


Figure 1.1. Block diagram showing the conventional procedure for model establishment starting from 2 proposed candidate models. Boldface blocks highlight the fundamental steps of the conventional process for model establishment.

Typically, the selection of the best model among a set of candidates is performed through the conduction of highly discriminative additional experiments designed through model-based design of experiments techniques for model discrimination (DoE or MBDoE for MD) [3, 13, 14]. Once the best model among the available ones has been selected, the quality of the parameter estimates associated to its non-measurable coefficients is assessed performing a statistical analysis highlighting the possibly

insufficient information content of the available experimental data. Unsatisfactory parameter estimates are amended gathering new information carrying out new trials designed through model-based design of experiments techniques for parameter precision (DoE or MBDoe for PP) [2-5]. All the information available on the system is then used to perform a new estimation of the parameters. The procedure is repeated until the desired accuracy on the estimates is achieved. In the following sections, the mathematical tools that have been developed in this framework for model identification will be explained more in detail focusing on the aspects functional to the work presented in this thesis. A section is also dedicated to the description of an unconventional method for model establishment employing an innovative model-based data mining technique to identify both the weaknesses of the model and the most unlikely experimental results.

1.2.1 The parameter estimation problem

When a model has already been selected among a set of candidates to describe a certain phenomenon, its identification reduces to the precise estimation of its non-measurable parameters. This section is dedicated to the definition of the problem of model identification taking into account the uncertainty intrinsically linked to the measurements and also to the description of the statistical instrument necessary to assess the quality of the results. All the models considered in this work are standard reduced models, consistently with the definition proposed by Bard [8]:

$$\hat{\mathbf{y}} = \mathbf{f}(\mathbf{x}, \mathbf{u}, \boldsymbol{\theta}) \quad (1.1)$$

Where \mathbf{f} represents a vector of N_m model equations, $\hat{\mathbf{y}}$ represents a vector of N_m directly measurable output variables, \mathbf{x} is a vector of N_x state variables, \mathbf{u} is a vector of N_u input variables that can be directly manipulated and $\boldsymbol{\theta}$ is a vector of N_θ model parameters (i.e. constant coefficients) that require estimation. Furthermore, it will be always assumed that the values measured in the i -th experiment for the inputs \mathbf{u}_i are not affected by significant errors while the measured values for the output variables \mathbf{y}_i are expected to differ significantly from their physical “true” quantity \mathbf{y}_i^* . Assume that the experimental data obtained in N_{exp} performed experiments are available. If the model is given, its identification reduces to the estimation of the set of parameters $\boldsymbol{\theta}$ that satisfies the constitutive equations of the model for all the experiments conducted:

$$\mathbf{y}_i - \mathbf{f}(\mathbf{x}, \mathbf{u}_i, \boldsymbol{\theta}) = \mathbf{0} \quad \forall \quad i = 1, \dots, N_{exp} \quad (1.2)$$

Where $\mathbf{0}$ is a column vector of null elements. In the great majority of the cases this problem is overspecified (i.e. the number of conditions $N_{exp}N_m$ outnumbers the parameters N_θ) and practically it will be impossible to satisfy the equations presented above because of two reasons:

- the measurements are affected by an error: i.e. $\mathbf{y}_i - \mathbf{y}_i^* \neq \mathbf{0}$;
- the set of equations included in the model is wrong or incomplete, thus resulting in the impossibility of satisfying the system even for the true values of the variables:
i.e. $\mathbf{y}_i^* - \mathbf{f}(\mathbf{x}, \mathbf{u}_i, \boldsymbol{\theta}) \neq \mathbf{0}$ for every non-trivial choice of $\boldsymbol{\theta}$.

Be $\hat{\mathbf{y}}_i(\boldsymbol{\theta}) = \mathbf{f}(\mathbf{x}, \mathbf{u}_i, \boldsymbol{\theta})$ the vector of output variables predicted by the model in the experimental conditions adopted in the i -th experiment, the quantity ρ_{ij} represents the difference between measured and predicted value for the j -th output variable in the i -th experiment:

$$\rho_{ij}(\boldsymbol{\theta}) = y_{ij} - \hat{y}_{ij}(\boldsymbol{\theta}) \quad (1.3)$$

The overspecified parameter estimation problem is then recast in terms of finding the best set of parameters $\boldsymbol{\theta}$ that minimises a certain objective function Φ that depends on the quantities $\rho_{ij}(\boldsymbol{\theta})$. This function could be simply defined as the sum of the squared residuals:

$$\min_{\boldsymbol{\theta}}\{\Phi\} = \min_{\boldsymbol{\theta}} \left\{ \sum_i^{N_{exp}} \sum_j^{N_m} [\rho_{ij}(\boldsymbol{\theta})]^2 \right\} \quad (1.4)$$

However, this approach does not take into account the uncertainty intrinsically associated to the measurements treating all the measured values with the same dignity to perform the fitting. The conditions under which a model is identified are never quite repeatable because of the random nature and the limited accuracy of any measurement technique. These disturbances are as much part of the physical reality as are the quantities appearing in the model. A model cannot be called complete if it does not take into account the casual nature of the measurements. In this work, the measured values for the output quantities appearing in the models will be treated as random variables. Since the parameter estimations $\hat{\boldsymbol{\theta}}$ are functions of the measurements, also these derived estimates will be treated as random variables.

The appropriate description of random events is made through the concept of probability (i.e. the extent to which a certain phenomenon is likely to happen). In a rigorous mathematical description, the complete characterisation of the behaviour of a random variable x is given by the definition of an

associated probability density function PDF which associates a probability of realisation to any possible value of the variable. Certainly one of the most popular PDF is represented by:

$$p(x) = \frac{1}{\sqrt{2\pi\sigma^2}} e^{-\frac{1}{2}\left(\frac{x-\mu}{\sigma}\right)^2} \quad (1.5)$$

Which is the univariate normal distribution with mean μ and standard deviation σ . The success of the normal distribution is not only due to its easily treatable mathematical structure, but also to the fact that it has been discovered to describe closely the errors associated to many measurements in nature [8]. Throughout this work, all the random variables are considered as normally distributed.

1.2.1.1 *The maximum likelihood estimate*

Assume that the measurement errors $y_{ij} - y_{ij}^* \forall i = 1, \dots, N_{exp}$ and $j = 1, \dots, N_m$ (i.e. the difference between the measured and the true values of the quantities appearing in the model as output variables), are normally distributed random variables with zero mean and a certain standard deviation (SDV) σ_{ij} . Also assume that the model used to fit the experimental data is correct; then it does exist a true value for the set of parameters $\boldsymbol{\theta}^*$ such that the model prediction for the output variables is exact (i.e. it does exist a value for $\boldsymbol{\theta}$ that satisfies $\hat{y}_{ij}(\boldsymbol{\theta}) = y_{ij}^* \forall i = 1, \dots, N_{exp}$ and $j = 1, \dots, N_m$). Thus, for that particular value of the parameters, the residuals $\rho_{ij}(\boldsymbol{\theta}^*)$ follow the same distribution of the measurement errors $y_{ij} - y_{ij}^*$, in fact:

$$\rho_{ij}(\boldsymbol{\theta}^*) = y_{ij} - \hat{y}_{ij}(\boldsymbol{\theta}^*) = y_{ij} - y_{ij}^* \quad (1.6)$$

Consider now the joint probability density function of the residuals $\rho_{ij}(\boldsymbol{\theta})$, assumed as completely uncorrelated, normally distributed random variables with zero mean and standard deviation equals to the SDV of the associated measurement σ_{ij} :

$$L(\boldsymbol{\theta}) = \prod_{i=1}^{N_{exp}} \prod_{j=1}^{N_m} \frac{1}{\sqrt{2\pi\sigma_{ij}^2}} e^{-\frac{1}{2}\left(\frac{\rho_{ij}(\boldsymbol{\theta})}{\sigma_{ij}}\right)^2} \quad (1.7)$$

The joint PDF of the residuals is also called likelihood function. The parameter estimation problem, can be recast in terms of finding the values for the parameters $\boldsymbol{\theta}$ which maximises the objective

function $L(\boldsymbol{\theta})$, causing the final residuals obtained after the maximisation to be distributed like the corresponding measurement errors:

$$\max_{\boldsymbol{\theta}}\{L(\boldsymbol{\theta})\} = \max_{\boldsymbol{\theta}} \left\{ \prod_{i=1}^{N_{exp}} \prod_{j=1}^{N_m} \frac{1}{\sqrt{2\pi\sigma_{ij}^2}} e^{-\frac{1}{2}\left(\frac{\rho_{ij}(\boldsymbol{\theta})}{\sigma_{ij}}\right)^2} \right\} \quad (1.8)$$

Different likelihood functions may be defined. The maximum likelihood estimate (MLE) does not usually possess any optimal property when the sample used to perform the fitting is small. It is generally biased unless a good knowledge on the statistic of the measurements is available [8]. However, it has been demonstrated to produce good estimates in many situations. Whereas different objective functions may perform better in a specific cases, a powerful argument for the use of the maximum likelihood method is the generality and relative ease of application [8].

Since the natural logarithm is a monotonic increasing function of its argument, the set of parameters maximising $L(\boldsymbol{\theta})$ also maximises $\ln(L(\boldsymbol{\theta}))$. The maximisation of $\ln(L(\boldsymbol{\theta}))$ frequently reduces the numerical complexity of the problem:

$$\max_{\boldsymbol{\theta}}\{\ln(L(\boldsymbol{\theta}))\} = \max_{\boldsymbol{\theta}} \left\{ \ln \left[\prod_{i=1}^{N_{exp}} \prod_{j=1}^{N_m} \frac{1}{\sqrt{2\pi\sigma_{ij}^2}} e^{-\frac{1}{2}\left(\frac{\rho_{ij}(\boldsymbol{\theta})}{\sigma_{ij}}\right)^2} \right] \right\} \quad (1.9)$$

This definition together with a modified version of the PE problem (presented in Section 1.2.3) will be used throughout this thesis. If one is willing to consider the effects of correlation among the measured variables, different, more complex forms of the likelihood function should be adopted. These are not treated in this work, but can be found on specialised text books (e.g. Bard, 1974 [8]).

Notice that only under the assumption of using an exact structural model it is rigorously acceptable to assume that residuals and measurement errors follow the same distribution. However, in a quasi-exact model this simplification is not cause of much harm and the non-perfect structure of the model is usually detected through a posterior analysis (e.g. performing a χ^2 -test). Furthermore, even if the model used to perform the fitting is exact, the number of measurements available will be always limited and might not be sufficient for a reliable estimate of the model parameters. In the following subsections the instruments necessary to assess the statistical quality of the estimates and the goodness of the fitting are described in detail.

1.2.1.2 The covariance matrix

Suppose that a certain objective function Φ , has been chosen to be maximised/minimised in order to estimate the set of model parameters $\boldsymbol{\theta}$. It is not legit to compute a value $\hat{\boldsymbol{\theta}}$ and state that the estimate obtained represents the “true” values of the parameters, in fact the computed value obtained depends on the measured values \mathbf{y}_i ($i = 1, 2, 3, \dots, N_{exp}$) which are affected by uncertainty. This section is dedicated to explaining the mathematical tool necessary to assess how the uncertainty associated to the measured values impacts the confidence we can assign on the estimated non-measurable parameters. Suppose that $\boldsymbol{\theta}$ is an N_θ -dimensional vector of model parameters and that a certain value $\hat{\boldsymbol{\theta}}$ has been computed maximising/minimising an objective function Φ . Practically, however, we are interested in knowing if changing the value of a specific parameter does not really have an important impact on the objective function (i.e. the model responses are not sensitive to specific parameters around $\hat{\boldsymbol{\theta}}$ for the chosen experimental conditions \mathbf{u}_i for $i = 1, 2, 3, \dots, N_{exp}$), or changing two parameters together does not impact the objective function (i.e. critical correlations between parameters resulting in their impossible individual identifiability) and also how the uncertainty intrinsically linked to the measured values of the dependent variables \mathbf{y}_i ($i = 1, 2, 3, \dots, N_{exp}$) influences the confidence we can assign to the estimates, or in other words, how a variation in the measurements impacts the location of $\hat{\boldsymbol{\theta}}$ in the N_θ -dimensional space of the parameters.

It is convenient to define a new column vector \mathbf{z} with dimension $N_{exp}N_m$ which contains all the vectors \mathbf{y}_i ($i = 1, \dots, N_{exp}$) in column:

$$\mathbf{z} = \left[y_{11}, \dots, y_{1N_m}, \dots, \dots, \dots, y_{N_{exp}1}, \dots, y_{N_{exp}N_m} \right]^T$$

Also column vectors $\delta\hat{\boldsymbol{\theta}}$ and $\delta\mathbf{z}$ with dimension N_θ and $N_{exp}N_m$ respectively are defined. The former represents a shift of the estimated value $\hat{\boldsymbol{\theta}}$ for the parameters derived from a variation $\delta\mathbf{z}$ in the measured values for the output variables. If $\hat{\boldsymbol{\theta}}$ has been computed maximising/minimising the objective function Φ , the following condition is satisfied:

$$\frac{\partial\Phi(\hat{\boldsymbol{\theta}}, \mathbf{z})}{\partial\boldsymbol{\theta}} = \mathbf{0} \quad (1.10)$$

Where the left-hand term represents the column vector of dimension N_θ whose elements represent the partial derivatives of the objective function Φ with respect to the parameters. If the function Φ is

continuous, a small variation in the measured values $\delta\mathbf{z}$ results in a small shift of the computed value $\hat{\boldsymbol{\theta}}$ in the space of the parameters.

$$\frac{\partial\Phi(\hat{\boldsymbol{\theta}} + \delta\hat{\boldsymbol{\theta}}, \mathbf{z} + \delta\mathbf{z})}{\partial\boldsymbol{\theta}} = \mathbf{0} \quad (1.11)$$

Expanding the condition to the first term of Taylor expansion it is possible to quantify approximately the variation of the estimated value for the parameters shift $\delta\hat{\boldsymbol{\theta}}$.

$$\frac{\partial\Phi(\hat{\boldsymbol{\theta}} + \delta\hat{\boldsymbol{\theta}}, \mathbf{z} + \delta\mathbf{z})}{\partial\boldsymbol{\theta}} \cong \frac{\partial\Phi(\hat{\boldsymbol{\theta}}, \mathbf{z})}{\partial\boldsymbol{\theta}} + \frac{\partial^2\Phi(\hat{\boldsymbol{\theta}}, \mathbf{z})}{\partial\boldsymbol{\theta}\partial\boldsymbol{\theta}}\delta\hat{\boldsymbol{\theta}} + \frac{\partial^2\Phi(\hat{\boldsymbol{\theta}}, \mathbf{z})}{\partial\boldsymbol{\theta}\partial\mathbf{z}}\delta\mathbf{z} \quad (1.12)$$

Notice that the first term of the expansion is equal to $\mathbf{0}$ because it has been supposed that $\hat{\boldsymbol{\theta}}$ represents an extremum point of the objective function. Also notice that:

$$\frac{\partial^2\Phi(\hat{\boldsymbol{\theta}}, \mathbf{z})}{\partial\boldsymbol{\theta}\partial\boldsymbol{\theta}} = \mathbf{H} \quad (1.13)$$

represents the symmetric Hessian matrix of function Φ evaluated with respect to the parameters, whose kl -th element is:

$$[\mathbf{H}]_{kl} = \frac{\partial^2\Phi(\hat{\boldsymbol{\theta}}, \mathbf{z})}{\partial\theta_k\partial\theta_l} \quad (1.14)$$

From the Taylor series the term $\delta\hat{\boldsymbol{\theta}}$ is isolated.

$$\frac{\partial^2\Phi(\hat{\boldsymbol{\theta}}, \mathbf{z})}{\partial\boldsymbol{\theta}\partial\boldsymbol{\theta}}\delta\hat{\boldsymbol{\theta}} + \frac{\partial^2\Phi(\hat{\boldsymbol{\theta}}, \mathbf{z})}{\partial\boldsymbol{\theta}\partial\mathbf{z}}\delta\mathbf{z} \cong \mathbf{0} \quad (1.15)$$

$$\delta\hat{\boldsymbol{\theta}} \cong -\mathbf{H}^{-1}\left(\frac{\partial^2\Phi(\hat{\boldsymbol{\theta}}, \mathbf{z})}{\partial\boldsymbol{\theta}\partial\mathbf{z}}\right)\delta\mathbf{z} \quad (1.16)$$

The covariance matrix associated to the estimates is defined as the expected value of the squared deviation of the parameters from their expected value $E(\boldsymbol{\theta})$:

$$\mathbf{V}_{\boldsymbol{\theta}} \equiv E\{[\boldsymbol{\theta} - E(\boldsymbol{\theta})][\boldsymbol{\theta} - E(\boldsymbol{\theta})]^T\} \quad (1.17)$$

If it is assumed that $E(\boldsymbol{\theta}) = \hat{\boldsymbol{\theta}}$ then the covariance matrix associated to the parameter estimates, approximated to the first term of the Taylor expansion, is evaluated as follows:

$$\mathbf{V}_{\boldsymbol{\theta}} \cong E \left[\left(-\mathbf{H}^{-1} \left(\frac{\partial^2 \Phi(\hat{\boldsymbol{\theta}}, \mathbf{z})}{\partial \boldsymbol{\theta} \partial \mathbf{z}} \right) \delta \mathbf{z} \right) \left(-\mathbf{H}^{-1} \left(\frac{\partial^2 \Phi(\hat{\boldsymbol{\theta}}, \mathbf{z})}{\partial \boldsymbol{\theta} \partial \mathbf{z}} \right) \delta \mathbf{z} \right)^T \right] \quad (1.18)$$

$$\mathbf{V}_{\boldsymbol{\theta}} \cong E \left[\mathbf{H}^{-1} \left(\frac{\partial^2 \Phi(\hat{\boldsymbol{\theta}}, \mathbf{z})}{\partial \boldsymbol{\theta} \partial \mathbf{z}} \right) \delta \mathbf{z} \delta \mathbf{z}^T \left(\frac{\partial^2 \Phi(\hat{\boldsymbol{\theta}}, \mathbf{z})}{\partial \boldsymbol{\theta} \partial \mathbf{z}} \right)^T \mathbf{H}^{-1} \right] \quad (1.19)$$

Notice that the only term containing random variables is $\delta \mathbf{z} \delta \mathbf{z}^T$, which represents the $N_{exp} N_m \times N_{exp} N_m$ covariance matrix associated to the measurements \mathbf{V}_z . It is therefore possible to rewrite explicitly the covariance matrix of the estimates:

$$\mathbf{V}_{\boldsymbol{\theta}} \cong \mathbf{H}^{-1} \left(\frac{\partial^2 \Phi(\hat{\boldsymbol{\theta}}, \mathbf{z})}{\partial \boldsymbol{\theta} \partial \mathbf{z}} \right) \mathbf{V}_z \left(\frac{\partial^2 \Phi(\hat{\boldsymbol{\theta}}, \mathbf{z})}{\partial \boldsymbol{\theta} \partial \mathbf{z}} \right)^T \mathbf{H}^{-1} \quad (1.20)$$

The formula, which is the one used throughout this thesis, applies for every choice of the objective function, however, for a specific class of functions Φ including the sum of squared residuals and the natural logarithm of the likelihood function $\ln(L)$, it can be demonstrated that also the following approximation holds:

$$\mathbf{V}_{\boldsymbol{\theta}} \cong \mathbf{H}^{-1} \quad (1.21)$$

The quality of the above approximation improves as the variance of the measurements decreases and the fitting of the model gets better [8].

1.2.1.3 The correlation matrix

As specified in Section 1.2.1.2, once a solution $\hat{\boldsymbol{\theta}}$ has been computed, further analysis on the estimates is absolutely necessary to assess the confidence interval in which we can expect to find the “true” value of the parameters. A problem which may arise when a model is proposed to fit measured data is that the mathematical structure of the equations involved may not allow for the identification. Let us consider as an example the following model:

$$y = \frac{\theta_1}{\theta_2} u \quad (1.22)$$

Assume that u and y can be measured without uncertainty and that parameters θ_1 and $\theta_2 \neq 0$ require estimation. The given model is used to fit the experimental data collected in 2 experiments:

- first experiment: $(u, y) = (1, 1)$;
- second experiment: $(u, y) = (2, 2)$.

It is simple to see that the problem admits infinite solutions in fact, the least squares method leads to the definition of an undetermined system of equations in the variables θ_1 and θ_2 :

$$\begin{pmatrix} \frac{\theta_1}{\theta_2} - 1, \theta_1(\theta_2 - \theta_1) \end{pmatrix} = \mathbf{0}^T \quad (1.23)$$

The impossibility of identifying separately the couple of coefficients is a consequence of the total correlation between the parameters that represents a weakness intrinsically linked to the model. The correlation coefficient r_{ij} between two parameters θ_i and θ_j , considered as random variables is defined as:

$$r_{ij} = \frac{V_{\theta,ij}}{\sqrt{V_{\theta,ii}V_{\theta,jj}}} = \frac{E\{[\theta_i - E(\theta_i)][\theta_j - E(\theta_j)]\}}{\sqrt{E\{[\theta_i - E(\theta_i)]^2\}E\{[\theta_j - E(\theta_j)]^2\}}} \quad (1.24)$$

Where $V_{\theta,ij}$ is the ij -th element of matrix \mathbf{V}_θ . If some of the correlation coefficients (i.e. r_{ij} $i \neq j$) are very close to 1 this might be interpreted either as a poorly informative data set or as a sign of weak model structure, in fact if high correlation among the parameters occurs that means that more than one set $\hat{\boldsymbol{\theta}}$ could potentially satisfy the model equations for the fitted data, highlighting the possible intrinsic non-identifiability of the model itself.

1.2.1.4 The t -test

The comparison of the variances associated to the estimated vector $\hat{\boldsymbol{\theta}}$ (i.e. the values on the diagonal of the computed matrix \mathbf{V}_θ) already gives good information about the parameters that require more attention and possible critical structural weaknesses of the model. However, to assess the statistical quality of the parameters, it is necessary to compare meaningfully the value of each parameter estimated with its confidence range. In other words, how large is the confidence region assigned to the parameter with respect to the absolute value of the parameter itself? Assume that a data set involving

N_{exp} times N_m measurements is used to solve a PE problem involving N_θ parameters. In this work, in order to assess the statistical value of the estimates, a one-tailed t -test with 95% of significance will be performed comparing the t -value of each estimated parameter $\hat{\theta}_i$ with the reference t -value of a Student distribution with degree of freedom $N_{exp}N_m - N_\theta$. The aim of the test is to answer the question: if the parameter estimation is the realisation of a normally distributed random variable, whose distribution is estimated from the available sample of measurements using the Student distribution of variable with degree of freedom $N_{exp}N_m - N_\theta$ and mean $\hat{\theta}_i$, is it possible to tell with at least 95% of confidence that the “true” value of the parameter lays in the range of approximately 2 SDVs of the evaluated distribution? In more rigorous terms, is the following condition satisfied?

$$\frac{\hat{\theta}_i}{t_{0.975}(N_{exp}N_m - N_\theta)\sqrt{V_{\theta,ii}}} > t_{0.95}(N_{exp}N_m - N_\theta) \quad \forall i = 1, \dots, N_\theta \quad (1.25)$$

Where the t -value appearing in the bottom part of the left-hand term is evaluated for a Student distribution with degree of freedom $N_{exp}N_m - N_\theta$ at a cumulated probability equals to 0.975 and the t -value of reference appearing in the right-hand side is evaluated at a cumulated probability of 0.95 to perform the one-tailed test with 95% of significance. The satisfaction of this condition will be considered as a proof of good estimation of the parameters.

1.2.1.5 Goodness of fit

In a conventional parameter estimation problem, a proposed model is used to fit a set of data. The model used might not reflect exactly the nature of the physical phenomenon, for example a model involving a quadratic law used to fit data collected from experiments performed on a linear phenomenon will perform decently only in a very limited range of experimental conditions and even though it would be possible to estimate the parameters with acceptable accuracy (i.e. $V_{\theta,ii}$ is small with respect to $\hat{\theta}_i$), the model will actually perform badly when used to make predictions. In order to detect a bad fitting, in this work, a χ^2 -test on the residuals with 95% of significance will be carried out. The χ_{ref}^2 will depend on the number of degrees of freedom $N_{exp}N_m - N_\theta$ specific of each case.

The test is necessary to understand if the residuals computed at the end of the parameter estimation problem can be justified by the measurement errors. Summing up $N_{exp}N_m - N_\theta$ squared random variables following the standard normal distribution, the result will be smaller than χ_{ref}^2 with a

probability of 95%. The reference value is compared to the squared weighted residuals obtained as solution of the PE problem:

$$\chi_{sample}^2 = \sum_{i=1}^{N_{exp}} \sum_{j=1}^{N_m} \left[\frac{\rho_{ij}(\hat{\theta})}{\sigma_{ij}} \right]^2 \quad (1.26)$$

If the model is exact and the sample used for the fitting is sufficiently large, the values computed for $\hat{\theta}$ are expected to be very close to the “true” values, thus the model identified would be very close to the “true” model and the residuals would be consequence of the measurement errors only. If these errors are normally distributed and the values of the SDVs associated to the measurements are known precisely and not underestimated, then $\chi_{sample}^2 \leq \chi_{ref}^2$ with a probability of 95%. If we are not sure about the measurement uncertainty and about the reliability of the model, and it happens that $\chi_{sample}^2 > \chi_{ref}^2$, that could be interpreted in 4 different ways:

- the assumption of having measurement errors following a normal distribution with zero mean is wrong;
- the values of the SDVs associated to the measurements have been globally underestimated;
- the model is wrong;
- a combination of the previous 4 cases.

1.2.2 Model-based design of experiments

Every model can present different strengths and weaknesses: different degrees of complexity and different descriptive capabilities. The holy grail of every researcher working on physical system modelling is to develop a simple model (i.e. involving a low number of physically meaningful parameters) which gives also accurate predictions in a vast range of experimental conditions. Complex models in fact might be capable of realising low residuals when they are used to fit the experimental data, but too high complexity may result in a very difficult identification of the parameters. In any case the identification of the model requires the execution of experiments which may involve the employment of costly facilities, resources and time. It is therefore of great importance planning carefully the experiments, taking into account the specific purpose which can be:

- identifying the best model for describing the reaction mechanism among a set of candidate models proposed by the researcher;

- identifying an already selected model through the improvement its parameters' estimates.

Following the seminal work by Box and Lucas [2] many researchers devoted their efforts to developing advanced MBDoe techniques for both MD and PP [3, 4]. These theories allow for the identification of the best experiment campaign even in complicated nonlinear dynamic systems through the numerical maximisation/minimisation of properly defined objective functions (dependent on both the purpose of the design and the amount of resources available for conducting the experiments). If the target of the design is to identify the best model among a given set, the objective function may be defined as the global divergence in the responses of the models in order to maximise the discriminating power of the experiments. If the target is to improve the precision of the parameters, then the objective function to minimise has to be a certain measure of the predicted covariance matrix associated to the parameter estimates \mathbf{V}_θ . The general and versatile mathematical framework in which these theories were developed made possible their successful application in various branches of science outside the field of chemical reaction kinetics: from nuclear physics and biophysics to econometrics and geophysical exploration [8]. The following subchapters will be dedicated to presenting better the mathematical tools and the techniques that have been developed regarding the design of experiments based on the model focusing on the aspects functional to the work presented in this thesis.

1.2.2.1 Metric of information

Considering the maximum likelihood estimate presented in Section 1.2.1.1, if Φ is defined as the logarithm of the likelihood function and the residuals are defined as $\rho_{ij} = \hat{y}_{ij} - y_{ij}$, the Hessian:

$$\mathbf{H} = \frac{\partial^2 \Phi}{\partial \theta \partial \theta} = \frac{\partial^2 \ln(L(\hat{\theta}))}{\partial \theta \partial \theta} \quad (1.27)$$

is also called Fisher information matrix and it quantifies the information carried by measurable random variables \mathbf{z} about non-measurable unknown parameters θ . Being this matrix the Hessian of a log-likelihood function, also the approximation $\mathbf{V}_\theta \cong \mathbf{H}^{-1}$ holds (Section 1.2.1.2). Intuitively, the covariance matrix \mathbf{V}_θ and the Fisher matrix \mathbf{H} represent two sides of the same coin. The higher the information carried by the measurements, the lower the uncertainty associated to the estimated parameters. Assume that a model is given to describe a certain physical phenomenon and that some experiments have been performed to obtain a first rough estimation of the parameters. We call this first estimate θ^0 with associated covariance matrix \mathbf{V}_{θ^0} . Assume now that we want to improve the

estimate reducing the elements of the covariance matrix associated to the parameters performing new experiments. It is possible to quantify approximately (also because it depends on the first available estimation $\boldsymbol{\theta}^0$) in advance the posterior covariance matrix $\mathbf{V}_{\boldsymbol{\theta}}$ after the conduction of N_{exp} experiments as:

$$\mathbf{V}_{\boldsymbol{\theta}} \cong \left[\mathbf{V}_{\boldsymbol{\theta}^0}^{-1} + \sum_{i=1}^{N_{exp}} \mathbf{H}_i \right]^{-1} \quad (1.28)$$

Where \mathbf{H}_i represents the information matrix associated to the i th experiment in a hypothetical campaign of N_{exp} experiments. The possibility of predicting the covariance matrix of the estimates simulating the trials with the available model represents a powerful tool for designing the best experiments for reaching the desired goal (which might be reducing the variance associated to a specific parameter or the covariance associated to a couple of parameters). An example for the application of this tool is proposed in Appendix I. Under certain conditions, it is possible to use an approximate form of the Fisher matrix. We refer to a log-likelihood function considering totally uncorrelated measured variables:

$$\Phi = \ln(L(\hat{\boldsymbol{\theta}})) = \frac{1}{2} \sum_{i=1}^{N_{exp}} \sum_{j=1}^{N_m} \left[\log(2\pi\sigma_{ij}^2) + \left(\frac{\hat{y}_{ij} - y_{ij}}{\sigma_{ij}} \right)^2 \right] \quad (1.29)$$

The kl -th element of the Fisher information matrix is also defined as the kl -th element of the Hessian matrix associated to function Φ :

$$[\mathbf{H}]_{kl} = \left[\frac{\partial^2 \ln(\Phi)}{\partial \boldsymbol{\theta} \partial \boldsymbol{\theta}} \right]_{kl} = \sum_{i=1}^{N_{exp}} \sum_{j=1}^{N_m} \left[\frac{1}{\sigma_{ij}^2} \left(\frac{\partial \hat{y}_{ij}}{\partial \theta_k} \frac{\partial \hat{y}_{ij}}{\partial \theta_l} \right) + \frac{1}{\sigma_{ij}^2} (\hat{y}_{ij} - y_{ij}) \frac{\partial^2 \hat{y}_{ij}}{\partial \theta_k \partial \theta_l} \right] \quad (1.30)$$

If residuals $\rho_{ij} = \hat{y}_{ij} - y_{ij}$ are small it is acceptable to write the following approximation:

$$[\mathbf{H}]_{kl} \cong \sum_{i=1}^{N_{exp}} \sum_{j=1}^{N_m} \left[\frac{1}{\sigma_{ij}^2} \left(\frac{\partial \hat{y}_{ij}}{\partial \theta_k} \frac{\partial \hat{y}_{ij}}{\partial \theta_l} \right) \right] \quad (1.31)$$

The term $\frac{\partial \hat{y}_{ij}}{\partial \theta_k}$ is called sensitivity of the j -th output variable with respect to the k -th parameter in the conditions investigated in the i -th experiment. Throughout this work, the above notation for the Fisher

matrix is be used to plot the information in the experimental design space in order to visualise the most informative experimental conditions. The trace of the matrix \mathbf{H} related to a single experiment is adopted as suitable scalar measure of the information.

1.2.2.2 *MBDoe for parameter estimation*

Suppose that a model is available together with preliminary experimental data which allowed for the solution of a PE problem leading to the computation of a first set of parameters $\boldsymbol{\theta}^0$. The evaluation of the covariance matrix $\mathbf{V}_{\boldsymbol{\theta}^0}$, the following statistical analysis of the correlation coefficients r_{ij} and the t -tests performed on the parameters will tell if it has been possible to get a satisfactory estimation or whether some parameters are affected by critical correlation and very high variance. If the second case occurs, it is necessary to amend the unsatisfactory estimates performing new experiments. As presented in Section 1.2.2.1, it is possible to quantify approximately the posterior covariance matrix $\mathbf{V}_{\boldsymbol{\theta}}$ (Equation 1.28) resulting by the execution of a certain set of N_{exp} experiments through the evaluation of the Fisher information matrix. By doing so, it is possible to design an experiment campaign with the aim of minimising a certain measure of the posterior covariance matrix $\mathbf{V}_{\boldsymbol{\theta}}$. In general, the covariance matrix of the estimates identifies a confidence ellipsoid in the N_{θ} -dimensional hyperspace. Improving the parameter estimates means reducing the size of this region of confidence choosing the proper scalar measure as target to minimise. Different meaningful scalar quantities can be chosen as objective function, but the most established and popular methods are:

- A-optimal: which considers the trace of $\mathbf{V}_{\boldsymbol{\theta}}$ as scalar function to be minimised. The trace of the covariance matrix associated to the parameter estimates quantifies the volume of the polyhedron circumscribing the confidence ellipsoid in the N_{θ} -dimensional space of the estimates;
- D-optimal: for which the determinant of the matrix $\mathbf{V}_{\boldsymbol{\theta}}$ is chosen as objective function. The determinant of the covariance matrix quantifies the volume of the confidence ellipsoid;
- E-optimal: in which the largest eigenvalue of $\mathbf{V}_{\boldsymbol{\theta}}$ is assumed as measure to minimise. The largest eigenvalue of the covariance matrix quantifies the length of the longest axis of the confidence ellipsoid.

In Appendix I an example of MBDoe application for parameter estimation adopting an A-optimal approach is presented for a yeast growth model obtained from literature [4]. In the example proposed in Appendix, two experiments are designed in sequence and performed virtually to reduce the size of the confidence region associated to the parameter estimates. In Figure 1.2 the confidence ellipsoids

referring to a couple of parameters are shown after the first experiment and after a second to highlight the reduction of the confidence region and the improved accuracy of the parameter estimates.

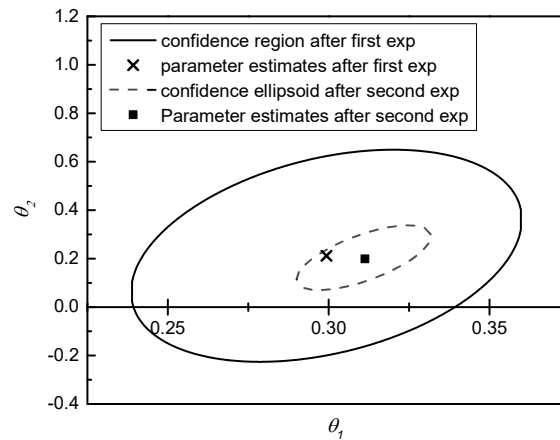


Figure 1.2. Reduction of the confidence region associated a couple of model parameters after the execution of a first experiment (solid line) and a second one (dotted line), both designed adopting an A-optimal approach.

1.2.3 *Alternative method for model identification*

A different approach for model identification with respect to the conventional one presented in the block diagram in Figure 1.1 is proposed in this section. This different procedure is shown schematically in Figure 1.3. Also this method starts from the availability of experimental data and related errors, but while the conventional approach involves the selection of the best model among a set of proposed ones, the method proposed here involves the gradual improvement of a “rough” model through its gradual modification guided by the identification its limits. Once the improved model has reached a satisfactory predictive capability for the phenomenon analysed, unsatisfactory parameter estimates are amended through techniques of MBD_{oE} for parameter precision, analogously to the conventional framework for model identification presented in Figure 1.1. The detection of the model weaknesses is performed through the application of a model-based data mining technique for parameter estimation (MBDM-PE), that can be fruitfully used either to remove the measurements affected by too high errors or to identify the experimental data the model is not able to fit by taking into account the uncertainty on the measurements.

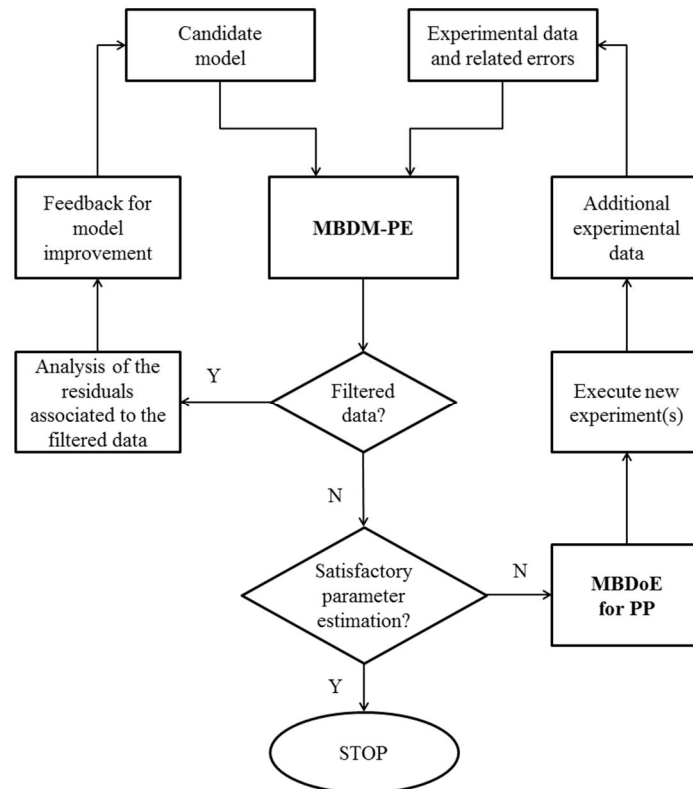


Figure 1.3. Systematic approach for model identification implementing the MBDM-PE filtering technique. Boldface blocks highlight the fundamental steps of this alternative process for model establishment.

The MBDM-PE method acts like a statistical filter estimating the parameters and simultaneously removing the measured values that are incompatible with the proposed model, highlighting either unlikely results or model weaknesses (if the model is known to be inexact) and possibly suggesting improvements. The filtering technique is based on the solution of a mixed integer nonlinear programming problem (MINLP) whose aim is the maximisation of a properly defined likelihood function acting on the set of parameters appearing in the candidate model (treated as continuous variables) and user-defined binary variables that act like switchers on critical experimental results. In the following paragraphs, the properties of the statistical filter based on the Gaussian distribution will be presented and explained.

1.2.3.1 The Gaussian filter

A statistical filter may be defined easily for any likelihood function involving uncorrelated measurements. The choice of the specific function, however, impacts directly the permissiveness of the associated filter. In this subsection the statistical filter based on the Gaussian distribution is considered to analyse the properties of the MBDM-PE method starting from the most general case in

which every measurement is associated to a switcher to the specific case functional for the analysis carried out in this thesis.

Consider, as usual, the case in which experimental data collected in N_{exp} experiments, each involving N_m measurements are used for defining an objective function to solve a parameter estimation problem. In the case of completely uncorrelated, normally distributed measurement errors, the likelihood function is simply defined as the product of the normal distributions associated to the residuals and it is function of the model parameters only (Equation 1.7). If one is willing to identify the most unlikely experimental results, the likelihood function can be modified adding an $N_{exp} \times N_m$ matrix $\mathbf{\Gamma}$ of binary variables γ_{ij} whose value can be either 1 or 0. The binary variable γ_{ij} is then added as exponent to the ij -th factor of the likelihood ($\forall i = 1, \dots, N_{exp} \wedge \forall j = 1, \dots, N_m$). The resulting objective function is then maximised with respect to $\boldsymbol{\theta}$, and $\mathbf{\Gamma}$.

$$\max_{\boldsymbol{\theta}, \mathbf{\Gamma}} \left\{ \prod_{i=1}^{N_{exp}} \prod_{j=1}^{N_m} \left[\frac{1}{\sqrt{2\pi\sigma_{ij}^2}} e^{-\frac{1}{2} \left(\frac{\rho_{ij}(\boldsymbol{\theta})}{\sigma_{ij}} \right)^2} \right]^{\gamma_{ij}} \right\} \quad (1.32)$$

The binary elements of matrix $\mathbf{\Gamma}$ act like switchers on critical single measurements, whose contribution to the objective function is lower than 1, removing them from the parameter estimation problem. Notice that the tolerance of the filter with respect to a residual ρ_{ij} changes with the SDV σ_{ij} of the residual itself. In the specific case of the statistical filter defined above (1.32), the tolerance region for a single measurement is shown in Figure 1.4a. Measurements with associated SDV higher than $1/\sqrt{2\pi} \cong 0.399$ cannot give a positive contribution to the likelihood (because the associated bell-shaped distribution does not surpass the value 1), and are rejected by the filter in any case. The maximum tolerance threshold for a residual is achieved by measurements with associated standard deviation equals to $1/\sqrt{2\pi e} \cong 0.242$. In Figure 1.4b the ratio between the maximum absolute residual admitted by the filter and the associated SDV is plotted highlighting with dashed lines some characteristic values for the filter:

- if the SDV $\sigma_{ij} > 1/\sqrt{2\pi e^9} \cong 0.004$, the condition $|\rho_{ij}| < 3\sigma_{ij}$ must occur for a residual to be accepted by the filter for taking part to the parameter estimation problem;
- if the SDV $\sigma_{ij} > 1/\sqrt{2\pi e^4} \cong 0.054$, the condition $|\rho_{ij}| < 2\sigma_{ij}$ must occur for a residual to be included the parameter estimation problem;
- if the SDV $\sigma_{ij} > 1/\sqrt{2\pi e} \cong 0.242$, the condition $|\rho_{ij}| < \sigma_{ij}$ must be verified by the residual to be considered for the parameter estimation problem;

- if the SDV $\sigma_{ij} > 1/\sqrt{2\pi} \cong 0.399$, the measurement is always rejected by the filter.

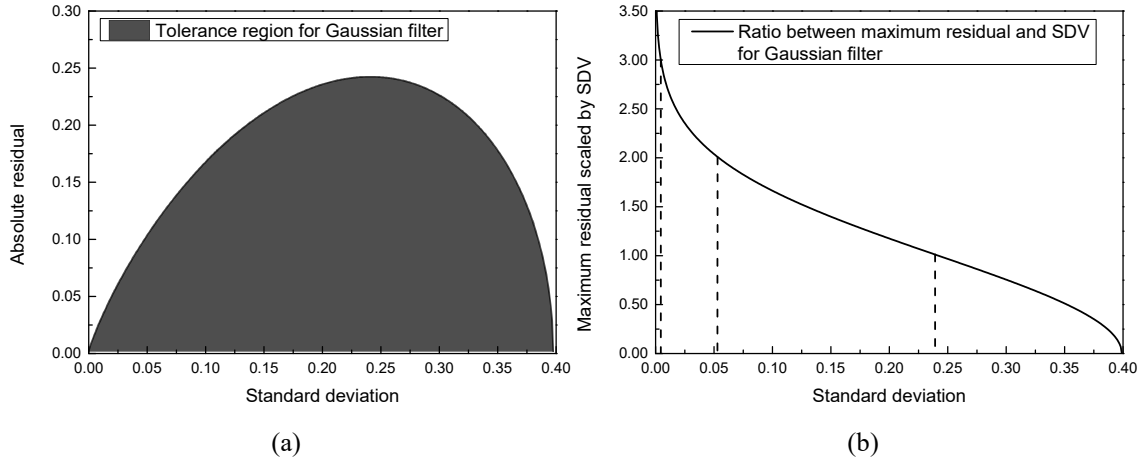


Figure 1.4. Tolerance region for the absolute residuals (grey-coloured area) plotted as function of the respective SDV in a statistical filter based on the normal distribution (a). Ratio between the maximum residual admitted and the associated SDV; dashed lines indicate characteristic values for the filter (b).

The tolerance region of the filter can be modified choosing properly the objective function. For example, a filter rejecting all the measurements whose associated absolute residual exceeds 3 SDVs can be defined as follows:

$$\max_{\theta, \Gamma} \left\{ \prod_{i=1}^{N_{exp}} \prod_{j=1}^{N_m} e \left[3^2 - \left(\frac{\rho_{ij}(\theta)}{\sigma_{ij}} \right)^2 \right] \gamma_{ij} \right\} \quad (1.33)$$

For the purposes of this work, a different filter is defined modifying the likelihood function based on the normal distribution adding two arrays of additional parameters α and β whose elements are binary values which can be either 1 or 0.

$$\alpha = [\alpha_1, \dots, \alpha_i, \dots, \alpha_{N_{exp}}] \quad \alpha_i = 1 \vee 0$$

$$\beta = [\beta_1, \dots, \beta_j, \dots, \beta_{N_m}] \quad \beta_j = 1 \vee 0$$

By adding the exponent $\alpha_i \beta_j$ to the ij -th factor of the likelihood function Φ and maximising the resulting modified likelihood function with respect to θ , α and β the result will be to estimate the model parameters θ removing simultaneously both the experiments and the measured variables the model is not able to fit. The binary elements of the arrays α and β act like switchers on critical experiments and measured variables respectively.

$$\max_{\theta, \alpha, \beta} \left\{ \prod_{i=1}^{N_{exp}} \prod_{j=1}^{N_m} \left[\frac{1}{\sqrt{2\pi\sigma_{ij}^2}} e^{-\frac{1}{2} \left(\frac{\rho_{ij}(\theta)}{\sigma_{ij}} \right)^2} \right]^{\alpha_i \beta_j} \right\} \quad (1.34)$$

The estimated parameters $\hat{\theta}$ will be the result of fitting a possibly limited set of experimental data given by the simultaneous estimation of parameters α and β with the aim of maximising the likelihood. The estimated values for the binary switchers will give information either on which aspects of the model should be strengthened or which are the most unlikely experimental results, depending on which confidence and correctness is assigned to the model and on which confidence is assigned to values set for the standard deviations of the measurements σ_{ij} .

1.3 gPROMS Model Builder

All the data analysis presented in this work has been carried out using the software gPROMS Model Builder 4.1 developed by Process System Enterprise (PSE). It is a computational framework which allows for advanced nonlinear dynamic model simulation and also implements powerful tools for model validation and process optimisation. It implements two standard solvers for the solution of sets of nonlinear algebraic equations named BDNLSOL and SPARSE:

- BDNLSOL (Block Decomposition NonLinear SOLver). It is an implementation of a general solver for sets of nonlinear equations recast to block triangular form. It is particularly suited when symmetric discontinuities are involved in the model (IF conditions).
- SPARSE. It is designed for the solution of nonlinear algebraic systems without block decomposition. It provides a sophisticated implementation of a Newton-type method.

The software also implements two standard mathematical solvers for the solution of mixed sets of differential and algebraic equations named DASOLV and SRADAU:

- DASOLV. Based on backward differentiation formulae (BDF), it has been proved to be efficient in a wide range of situations.
- SRADAU. Implementing a fully-implicit Runge-Kutta method, it has been proved to be efficient for the solution of problems arising from the discretisation of partial differential algebraic equations (PDAEs). Particularly effective in the presence of strong transport phenomena and models with frequent discontinuities.

Throughout this work the solvers SPARSE and DASOLVE will be used for the simulations. Regarding the tools available for model validation, these are all founded on the maximisation of certain objective functions. In the case of the parameter estimation tool, the objective function implemented is the log-likelihood. When a PE is performed in gPROMS, also an evaluation of parameters statistics (consistent with the methods explained in Section 1.2.1.1), is proposed to the user to assess the quality of the results. The software facilitates also the design of experiments based on the models. In this case the objective function is built by the program depending on the design criterion chosen (Section 1.2.2.2) and on the boundaries and settings defined by the operator through a user-friendly interface. If the user needs to optimise a certain variable, which could represent for example a cost function, embedded in a complex process, also an optimisation feature is made available for the maximisation of user defined objective functions. For the optimisation purposes, gPROMS implements different solvers. The standard one, which will be also used throughout this thesis, is CVP_SS. It can solve optimisation problems with both discrete and continuous decision variables (i.e. mixed integer optimisation) and it supports both steady-state and dynamic problems. In Figure 1.5 an example of gPROMS Model Builder interface is proposed.

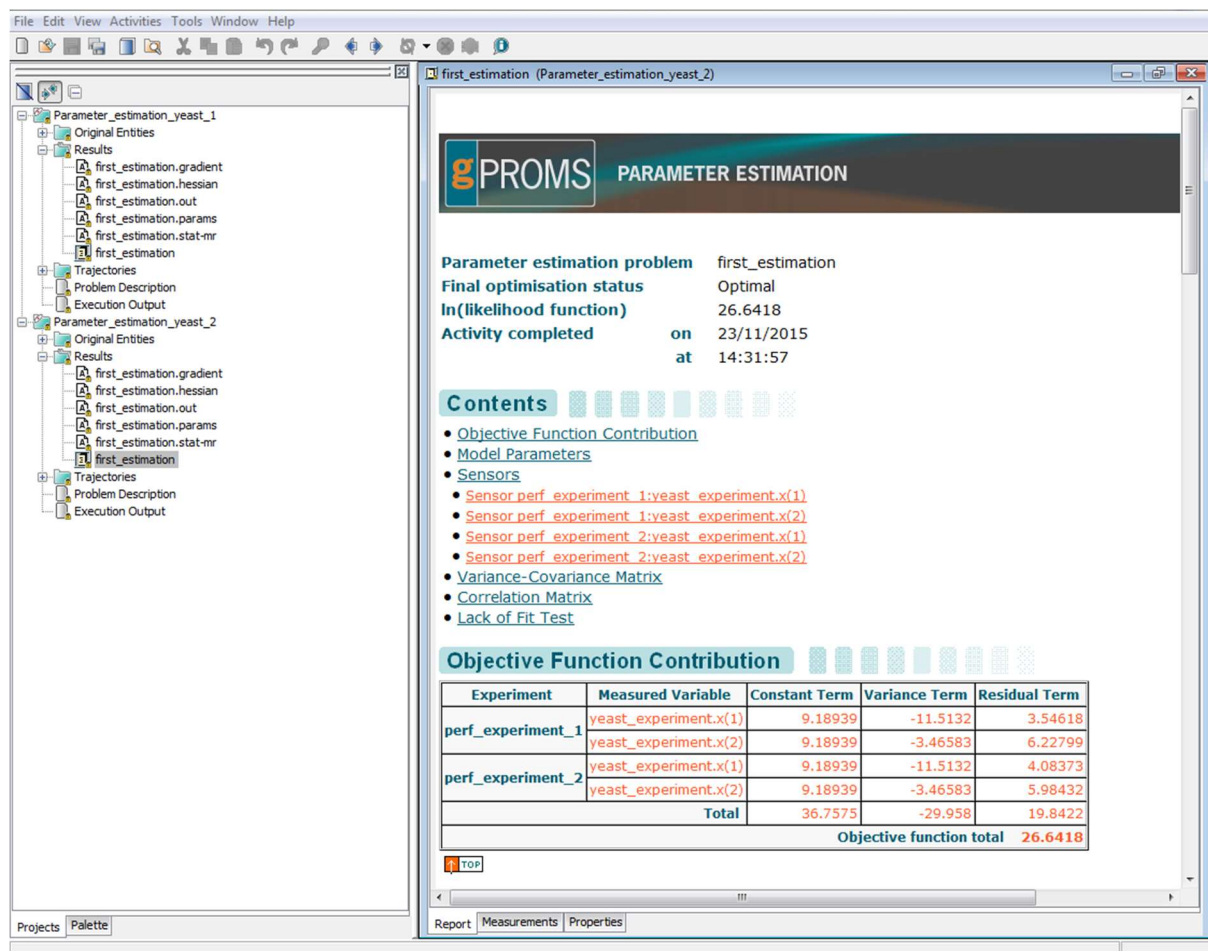


Figure 1.5. gPROMS ModelBuilder's interface.

Chapter 2: Case study, experimental setup and available data sets

The case study analysed in this work is introduced in this chapter. An introductory section is dedicated to presenting the key kinetic mechanisms that are supposed to occur during the catalytic oxidation of methanol on silver. This is to clarify some aspects that are useful for a better understanding of the topics discussed afterwards. The experimental setup, the devices used and the measurement system are then described.

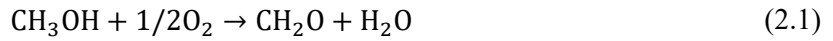
A section is dedicated to presenting the data sets that were made available for the targets chased in this work. These experimental sets of data present very few similarities:

- they were collected in 3 different years: 2008, 2013 and 2015; using catalysts that have been synthesised separately and might behave differently;
- to perform the experiments, 5 reactors with different geometries have been used;
- different ranges of experimental conditions have been investigated in each reactor.

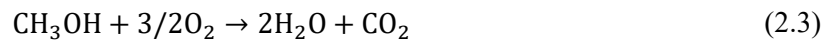
The sets collected in each of the reactors are first analysed individually to assess the repeatability and consistency of the results, highlighting odd trends and experimental errors. Then, some experiments are selected to compare qualitatively the reactivity of the catalysts present in the different setups.

2.1 Kinetic mechanism

Under industrial conditions, the partial oxidation of methanol to formaldehyde on silver catalyst is usually carried out at atmospheric pressure at a temperature around 900K. The overall mechanism involves the conversion of methanol CH_3OH to formaldehyde CH_2O , through both oxidation and dehydrogenation phenomena:



The main by-products are: molecular hydrogen H_2 , water H_2O , carbon dioxide CO_2 , formic acid CH_2O_2 and traces of carbon monoxide CO . The industrial process is always carried out with high inlet methanol/oxygen molar ratio ($y_{\text{CH}_3\text{OH}}^{\text{IN}}/y_{\text{O}_2}^{\text{IN}} = 2.4 - 2.5$) introducing steam for achieving high selectivity. The main undesired reactions occurring in the system, impacting negatively the selectivity of formaldehyde, involve the complete oxidation of methanol and the decomposition of formaldehyde to carbon dioxide:



This process has been studied extensively, but despite the great industrial importance of this reaction mechanism, the key phenomena occurring on the catalyst surface are yet to be completely understood. There are in fact cases in which the system behaves in unexpected ways. The low quantities of hydrogen found at the outlet with some silver catalysts suggests the presence of a hydrogen oxidation reaction which is instead expected to occur at higher temperature [15]:



In the following sections, the basic mechanisms introduced here are mentioned to analyse the experimental data made available for the objectives of this work.

2.2 Experimental setup

For the purposes of model identification some data sets for the partial oxidation of methanol to formaldehyde over silver catalyst have been made available. These data sets were collected using microreactors. Microreactors are small devices, typically operating as continuous flow reactors, which are employed in reaction engineering for the fruitful collection of information on reacting systems. The small dimensions of the channels in microreactors permits to study the reactions under the assumptions of negligible diffusion resistance and negligible temperature gradients allowing for meaningful data collection for the investigation of kinetic mechanisms.

The microreactors employed for the data collection functional to this work are presented schematically in Table 2.1 with concise information on reactor geometry and catalyst film length. The grey-coloured area in the drawings represents the section occupied by the catalyst film while the dark-coloured area, located downstream with respect to the catalyst, represents the retainer (i.e. a sieve to prevent particles of catalyst from being scraped off the reactor by the gas flow). As one can see from table, 3 different geometries of reactors were employed in the years for the data collection:

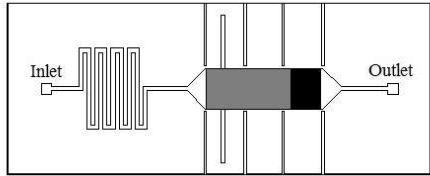
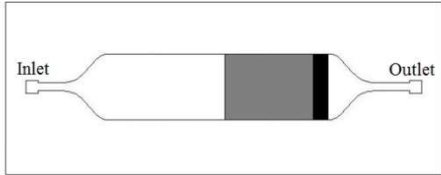
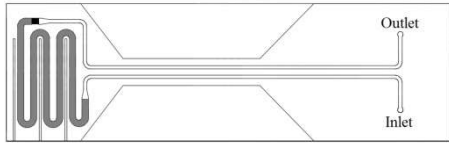
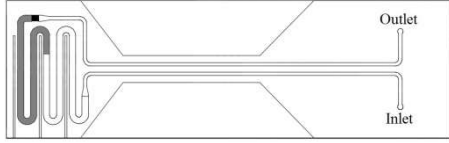
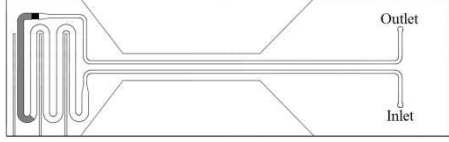
- wide-channel reactor C1;
- wide-channel reactor C2;
- serpentine reactors R1, R2 and R3.

The serpentine reactors were loaded with different quantities of catalysts, indeed the silver film length decreases going from R1 to R3.

All these microreactors had been fabricated through photolithography and deep reacting ion etching. The silver catalyst was deposited on the channel floors through sputtering. The overall assembly was insulated with ceramic material to reduce the heat losses. COMSOL simulations have been performed to demonstrate the isothermal state of the catalyst film and the negligible effect of diffusion in the experimental conditions investigated [5]. The relatively large cross-sectional areas of the main channel in microreactors C1 and C2 (0.72 mm^2 and 0.96 mm^2 respectively), justifies the assumption of having negligible pressure drops along the section occupied by the catalyst. It will be therefore assumed throughout this work that the only source of pressure drops in the wide-channel reactors is the retainer (i.e. the pressure in the section occupied by the catalyst will be assumed constant and equals to the pressure at the inlet). In the serpentine reactors R1, R2 and R3, used to perform the experiments in 2015, the cross-sectional area of the main channel is an order of magnitude smaller (around 0.11 mm^2), making unacceptable the assumption of having negligible pressure drops along the catalyst film region. A more detailed description of the reactors and the setups can be found in the literature [16].

Experiments were performed in steady-state conditions injecting the gaseous mixture containing the reactants (i.e. methanol and oxygen), water and helium (used as inert carrier), through the microreactors using syringe pumps. The samples collected were analysed through gas chromatography to identify the outlet composition.

Table 2.1. Schematic representation of the setups and concise information on channel and catalyst film geometries. The grey-coloured area represents the catalyst film; black-coloured area indicates the retainer. Boldface numbers highlight the length of the catalyst film. Drawings have different scales.

Microreactor	Main channel	Inlet channel	Outlet channel	Catalyst film
<p>C1 - wide-channel - 2008</p> 	Length 27.7 mm Width 6.0 mm Depth 0.12 mm	Length 102.8 mm Width 0.6 mm Depth 0.12 mm	Neglected	Length 12.5 mm Width 6.0 mm
<p>C2 – wide-channel - 2013</p> 	Length 27.7 mm Width 8.0 mm Depth 0.12 mm	Neglected	Neglected	Length 12.5 mm Width 8.0 mm
<p>R1 – serpentine – 2015</p> 	Length 79.3 mm Width 0.9 mm Depth 0.12 mm	Length 52.0 mm Width 0.5 mm Depth 0.12 mm	Length 63.1 mm Width 0.5 mm Depth 0.12 mm	Length 78.1 mm Width 0.9 mm
<p>R2 – serpentine - 2015</p> 	Length 79.3 mm Width 0.9 mm Depth 0.12 mm	Length 52.0 mm Width 0.5 mm Depth 0.12 mm	Length 63.1 mm Width 0.5 mm Depth 0.12 mm	Length 35.7 mm Width 0.9 mm
<p>R3 – serpentine - 2015</p> 	Length 79.3 mm Width 0.9 mm Depth 0.12 mm	Length 52.0 mm Width 0.5 mm Depth 0.12 mm	Length 63.1 mm Width 0.5 mm Depth 0.12 mm	Length 17.8 mm Width 0.9 mm

2.2.1 Measurement system

The result produced by the steady-state experiments performed on the microreactors presented in Section 2.2 are samples that require to be analysed to identify the outlet composition of the mixture. This analysis is carried out through gas chromatography. A gas chromatograph is an instrument capable of separating and quantifying the single components present in complex gaseous samples

[17]. The compounds involved in the sample move between two phases: a stationary bed with a large exchange area and the gas phase of the sample. The mixture that requires to be analysed is vaporised and injected through a narrow tube filled with the stationary bed, namely the column. The single compounds undergo a series of reversible reactions being adsorbed and freed from the stationary phase with a rate that depends on the relative vapour pressure and the chemical affinity of each component with the bed. Thus, different components then require different times to reach the end of the pipe where they are independently detected through electronic signals. Concerning the specific measurement systems, in 2008 the compositions were detected using a ThermoQuest Trace and a Shimadzu gas chromatographs. In 2013 and 2015 (i.e. in the experiments carried out on C2, R1, R2 and R3) an Agilent 7890A GC was used instead.

2.3 Data sets and experimental conditions

The set of independent experimental conditions that can be directly manipulated by the experimentalist in the described setups involve the following physical quantities:

- inlet volumetric flowrate F_{STC}^{IN} , which will be always referred to the standard conditions STC (i.e. $T^* = 273.15$ K; $P^* = 101325$ Pa);
- operating temperature T ;
- the inlet composition of the gaseous mixture at the inlet of the reactor, expressed in terms of molar fractions of methanol, oxygen, water (i.e. $y_{CH_3OH}^{IN}$, $y_{O_2}^{IN}$ and $y_{H_2O}^{IN}$ respectively).

The measurable output variables of the system are instead:

- outlet volumetric flowrate F_{STC}^{OUT} , still expressed in STC (the values F_{STC}^{IN} and F_{STC}^{OUT} are different because of a change in the molarity of the mixture during the reaction);
- inlet and outlet pressure P^{IN} and P^{OUT} ;
- the outlet composition, expressed in terms of molar fractions of methanol, oxygen, water, formaldehyde, hydrogen, carbon dioxide and carbon monoxide (i.e. $y_{CH_3OH}^{OUT}$, $y_{O_2}^{OUT}$, $y_{H_2O}^{OUT}$, $y_{CH_2O}^{OUT}$, $y_{H_2}^{OUT}$, $y_{CO_2}^{OUT}$ and y_{CO}^{OUT} respectively).

In the cases of the wide-channel reactors C1 and C2, the outlet pressure P^{OUT} and the outlet molar fraction of carbon dioxide y_{CO}^{OUT} are not reported. In the data sets collected on R1, R2 and R3 the outlet composition is given in terms of conversion of the reactants X_i ($i = CH_3OH, O_2$) and selectivity

of the products S_j ($j = \text{CH}_2\text{O}, \text{H}_2, \text{H}_2\text{O}, \text{CO}_2, \text{CO}$); the measured values for the molar fractions have been derived from the definitions:

$$X_i = \frac{y_i^{\text{IN}} F_{\text{STC}}^{\text{IN}} - y_i^{\text{OUT}} F_{\text{STC}}^{\text{OUT}}}{y_i^{\text{IN}} F_{\text{STC}}^{\text{IN}}} \quad i = \text{CH}_3\text{OH}, \text{O}_2 \quad (2.6)$$

$$S_j = \frac{y_j^{\text{OUT}} F_{\text{STC}}^{\text{OUT}} - y_j^{\text{IN}} F_{\text{STC}}^{\text{IN}}}{X_{\text{CH}_3\text{OH}} y_{\text{CH}_3\text{OH}}^{\text{IN}} F_{\text{STC}}^{\text{IN}}} \quad j = \text{CH}_2\text{O}, \text{H}_2, \text{H}_2\text{O}, \text{CO}_2, \text{CO} \quad (2.7)$$

The experimental conditions investigated in the different setups are reported in Table 2.2. The detailed results for all the experiments can be found in Appendix II:

- the first data set was collected in 2008 on the wide-channel reactor C1. It includes 20 experiments performed varying one factor at time, assessing the effect of a variation in temperature keeping the inlet composition constant and also changing the composition at the inlet keeping the same value of temperature; the inlet volumetric flowrate set in the trials is always the same;
- the second data set collected in 2013 on the wide-channel reactor C2 consists in 4 experiments carried out keeping constant the temperature T and varying the flowrate $F_{\text{STC}}^{\text{IN}}$ (i.e. investigating the effect of a variation in the residence time at constant temperature);
- the third data set was collected on the serpentine reactor R1 in 2015. 13 trials were carried out on this setup investigating the effects of a variation in temperature T , inlet flowrate $F_{\text{STC}}^{\text{IN}}$ and inlet composition;
- the fourth set of data was collected in 2015 on R2. 3 experiments were executed at the same temperature T varying the inlet flowrate $F_{\text{STC}}^{\text{IN}}$ (analogously to C2);
- the fifth set of experimental data was obtained in 2015 running experiments in the serpentine reactor R3 investigating the effects of variations in temperature T and flowrate $F_{\text{STC}}^{\text{IN}}$ and keeping always the same inlet composition.

One of the most critical aspects to consider when performing experiments aimed at identifying the reaction kinetic in catalytic systems is quantifying the reactivity of the catalyst detecting also its unstable behaviour. The reactivity in fact can change over time and it strongly depends on the specific procedure followed to synthesize the catalyst and on the experimental conditions adopted in the trials. In Section 2.3.1, a check on the repeatability of the experimental results is performed for each data set independently.

Table 2.2. Experimental conditions investigated in all the available experiments. The volumetric flowrate is expressed in STC*. Helium, used as inert carrier, represents the remaining molar fraction.

C1 – wide-channel reactor - 2008					
N° experiments	T [K]	F_{STC}^{IN} [ml/min]	$y_{CH_3OH}^{IN}$	$y_{O_2}^{IN}$	$y_{H_2O}^{IN}$
1-5	725 – 805	26.5	0.0982	0.0436	0.0744
6-9	764 – 826	26.6	0.1483	0.0606	0.1123
10-14	783	26.5	0.1047	0.0269 – 0.0962	0.0793
15-16	783	26.4	0.0684 – 0.1395	0.0445	0.0782
17-20	783	26.5	0.1042	0.0435	0.0184 – 0.2114
C2 – wide-channel reactor - 2013					
N° experiments	T [K]	F_{STC}^{IN} [ml/min]	$y_{CH_3OH}^{IN}$	$y_{O_2}^{IN}$	$y_{H_2O}^{IN}$
1-4	783	13.7 – 58.8	0.0990	0.0441	0.0750
R1 – serpentine reactor – 2015					
N° experiments	T [K]	F_{STC}^{IN} [ml/min]	$y_{CH_3OH}^{IN}$	$y_{O_2}^{IN}$	$y_{H_2O}^{IN}$
1-3	783	29.1 – 73.1	0.0996	0.0414	0.0754
4-7	733 – 826	50.9	0.1468	0.0975	0.2293
8-10	765 – 826	93.9	0.1469	0.0980	0.2296
11-13	800 – 900	54.5	0.2590	0.1064	0.2122
R2 – serpentine reactor – 2015					
N° experiments	T [K]	F_{STC}^{IN} [ml/min]	$y_{CH_3OH}^{IN}$	$y_{O_2}^{IN}$	$y_{H_2O}^{IN}$
1-3	783	29.1 – 73.1	0.0996	0.0414	0.0754
R3 – serpentine reactor – 2015					
N° experiments	T [K]	F_{STC}^{IN} [ml/min]	$y_{CH_3OH}^{IN}$	$y_{O_2}^{IN}$	$y_{H_2O}^{IN}$
1-3	783	29.1 – 73.1	0.0996	0.0414	0.0754
4-8	783 – 933	41.7	0.0997	0.0414	0.0755

STC reference conditions of: temperature $T^ = 273.15$ K; pressure $P^* = 101325$ Pa.

By analysing the sets of experimental conditions reported in Table 2.2, it can be noticed that there is a set of inlet compositions that was tested in all the setups:

- inlet molar fraction of methanol $y_{CH_3OH}^{IN} \cong 0.099$;
- inlet molar fraction of oxygen $y_{O_2}^{IN} \cong 0.041$;
- inlet molar fraction of water $y_{H_2O}^{IN} \cong 0.075$;

Among the experiments carried out at the above inlet composition, all the data sets include trials performed at the temperature $T = 783$ K:

- C1 wide-channel reactor: experiments 11 and 18;
- C2 wide-channel reactor: experiments 1, 2, 3 and 4;

- R1 serpentine reactor: experiments 1, 2 and 3;
- R2 serpentine reactor: experiments 1, 2 and 3;
- R3 serpentine reactor: experiments 1, 2, and 3.

The only factors varying among the experiments listed above are the inlet flowrate F_{STC}^{IN} and the reactor on which the experiments were performed on. The results obtained in these trials are considered in Section 2.3.2 to compare qualitatively the reactivity of the catalysts present in the different setups.

2.3.1 Data quality

Graphs presented in this section will give an overview on all the experimental data collected from the different setups: 1) wide-channel C1; 2) wide-channel C2; 3) serpentine R1; 4) serpentine R2; 5) serpentine R3. The aim of this assessment is to understand if the data collected within the same setup are consistent for performing a model fitting or whether there are some unlikely, strongly inconsistent results. Some data are presented as function of the residence time τ , which is a quantity that cannot be measured directly. τ is evaluated approximately from the arithmetic average between the inlet and the outlet gas velocities v^{IN} and v^{OUT} . The velocity is obtained assuming ideal behaviour for the gas through the following formula:

$$\tau = \frac{L_C}{\frac{v^{IN} + v^{OUT}}{2}} = \frac{2AL_C}{\left(\frac{F_{STC}^{IN}}{P^{IN}} + \frac{F_{STC}^{OUT}}{P^{OUT}}\right) \left(\frac{P^*}{T^*}\right) T} \quad (2.8)$$

Where A is the cross-sectional area of the main channel of the reactor and L_C is the length of the catalyst film. F_{STC}^{IN} and F_{STC}^{OUT} represents the inlet and outlet volumetric flowrates in STC (i.e. $T^* = 273.15$ K; $P^* = 101325$ Pa), P^{IN} and P^{OUT} are the measured pressures at the inlet and outlet of the microreactor respectively, and T is the operating temperature set in the trial. For the specific cases of the wide-channel reactors C1 and C2, P^{OUT} is not reported, but since pressure drops before the retainer can be reasonably assumed negligible for these two setups (see Section 2.2 for further details), it will be assumed that $P^{OUT} = P^{IN}$.

Throughout this analysis it is assumed that: 1) the only variables whose measurements are affected by significant errors are the outlet molar fractions; 2) they are affected by a normally distributed error with zero mean and SDV equals to 1% of the measured value; 3) the input variables defining the

experimental conditions as well as the outlet flowrate F_{STC}^{OUT} and pressures are measurable with negligible uncertainty. Deviation bars will be shown in the graphs for both measured and derived quantities (i.e. conversions and selectivities), whose uncertainty was evaluated calculating the propagation of the errors from the measurements.

2.3.1.1 C1 wide-channel reactor

Table 2.3. Experimental conditions investigated in the trials performed on C1. The volumetric flowrate is expressed in STC*. Helium, used as inert carrier, represents the remaining molar fraction.

C1 – wide-channel - 2008							
N° exp	T [K]	Site	P [Pa]	$F_{STC} \left[\frac{\text{ml}}{\text{min}} \right]$	y_{CH_3OH}	y_{O_2}	y_{H_2O}
1	725	Inlet	159200	26.5	0.0982	0.0436	0.0744
2	744	Inlet	160600	26.5	0.0982	0.0436	0.0744
3	765	Inlet	162000	26.5	0.0982	0.0436	0.0744
4	784	Inlet	163400	26.5	0.0982	0.0436	0.0744
5	805	Inlet	164700	26.5	0.0982	0.0436	0.0744
6	764	Inlet	162000	26.6	0.1483	0.0606	0.1123
7	785	Inlet	163400	26.6	0.1483	0.0606	0.1123
8	804	Inlet	164700	26.6	0.1483	0.0606	0.1123
9	826	Inlet	164700	26.6	0.1483	0.0606	0.1123
10	783	Inlet	163400	26.4	0.1029	0.0269	0.078
11	783	Inlet	163400	26.5	0.1038	0.0443	0.0786
12	783	Inlet	163400	26.5	0.1063	0.0504	0.0805
13	783	Inlet	163400	26.5	0.1042	0.0659	0.079
14	783	Inlet	163400	26.5	0.1064	0.0962	0.0806
15	783	Inlet	163400	25.8	0.1395	0.0462	0.079
16	783	Inlet	163400	27.1	0.0684	0.0428	0.0775
17	783	Inlet	163400	26.4	0.1035	0.0427	0.0184
18	783	Inlet	163400	26.5	0.1038	0.0443	0.0786
19	783	Inlet	163400	26.5	0.1038	0.0443	0.143
20	783	Inlet	163400	26.5	0.1057	0.043	0.2114

STC reference conditions of: temperature $T^ = 273.15$ K; pressure $P^* = 101325$ Pa.

20 experiments were performed on the wide-channel reactor C1. The experimental conditions investigated are illustrated in Table 2.3. From the table, it can be noticed that experiments 11 and 18 were performed at the same experimental conditions. Considering the available data, some graphs have been produced for assessing the repeatability of the results. A first check is performed comparing the results obtained in experiments 1-5 and experiments 10-14:

- experiments 1-5 were performed at the same inlet composition varying the temperature in the range 725 K – 805 K and adopting a molar fraction of oxygen at the inlet equal to 0.0436;

- experiments 10-14 were carried out varying the inlet molar fraction of oxygen in the range 0.0269 – 0.0962 keeping the temperature constant at 783 K. The values of all the other input variables are the same.

Thus, the experimental conditions assessed in these two subsets cross each other in the experimental design subspace identified by the input variables: 1) temperature T ; 2) inlet molar fraction of oxygen $y_{O_2}^{IN}$. Experimental data for methanol conversion and selectivity of formaldehyde, considering experiments 1-5 and experiments 10-14 are presented in Figure 2.1 with respect to temperature T and inlet ratio $y_{CH_3OH}^{IN}/y_{O_2}^{IN}$.

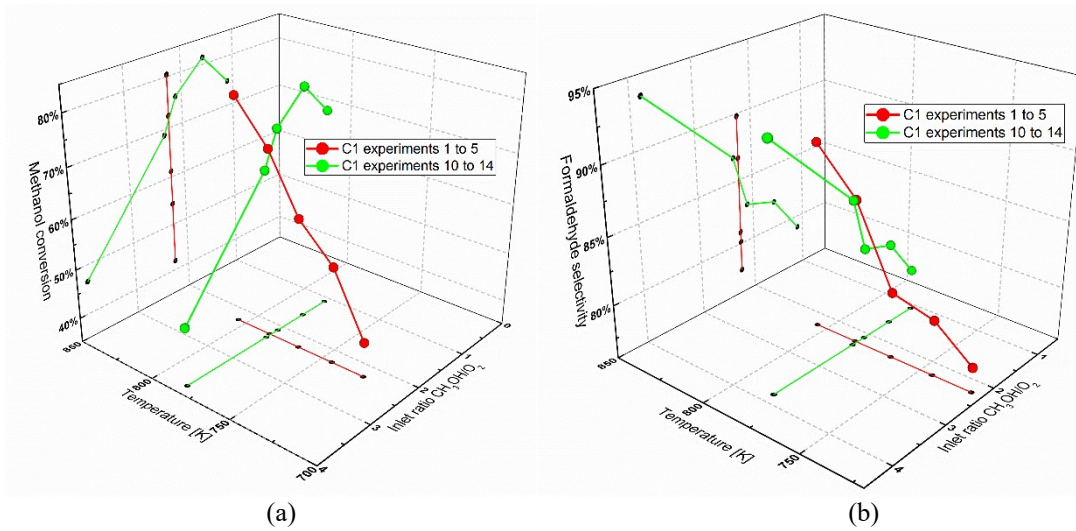


Figure 2.1. Experimental data obtained from experiments 1-5 (red dots) and experiments 10-14 (green dots) carried out on C1: (a) methanol conversion and (b) formaldehyde selectivity are shown with respect to a variation of the operating temperature and the inlet molar ratio $y_{CH_3OH}^{IN}/y_{O_2}^{IN}$.

Both methanol conversion and formaldehyde selectivity are positively influenced by temperature, but they show an opposite trend with respect to the inlet methanol/oxygen ratio. This can be explained by the fact that in presence of rich mixtures, partial methanol oxidation occurs at a much higher rate than formaldehyde decomposition reaction, resulting in a quick consumption of oxygen, which is not sufficient to complete the oxidation. It is possible to appreciate that the experiments shown in Figure 2.1 give consistent results. Since similar outcomes were obtained adopting similar experimental conditions, repeatability is achieved.

A second comparison is proposed between experiments 1-5 and experiments 6-9 in Figure 2.2:

- experiments 1-5 were performed varying the temperature at constant inlet composition with an inlet molar ratio $y_{CH_3OH}^{IN}/y_{O_2}^{IN} = 2.25$ and an inlet fraction of water $y_{H_2O}^{IN} = 0.0744$;

- experiments 6-9 were conducted varying the temperature at constant inlet composition, but adopting an inlet molar ratio $y_{CH_3OH}^{IN}/y_{O_2}^{IN} = 2.44$ and an inlet fraction of water $y_{H_2O}^{IN} = 0.1123$.

The different inlet composition adopted in these two groups of experiments does not allow for a direct comparison of the results, however the trend shown by the experimental results in the two cases is consistent.

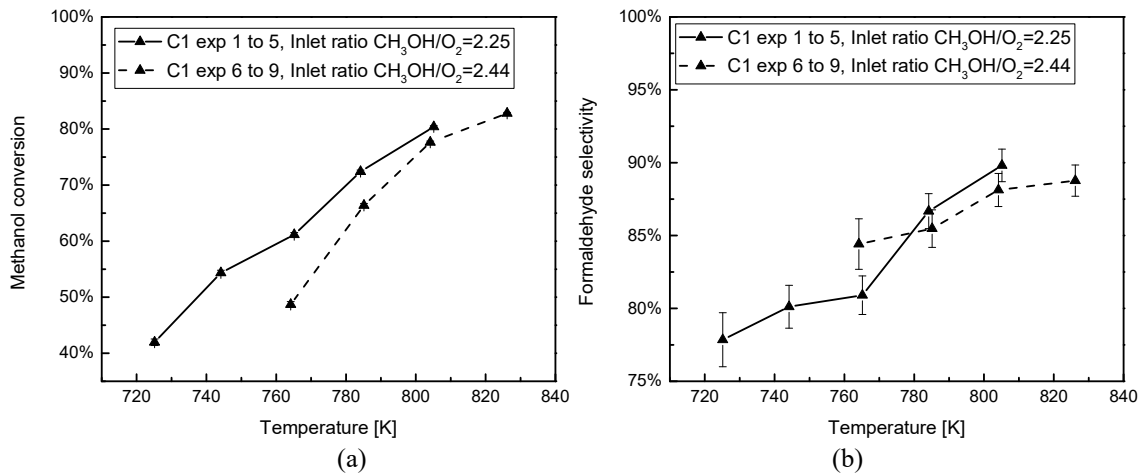


Figure 2.2. Experimental results obtained in experiments 1-5 (solid line) and experiments 6-9 (dashed line) carried out on C1: (a) methanol conversion and (b) formaldehyde selectivity with respect to a variation of the operating temperature.

Experiments 10-14, and 15-16 can be compared because they were carried out at the same operating temperature, keeping the inlet molar fraction of water $y_{H_2O}^{IN}$ always around 0.078 – 0.079 and varying the inlet molar ratio methanol/oxygen, but:

- in experiments 10-14 the ratio $y_{CH_3OH}^{IN}/y_{O_2}^{IN}$ is changed acting on the oxygen, keeping the inlet fraction of methanol constant;
- in experiments 15 and 16 the ratio $y_{CH_3OH}^{IN}/y_{O_2}^{IN}$ is modified acting on methanol at constant inlet fraction of oxygen.

In Figure 2.3 results from experiments 10-14, 15-16 are shown separately. It can be noticed that experiments 13 and 16 were performed at the same inlet molar ratio $y_{CH_3OH}^{IN}/y_{O_2}^{IN}$, but since the inlet compositions adopted in these two experiments are different the results are not directly comparable. The lower conversion achieved in experiment 16 is due to the high inlet fraction $y_{CH_3OH}^{IN}$ adopted (i.e. 0.139) with respect to that tested in experiments 10-14 (around 0.10); thus requiring a longer

residence time to achieve the same level of conversion. However, the consistency of the data is proved by experiment 15, conducted adopting a lower inlet fraction of methanol, which gave results compatible with the trend observed for experiments 10-14.

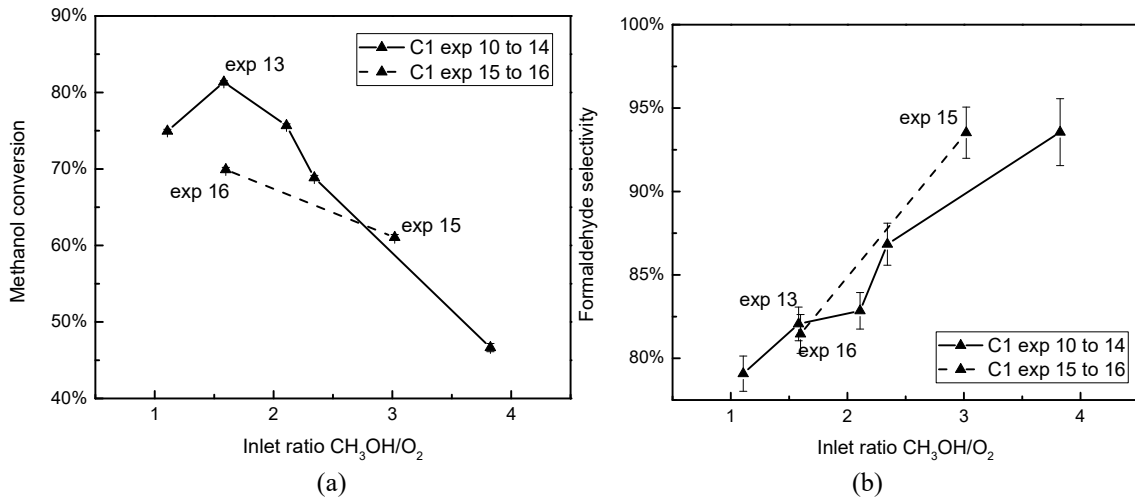


Figure 2.3. Experimental results obtained in experiments 10-14 (connected by the solid line), and experiments 15 and 16 (connected by the dashed line) carried out on C1: (a) methanol conversion and (b) formaldehyde selectivity with respect to a variation of the inlet molar ratio $y_{CH_3OH}^IN/y_{O_2}^IN$.

The last comparison proposed among the trials carried out in C1 is related to experiments 17-20. These experiments were carried at different inlet molar fraction of water $y_{H_2O}^IN$. Since experiment 18 and experiment 11 were carried out at the same conditions, their results can be compared. Experimental results obtained in experiments 17-20, 11 are shown in Figure 2.4. As one can see the conversions of methanol achieved in experiment 11 and experiment 18 are overlapped. The selectivity of formaldehyde is different (87% in experiment 11 and 90% in experiment 18), but the difference can be justified by the propagation of the measurement errors in the evaluation of selectivity, so that the condition of repeatability in these experiments is achieved. The experimental results obtained using the wide-channel reactor C1 have shown both repeatability and consistency, thus these experimental data can be used in the parameter estimation problem.

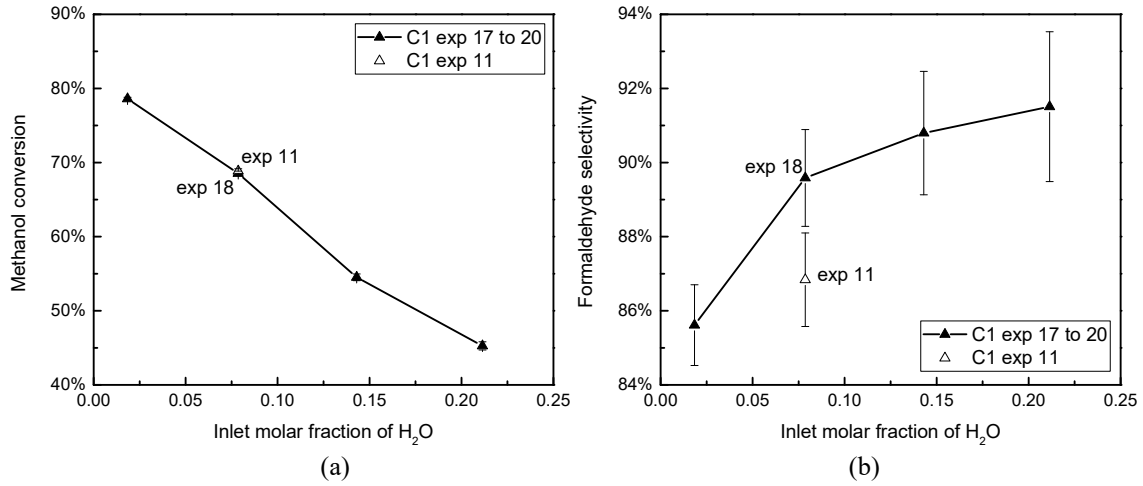


Figure 2.4. Experimental results obtained in experiments 17-20 (connected by the solid line) and experiment 11 (represented by the white triangle) carried out on C1: (a) methanol conversion and (b) formaldehyde selectivity with respect to a variation of the inlet molar fraction of water.

2.3.1.2 C2 wide-channel reactor

Four experiments were carried out in the wide-channel reactor C2. All these experiments were performed at the same temperature and with the same inlet composition. The input variable modified in these experiments is the inlet flowrate (that directly has an impact on the residence time τ). Experimental conditions sampled in C2 setup are presented in Table 2.4. Results obtained for methanol conversion are consistent. The derived values for the selectivities of the products containing carbon are shown in Figure 2.5. Inconsistent results are observed for the selectivity of formaldehyde, which increases with the residence time when it is expected to decrease because of the decomposition reaction (i.e. the complete oxidation of formaldehyde to carbon dioxide, Section 2.1). Also notice that if it is assumed that the only products containing carbon are formaldehyde, carbon dioxide and carbon monoxide (i.e. the detected ones), the sum of their selectivities should be equal to 1¹. Increasing trend for the selectivities of all these products are interpreted as the result of a systematic error affecting the measurements.

¹ From equations (2.6) and (2.7), the sum of the selectivities associated to the products containing carbon is:

$$S_{CH_2O} + S_{CO_2} + S_{CO} = \frac{(y_{CH_2O}^{OUT} + y_{CO_2}^{OUT} + y_{CO}^{OUT})F_{STC}^{OUT}}{y_{CH_3OH}^{IN}F_{STC}^{IN} - y_{CH_3OH}^{OUT}F_{STC}^{OUT}}$$

The fraction in the right hand term represents the ratio between the mols of formaldehyde, carbon dioxide and carbon monoxide generated and the mols of methanol converted in the reactor. Since all the products appearing in the top part of the fraction contain only one atom of carbon, the ratio must be equal to 1.

Table 2.4. Experimental conditions investigated in the trials carried out on C2. The volumetric flowrate is expressed in STC*. Helium, used as inert carrier, represents the remaining molar fraction.

C2 – wide-channel reactor – 2013							
N° exp	T [K]	Site	P [Pa]	F_{STC} [$\frac{ml}{min}$]	y_{CH_3OH}	y_{O_2}	y_{H_2O}
1	783	Inlet	163400	58.8	0.0996	0.0441	0.0754
2	783	Inlet	163400	29.6	0.0990	0.0442	0.0750
3	783	Inlet	163400	20.5	0.0986	0.0442	0.0746
4	783	Inlet	163400	13.7	0.0991	0.0441	0.0750

STC reference conditions of: temperature $T^ = 273.15$ K; pressure $P^* = 101325$ Pa.

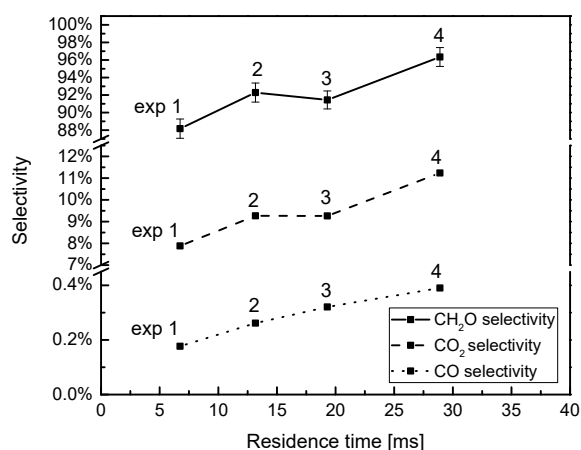


Figure 2.5. Experimental results obtained in the 4 experiments carried out on C2. Measured selectivities of the products at different residence time: formaldehyde (solid line); carbon dioxide (dashed line); carbon monoxide (dotted line).

2.3.1.3 R1 serpentine reactor

R1 is the serpentine reactor with the longest catalyst film length. Experimental conditions investigated in the 13 trials carried out on it are summarised in Table 2.5. Experiments were performed varying the inlet flowrate, temperature and inlet mixture composition. Only experiments 4-10 were executed at the same inlet composition, allowing for a paired check for repeatability. The two subsets involving experiments 1-3 and 11-13 are presented independently to assess the consistency of the data. Experiments 1-3 were carried out at the same temperature and inlet composition, but different residence time. In all these experiments oxygen is completely consumed. The conversion of methanol in these experiments is around 89%. For increasing residence time, the selectivity of formaldehyde decreases, but an inconsistency arises if one looks also at the selectivities measured for carbon dioxide and carbon monoxide shown in Figure 2.6.

Table 2.5. Experimental conditions investigated in the trials carried out on R1. The volumetric flowrate is expressed in STC*. Helium, used as inert carrier, represents the remaining molar fraction.

R1 – serpentine reactor – 2015							
N° exp	T [K]	Site	P [Pa]	F_{STC} [$\frac{ml}{min}$]	y_{CH_3OH}	y_{O_2}	y_{H_2O}
1	783	Inlet	260000	73.1	0.0994	0.0415	0.0753
2	783	Inlet	220000	41.7	0.0997	0.0414	0.0755
3	783	Inlet	200000	29.1	0.0996	0.0414	0.0755
4	733	Inlet	220000	50.9	0.1468	0.0975	0.2293
5	765	Inlet	226000	50.9	0.1468	0.0975	0.2293
6	796	Inlet	235000	50.9	0.1468	0.0975	0.2293
7	826	Inlet	240000	50.9	0.1468	0.0975	0.2293
8	765	Inlet	280000	93.9	0.1469	0.0980	0.2296
9	796	Inlet	286000	93.9	0.1469	0.0980	0.2296
10	826	Inlet	295000	93.9	0.1469	0.0980	0.2296
11	800	Inlet	240000	54.6	0.2590	0.1064	0.2122
12	850	Inlet	245000	54.6	0.2590	0.1064	0.2122
13	900	Inlet	252000	54.6	0.2590	0.1064	0.2122

STC reference conditions of: temperature $T^ = 273.15$ K; pressure $P^* = 101325$ Pa.

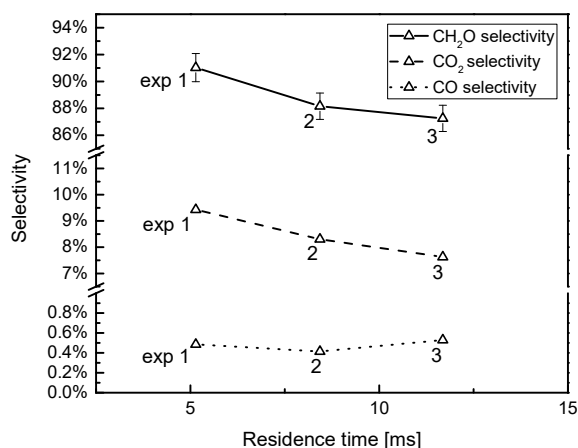


Figure 2.6. Experimental results obtained in experiments 1-3 carried out on R1. Measured selectivities of the products at different residence time: formaldehyde (solid line); carbon dioxide (dashed line); carbon monoxide (dotted line).

All the selectivities decrease from experiment 1 to experiment 2. Both formaldehyde and carbon dioxide selectivities decrease from experiment 2 to experiment 3 while the selectivity for carbon monoxide slightly increases. However, this increment is not sufficient to justify the drop of selectivity on the previous two compounds. This inconsistency, similar to the one highlighted for C2 (Section 2.3.1.2), can be explained by the fact that a less reliable GC was used to measure the outlet composition of the samples in 2013 and 2015 (Section 2.2.1).

Experiments 4-10 were carried out using the same inlet composition, but adopting 2 different values for the flowrate (50.9 ml/min in experiments 4-7 and 93.9 ml/min in experiments 8-10). However, the

same temperature was investigated in experiments 5 and 8, 6 and 9, and 7 and 10 (see Table 2.5). These experiments allow for a meaningful assessment of the impact played by τ , which is the only factor varying between the three couples of experiments. In these trials, whose results are proposed in Figure 2.7, it can be noticed that the outcomes are not particularly affected by the residence time. This is because already with the low residence time adopted in experiments 8-10 the equilibrium is nearly reached and almost all the oxygen is consumed (See Appendix II).

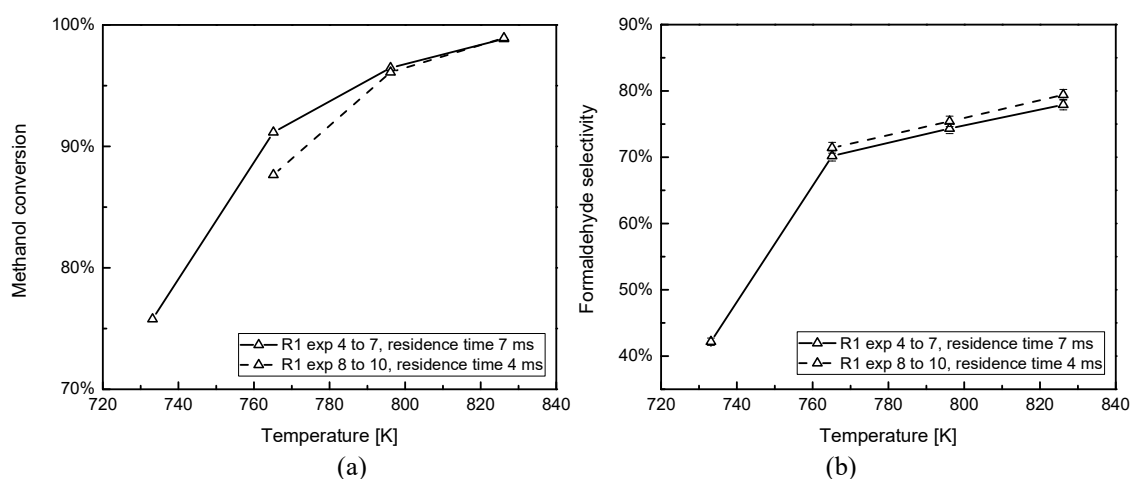


Figure 2.7. Experimental results obtained in experiments 4-7 (connected by the solid line) and experiments 8-10 (connected by the dashed line), carried out on R1: (a) methanol conversion and (b) formaldehyde selectivity at different temperature.

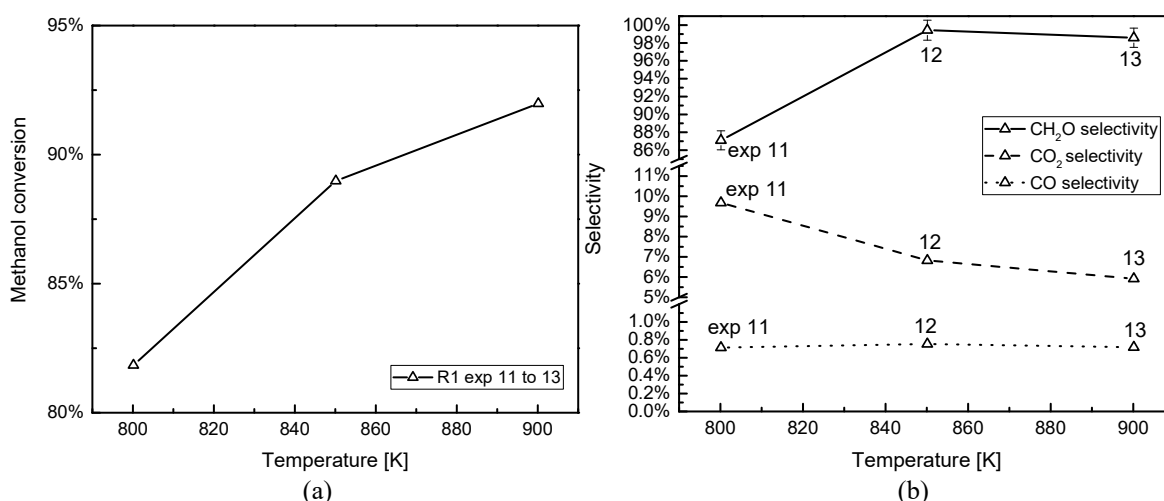


Figure 2.8. Experimental results obtained in the experiments 11-13 carried out on R1. (a) Measured conversion of methanol and (b) measured selectivities of the products at different temperature: formaldehyde (solid line); carbon dioxide (dashed line); carbon monoxide (dotted line).

Also in experiments 10-13 the reaction reaches the equilibrium point. Oxygen conversion is over 99.9% in experiment 10 and a basically complete conversion is observed in experiments 12 and 13 (See Appendix II). Despite of the fact that the composition at the inlet is the same, the conversion of methanol at the outlet, shown in Figure 2.8a, is different, increasing with the temperature. In Figure 2.8b the selectivities for the products containing carbon are shown. There are not particular inconsistencies to highlight in the trends, even though values obtained summing up the selectivities of the products containing carbon (i.e. 0.97, 1.06 and 1.05 in experiments 11, 12 and 13 respectively) show the presence of non-negligible experimental errors.

2.3.1.4 R2 serpentine reactor

In the middle-length serpentine reactor R2 three experiments were carried out at the same temperature and inlet composition varying the residence time acting on the inlet flowrate as one can see in Table 2.6.

Table 2.6. Experimental conditions investigated in the trials carried out on R2. The volumetric flowrate is expressed in STC*. Helium, used as inert carrier, represents the remaining molar fraction.

R2 – serpentine reactor – 2015							
N° exp	T [K]	Site	P [Pa]	F_{STC} [$\frac{ml}{min}$]	y_{CH_3OH}	y_{O_2}	y_{H_2O}
1	783	Inlet	290000	73.1	0.0994	0.0415	0.0753
2	783	Inlet	240000	41.7	0.0997	0.0414	0.0755
3	783	Inlet	220000	29.1	0.0996	0.0414	0.0755

STC reference conditions of: temperature $T^ = 273.15$ K; pressure $P^* = 101325$ Pa.

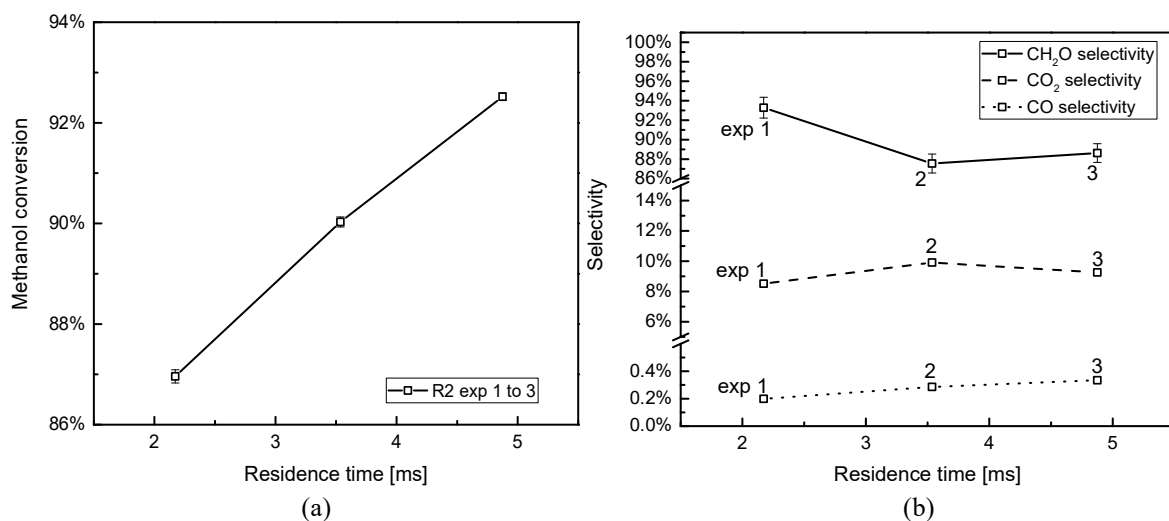


Figure 2.9. Experimental results obtained in the experiments carried out on R2. (a) Measured conversion of methanol and (b) measured selectivities of the products at different residence time: formaldehyde (solid line); carbon dioxide (dashed line); carbon monoxide (dotted line).

Experimental results for methanol conversion and the selectivities for the products containing carbon are shown in Figure 2.9. Selectivity for formaldehyde shows a decreasing but not definite trend for increasing residence time τ , from 93.3% in the first experiment with 2.17 ms residence time to 87.5% in the second experiment with a residence time of 3.53 ms and 88.6% in the third experiment where the residence time is around 4.87 ms. On the other hand, neglecting the low amount of carbon monoxide detected at the outlet, the selectivity of carbon dioxide shows a specular trend to the one shown by formaldehyde, but with different magnitude, going from 8.5% in the first experiment to 9.9% in the second and to 9.2% in the third. These experimental results confirm the presence of systematic errors related to the measurement system.

2.3.1.5 R3 serpentine reactor

As reported in Table 2.7, 8 experiments were performed on R3 adopting the same inlet composition. Experiments 2 and 4 were conducted adopting the same conditions allowing for a repeatability assessment. Experiments performed on this setup have been divided in two groups:

- experiments 1-3 carried out at constant temperature but different residence time;
- experiments 4-8 executed at constant residence time but different temperature.

Methanol conversion and formaldehyde selectivity are plotted in Figure 2.10 for a comparison. It is evident the fact that although experiments 2 and 4 were carried out at the same experimental conditions, their outcomes are completely different. The selectivity of formaldehyde in experiment 2 exceeds 100%, highlighting, also in this data set, the presence of relevant measurement errors.

Table 2.7. Experimental conditions investigated in the trials performed in R3. The volumetric flowrate is expressed in STC*. Helium, used as inert carrier, represents the remaining molar fraction.

R3 – serpentine reactor – 2015							
N° exp	T [K]	Site	P [Pa]	F_{STC} [$\frac{ml}{min}$]	y_{CH_3OH}	y_{O_2}	y_{H_2O}
1	783	Inlet	290000	73.1	0.0994	0.0415	0.0753
2	783	Inlet	240000	41.7	0.0997	0.0414	0.0755
3	783	Inlet	220000	29.1	0.0996	0.0414	0.0755
4	783	Inlet	240000	41.7	0.0997	0.0414	0.0755
5	813	Inlet	250000	41.7	0.0997	0.0414	0.0755
6	843	Inlet	260000	41.7	0.0997	0.0414	0.0755
7	883	Inlet	270000	41.7	0.0997	0.0414	0.0755
8	933	Inlet	280000	41.7	0.0997	0.0414	0.0755

STC reference conditions of: temperature $T^ = 273.15$ K; pressure $P^* = 101325$ Pa.

The lower values of conversion and selectivity obtained in experiments 4-8 with respect to experiments 1-3 could be explained with the deactivation of the catalyst and a consequent increment of the activation energy. In Figure 2.11 selectivities of formaldehyde and carbon dioxide are shown to highlight again the low reliability of the measurement system that produced results violating the carbon balance (see Section 2.3.1.6): the selectivity of carbon dioxide lays in the interval 3.3% and 3.8% while the selectivity of formaldehyde varies in the range between 75% and 90%.

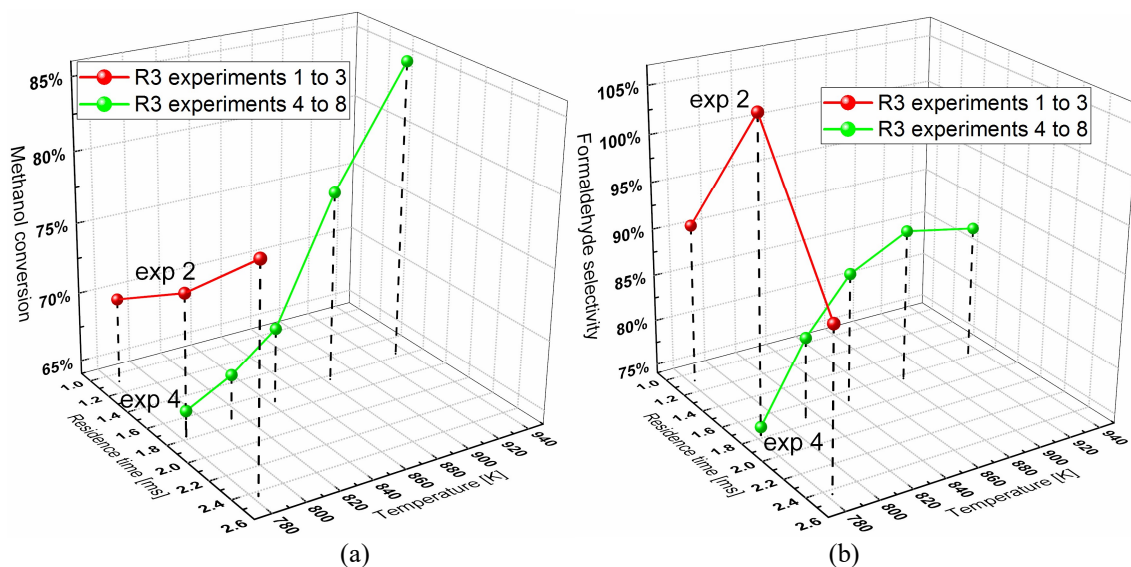


Figure 2.10. Experimental results obtained in experiments 1-3 (red dots) and experiments 4-8 (green dots) carried out in R3: (a) methanol conversion and (b) formaldehyde selectivity with respect to a variation of the operating temperature and the residence time.

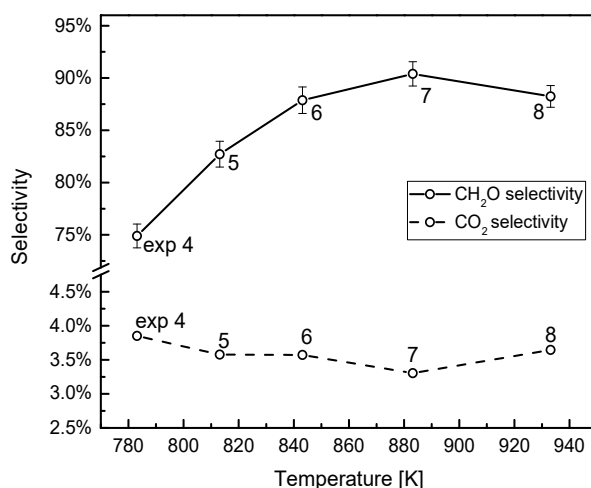


Figure 2.11. Experimental results obtained in the experiments carried out in R3. Measured selectivity of products at different temperature: formaldehyde (solid line); carbon dioxide (dashed line).

2.3.1.6 Carbon balance

In order to summarise the results of the analysis carried out on data consistency and results reliability, a carbon balance evaluation has been performed for all the available experiments. This analysis requires calculating how many atoms of carbon are “generated” or “disappear” during the experiments because of measurement errors. To evaluate the carbon balance CB for a single experiment, the ratio between the atoms of carbon measured at the outlet and the atoms of carbons available at the inlet is considered:

$$CB = \frac{(y_{CH_3OH}^{OUT} + y_{CH_2O}^{OUT} + y_{CO_2}^{OUT} + y_{CO}^{OUT}) F_{STC}^{OUT}}{y_{CH_3OH}^{IN} F_{STC}^{IN}} \quad (2.9)$$

Table 2.8. Carbon balances expressed in terms of percentage for all the available experiments.

C2 – wide-channel reactor – 2008		R1 – serpentine reactor – 2015	
N° exp	CB%	N° exp	CB%
1	99.7	1	100.8
2	100.6	2	97.2*
3	99.6	3	95.9*
4	100.0	4	84.8*
5	100.3	5	99.4
6	99.7	6	97.2*
7	99.5	7	101.2*
8	99.6	8	97.9*
9	99.0	9	99.8
10	100.5	10	101.0
11	100.3	11	98.0*
12	100.1	12	106.2*
13	100.3	13	104.8*
14	99.9	R2 – serpentine reactor – 2015	
15	100.7	N° exp	CB%
16	98.1*	1	101.7*
17	99.5	2	98.0*
18	101.4*	3	98.4*
19	101.0	R3 – serpentine reactor – 2015	
20	99.8	N° exp	CB%
C2 – wide-channel reactor – 2013		1	97.3*
N° exp	CB%	2	96.4*
1	97.0*	3	109.2*
2	101.5*	4	86.0*
3	100.9	5	90.8*
4	107.2*	6	94.1*
		7	95.1*
		8	93.3*

*CB% balance outside 1% range.

The carbon balances calculated for each available experiment are presented in Table 2.8 in terms of percentage. Also an average carbon balance error ACB_{err}^k ($k = C1, C2, R1, R2, R3$), is evaluated for each of the 5 data sets to assess the decreasing reliability of the measurements going from the earliest sets of experiments to the latest ones.

$$ACB_{err}^k = \frac{1}{N_{exp}^k} \sum_{i=1}^{N_{exp}^k} \sqrt{(CB_i - 1)^2} \quad k = C1, C2, R1, R2, R3 \quad (2.10)$$

Where N_{exp}^k represents the number of experiments involved in the k -th data set. The average errors on the carbon balance are presented in Table 2.9.

Table 2.9. Average carbon balance errors, divided by dataset, expressed in terms of percentage.

	C1 - 2008	C2 - 2013	R1 - 2015	R2 - 2015	R3 - 2015
$ACB_{err}\%$	0.54%	3.16%	3.38%	1.80%	7.02%

2.3.2 Assessment of catalyst reactivity

It has already been noticed that different ranges of experimental conditions were investigated in the different setups, however, as it has been already mentioned in the introduction of Section 2.3, there is a set of experimental conditions that has been tested at least in one experiment in every reactor:

- inlet composition $[y_{CH_3OH}^{IN}, y_{O_2}^{IN}, y_{H_2O}^{IN}] \cong [0.099, 0.041, 0.075]$;
- operating temperature $T = 783$ K.

The comparison proposed in this section takes into account only the experiments performed at these experimental conditions, i.e.:

- experiments 11 and 18 in C1;
- experiments 1-4 in C2;
- experiments 1-3 in R1;
- experiments 1-3 in R2;
- experiments 1-3 in R3.

Pressure is taken into account only to evaluate the residence time τ characteristic of each experiments, as explained in the introduction of Section 2.3, but potential different impacts of pressure on the

experimental results are not treated in this comparison. Experiments 11 and 18 performed on C1 were conducted at the same experimental conditions giving very similar results, thus, only experiment 11 is considered for this analysis. Since the measurements collected on C1 (Section 2.3.1.1), have been proved to be very consistent, experiment 11 can be reasonably assumed as good candidate to represent the behaviour of the catalyst present in C1. Concerning the other data sets, also results affected by high measurement errors are included in the graphs presented in this section (see Section 2.3.1). The aim of the graphical assessment proposed here in fact is to capture the general trend of the measurements collected in the different setups to make comparisons and not to highlight inconsistencies.

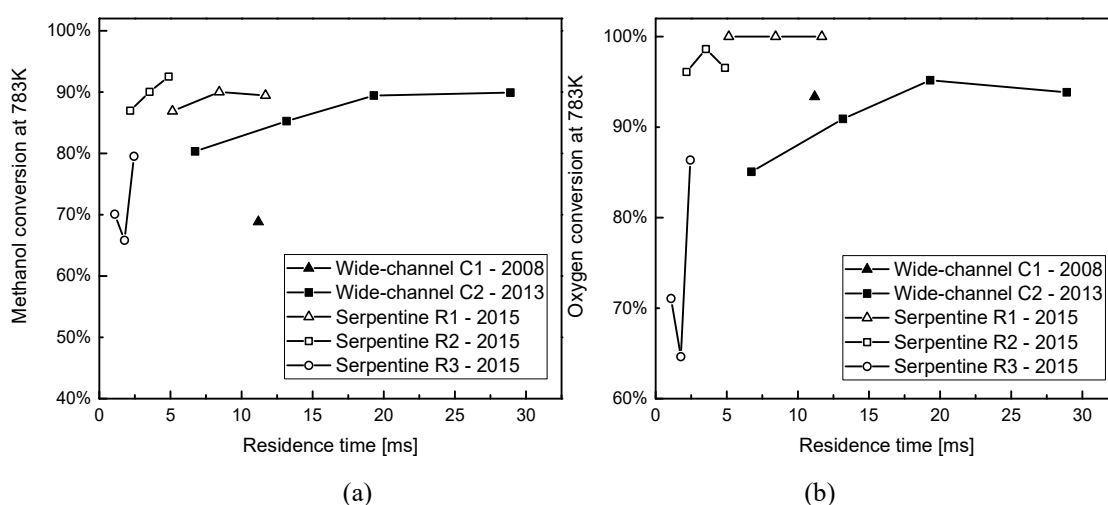


Figure 2.12. Selected experimental data points obtained in C1, C2, R1 R2 and R3: (a) methanol conversion and (b) oxygen conversion. All the experiments shown were performed adopting the same inlet composition and temperature.

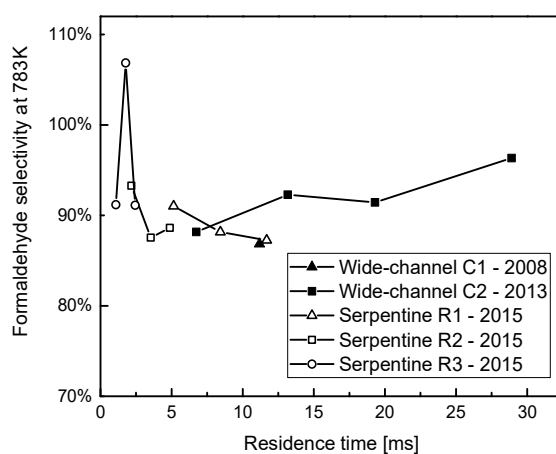


Figure 2.13. Selected experimental data points obtained in C1, C2, R1 R2 and R3: selectivity of formaldehyde. All the experiments shown were performed adopting the same inlet composition and temperature.

Values for the conversion of reactants are shown in Figure 2.12. It can be noticed from the graph that the slowest conversion is achieved in the experiment 11 carried out on C1, but it can be also appreciated the fact that in R1 the conversion of methanol is faster than in C2. Very quick consumption of methanol is achieved in all the serpentine reactors used in 2015. The different velocities of conversion can be explained by a different level of reactivity of the catalysts present in the setups. Also concerning the conversion of oxygen, different results were obtained in the different reactors showing the fact that reactants were consumed at different rates. Very high values for formaldehyde selectivity, reported in Figure 2.13, are achieved in all the considered experiments, regardless of the different residence time and the different setup.

2.4 Summary of results

The results obtained from the analysis carried out through this chapter on the consistency and the differences in the available experimental results brings to assigning the highest reliability to the measurements of the oldest data set collected in 2008. Since the results obtained on the wide-channel reactor C1 have been proved to be both consistent and affected by very low measurement errors (see Table 2.9), it is reasonable to use them for defining a parameter estimation problem aimed at identifying a deterministic phenomenological model.

Concerning the other sets collected in 2013 and 2015, higher errors in the measurement occurred, possibly due to the fact that the outlet composition was measured with a different gas chromatograph with respect to the ones used in 2008 (Section 2.2.1). Furthermore, the analysis of the measurements collected on C3 shows that repeated experiments produced different results, possibly because of the deactivation of the catalyst.

In the next chapters, a candidate model for the partial oxidation of methanol is identified using the richest and most consistent data set available (i.e. the experiments carried out in 2008 on C1). This model is then used as reference for quantifying the reactivity of the catalysts present in the other setups as well as removing the most unlikely or irrelevant experiments from the analysis (i.e. removing both the experiments affected by high measurement errors and the experiments carried out with a deactivated catalyst).

Chapter 3: Identification of a simplified kinetic model

The objective of this Chapter is the identification of a simplified kinetic model for the partial oxidation of methanol over silver catalyst considering only the experiments carried out in 2008 on C1. The main channel of the experimental apparatus is modelled as plug flow reactor. Two kinetic models proposed in literature will be taken into account. Their predicting capability and their limitations will be compared in order to identify the best model for the considered data set. The best model identified will be eventually used as reference to quantify the different reactivity of the catalysts present in the latest reactors used.

3.1 Assumptions

The assumptions adopted for the purpose of model identification are explained in detail in the next sections. The microchannel is assumed to be well described by an ideal plug flow reactor whose equations are reported and explained in Section 3.1.1. In Section 3.1.2 two candidate kinetic models for partial methanol oxidation are presented. The fitting capability of the proposed simplified kinetic models is compared by fitting the experimental data collected on C1 in 2008.

3.1.1 *The plug flow reactor model*

All the microreactors used to collect the experimental data functional to this work can be represented schematically by a single tubular reactor. Since the cross-sectional dimensions of the microchannels are much smaller than the length, it has been decided to neglect the radial coordinates studying the reactors as one-dimensional systems defining only an axial spatial coordinate z . The channel of a

generic single channel microreactor is shown schematically in Figure 3.1. Four well defined stages can be identified in all the reactors considered in this thesis (see also Section 2.2):

- inlet channel from coordinate z_{IN} to z_{MC} ;
- main channel from coordinate z_{MC} to z_R ;
- retainer from coordinate z_R to z_{OC} ;
- outlet channel from coordinate z_{OC} to z_{OUT} .

The coordinate z_C laying in the range between z_{MC} and z_R denotes the beginning of the zone occupied by the catalyst, thus, $z_R - z_C$ represents the length of the catalyst film.

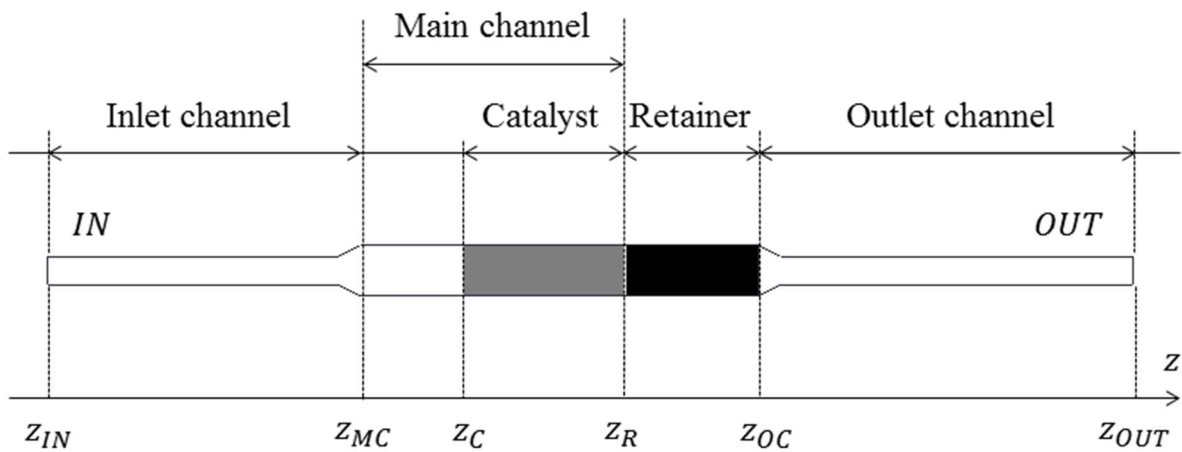


Figure 3.1. General schematic representation of the microchannel. The grey-coloured area represents the catalyst film region; black-coloured area represents the retainer. Drawing is not in scale.

In this work, reactions are assumed to occur only in the stage occupied by the silver catalyst, thus, the identification of the kinetic models presented in the next sections is fulfilled simulating the physical system only from coordinate z_C to coordinate z_R (i.e. only along the stage occupied by the catalyst).

The fluid dynamic behaviour of the microchannel is assumed to be well approximated by a plug flow reactor (PFR), which is used throughout this work for simulating the behaviour of the gas mixture in all the reactors (i.e. C1, C2, R1, R2 and R3), along the catalyst film. The PFR equations involving the mass balances, the reaction kinetics and the pressure profile along the channel are listed below:

$$\frac{\partial C_i(t, z)}{\partial t} = -\frac{\partial \dot{n}_i(t, z)}{\partial z} + \sum_{j=1}^{N_R} \nu_{ij} r_j(t, z) \quad \forall i = 1, \dots, N_C \quad (3.1)$$

$$\dot{n}_{tot}(t, z) = \sum_{i=1}^{N_C} \dot{n}_i(t, z) \quad (3.2)$$

$$r_j(t, z) = k_j \prod_{i=1}^{N_C} C_i(t, z)^{O_{ij}} \quad \forall j = 1, \dots, N_R \quad (3.3)$$

$$C_i(t, z) = \frac{\dot{n}_i(t, z) P(z)}{\dot{n}_{tot}(t, z) R_g T} \quad \forall i = 1, \dots, N_C \quad (3.4)$$

$$P(z) = P(z_C) - \left(\frac{P(z_C) - P(z_R)}{z_R - z_C} \right) z \quad (3.5)$$

Where N_C is the number of components considered in the gaseous mixture and N_R is the number of reactions considered by the specific kinetic model analysed. The variable time is expressed by t and the spatial coordinate is expressed by z . C_i represents the concentration of the i -th component in the mixture expressed in mol/m³, \dot{n}_i is the molar flowrate of the i -th component in the mixture per units of surface expressed in mol/m²s, \dot{n}_{He} is the helium molar flowrate, which is assumed to be constant along the reactor. P represents the pressure, R_g is the ideal gas constant, T is the operating temperature (assumed to be uniform in the micro-reactors analysed). ν_{ij} and O_{ij} are respectively the stoichiometric coefficient and the reaction order of the i -th component in the j -th reaction; r_j is the reaction rate (expressed in mol/m³s) of the j -th reaction whose kinetic constant k_j is described by an Arrhenius-type equation:

$$k_j = A_j e^{-\frac{E_{aj}}{R_g T}} \quad \forall j = 1, \dots, N_R \quad (3.6)$$

The kinetic constant k_j is defined by two kinetic parameters: 1) a pre-exponential factor A_j ; 2) an activation energy E_{aj} .

The PFR is always used in this work to simulate experiments in steady-state conditions, thus all the variables are only space dependent and the time derivatives are assumed to be equal to zero. The models studied in this work involve 7 mass balances for the species: methanol, oxygen, water, formaldehyde, hydrogen, carbon dioxide and helium. Carbon monoxide is never considered. Diffusion phenomena are completely neglected.

The pressure profile along the microchannel is not directly controllable in the experiment. The pressures measured at the inlet and outlet of the reactor depend on the other experimental conditions

set in the trial and on the channel geometry (see Section 2.3). Despite the fact that pressure is a dependent variable, it will be assigned (i.e. treated as independent experimental condition), for the purpose of model identification. Linear pressure drops are assumed between the two extrema of the catalyst film region:

- in the serpentine reactors R1, R2 and R3, being the pressure drops in the main channel non-negligible, the values for pressure $P(z_C)$ and $P(z_R)$ at the beginning and at the end of the catalyst film are evaluated with a correlation explained in Appendix III.
- in the wide-channel reactors C1 and C2, since the major source of pressure losses is the retainer (located downstream with respect to the catalyst film) and the pressure at the outlet is not reported in the data sets, it will be assumed $P(z_R) = P(z_C) = P^{IN}$ where P^{IN} is the pressure measured at the inlet of the reactor.

The set of reaction rates r_j ($j = 1, \dots, N_R$) as well as the stoichiometric coefficients ν_{ij} characterises the kinetic model. Two simplified kinetic models, already proposed in literature [5, 7] are considered throughout this work as candidates for fitting the available experimental data.

3.1.2 Kinetic models

The experimental data collected in 2008 are used to identify a simplified kinetic model based on Arrhenius-type equations. Two models, A and B, proposed in literature are considered for the identification. Their structural identifiability is assessed through a sensitivity analysis and eventually their predictive capability is compared highlighting strengths and weaknesses. The two models take into account the same 6 species (i.e. methanol, oxygen, water, formaldehyde, hydrogen and carbon dioxide), but consider different sets of reactions among the ones presented in Table 3.1:

- Model A: it represents the simplified kinetic model proposed by Andreasen et al. in 2005 [7] which is derived from a micro-kinetic model proposed by the same authors in 2003 [12]. It considers only 2 limiting steps out of the global mechanism: reaction 1 (i.e. the partial oxidation of methanol to formaldehyde) and reaction 2 (i.e. the decomposition of formaldehyde to carbon dioxide);
- Model B: it is a simplified model involving reactions 1, 2 and 3. It is derived from Andreasen's one adding the third reaction for the oxidation of hydrogen to water. This model was proposed by Galvanin et al. in 2015 [5] in a paper considering the same data collected in

2008 analysed in this work. The third reaction, expected to occur only at higher temperatures [15], was included to represent the low amounts of hydrogen measured at the outlet.

Only pre-exponential factors and activation energies are considered as non-measurable parameters requiring estimation (reaction orders O_{ij} are assumed to be known), thus, the identification of Model A requires the estimation of 4 parameters: 2 pre-exponential factors (i.e. A_1 and A_2) and 2 activation energies (i.e. E_{a1} and E_{a2}); the identification of Model B is more complex since 2 additional parameters (i.e. A_3 and E_{a3}) are involved in the estimation problem.

Table 3.1. Reactions involved in the considered kinetic models. Stoichiometries and reaction rates are also given in the table.

ID	Stoichiometry	Rate	Model A	Model B
1	$\text{CH}_3\text{OH} + \frac{1}{4}\text{O}_2 \leftrightarrow \text{CH}_2\text{O} + \frac{1}{2}\text{H}_2 + \frac{1}{2}\text{H}_2\text{O}$	$r_1 = A_1 e^{-\frac{E_{a1}}{RgT}} \frac{C_{\text{CH}_3\text{OH}} C_{\text{O}_2}^{0.25}}{C_{\text{H}_2\text{O}}^{0.5}}$	Included	Included
2	$\text{CH}_2\text{O} + \frac{1}{2}\text{O}_2 \leftrightarrow \text{H}_2 + \text{CO}_2$	$r_2 = A_2 e^{-\frac{E_{a2}}{RgT}} \frac{C_{\text{CH}_2\text{O}} C_{\text{O}_2}^{0.5}}{C_{\text{H}_2}^{0.5}}$	Included	Included
3	$\text{H}_2 + \frac{1}{2}\text{O}_2 \rightarrow \text{H}_2\text{O}$	$r_3 = A_3 e^{-\frac{E_{a3}}{RgT}} C_{\text{H}_2} C_{\text{O}_2}^{0.5}$	Not included	Included

3.2 Model identification

In this section, the experimental data collected in 2008 on C1 are used for the identification of a kinetic model for the partial oxidation of methanol comparing the fitting capabilities of the candidate models presented in Section 3.1.2. The identification and simulation of the kinetic models together with the PFR equations presented in Section 3.1.1 is performed in gPROMS.

Since the reaction orders are assumed to be already known, two non-measurable parameters are involved in each reaction included in the kinetic model (i.e. the pre-exponential factor and the activation energy), thus Model A requires the estimation of 4 parameters (i.e. A_1 , A_2 , E_{a1} and E_{a2}) while Model B requires the estimation of 6 parameters (i.e. A_1 , A_2 , A_3 , E_{a1} , E_{a2} and E_{a3}). In order to reduce the numerical complexity of the problem it is convenient to scale the parameters to a comparable order of magnitude; for this reason, the following form of the kinetic constant is implemented in gPROMS:

$$A_j e^{-\frac{E_{aj}}{R_g T}} = e^{\ln(A_j) - \frac{E_{aj}}{R_g T}} = e^{\theta_{j1} - \frac{\theta_{j2} \cdot 10^4}{R_g T}} \quad (3.7)$$

Parameters θ_{j1} and θ_{j2} ($j = 1, \dots, N_R$) are computed in the PE problem assigning a lower bound equal to zero (i.e. negative computed values for these parameters are not physically acceptable); the pre-exponential factors A_j and the activation energies E_{aj} ($j = 1, \dots, N_R$) are subsequently derived.

The only data fitted in the parameter estimation problem defined in this work are the molar fractions measured at the outlet for methanol, oxygen, water, formaldehyde, hydrogen and carbon dioxide (i.e. $y_{CH_3OH}^{OUT}$, $y_{O_2}^{OUT}$, $y_{H_2O}^{OUT}$, $y_{CH_2O}^{OUT}$, $y_{H_2}^{OUT}$ and $y_{CO_2}^{OUT}$), or a reduced set of outlet fractions selected among them. The outlet flowrate referred to the standard conditions F_{STC}^{OUT} , reported in the data sets, is not considered in any of the parameter estimation problems proposed in this thesis.

All the results shown here have been obtained through a maximum likelihood parameter estimation implemented in gPROMS (see Section 1.2.1.1). The standard deviation associated to the measurement errors is assumed equal to $3 \cdot 10^{-3}$ for all the outlet molar fractions in order to weight evenly the different species in the parameter estimation problems.

3.2.1 Preliminary discrimination

In this subsection, 4 parameter estimation problems are defined and solved to assess and compare the fitting capability of the kinetic models A and B presented in Section 3.1.2. Only experimental data collected in 2008 on C1 are considered. The first and the second parameter estimation problems are defined with the aim of identifying model A, while the third and the fourth are defined with the aim of identifying model B:

- Case A1: The parameter estimation problem is defined fitting with Model A the outlet molar fractions measured in experiments 1-20 (i.e. all the experiments performed on C1) for three species: methanol, oxygen and carbon dioxide;
- Case A2: The parameter estimation problem is defined employing Model A, including in the likelihood function the outlet molar fractions measured in experiments 1-20 for a different set of species: methanol, formaldehyde and carbon dioxide.
- Case B1: The parameter estimation problem is defined fitting with Model B the outlet molar fractions measured in experiments 1-20 (i.e. all the experiments performed on C1) for three species: methanol, oxygen and carbon dioxide (analogously to Case A1);

- Case B2: The parameter estimation problem is defined fitting with Model B the outlet molar fractions of all the species (carbon monoxide excluded) measured in experiments 1-20.

These 4 cases are summarised in Table 3.2. In the following sections the results obtained solving the just defined PE problems are presented and analysed evaluating the goodness of fit and the structural identifiability of the candidate models.

Table 3.2. Definition of the parameter estimation problems analysed: model considered, experiments included, measured species included.

PE problem	Model	Exp.	$y_{CH_3OH}^{OUT}$	$y_{O_2}^{OUT}$	$y_{H_2O}^{OUT}$	$y_{CH_2O}^{OUT}$	$y_{H_2}^{OUT}$	$y_{CO_2}^{OUT}$
Case A1	A	1-20	Included	Included	-	Included	-	-
Case A2	A	1-20	Included	-	-	Included	-	Included
Case B1	B	1-20	Included	Included	-	Included	-	-
Case B2	B	1-20	Included	Included	Included	Included	Included	Included

3.2.1.1 Parameter estimation results

Considering the two-equation Model A, two parameter estimations: 1) Case A1 and 2) Case A2 have been performed adopting two different sets of measured variables:

- Case A1: the first estimate for Model A is obtained fitting only the outlet molar fractions of methanol, oxygen and formaldehyde is reported in Table 3.3;
- Case A2: the second estimate for Model A is computed fitting the outlet molar fractions available for methanol, formaldehyde and carbon dioxide is reported in Table 3.4.

In both cases, the whole set of experiments has been used (i.e. experiments 1-20). As one can see from the tables, the value computed for the activation energy of the second reaction E_{a2} is null in both cases. The corresponding statistics have not been computed because the parameter hit the lower bound zero during the estimation, making the estimate not satisfactory. Despite the fact that the estimated value for this parameter is physically unacceptable, the information content of the experiments has been sufficient to estimate the other parameters with acceptable accuracy in both cases A1 and A2 (i.e. all the non-null parameters in both cases A1 and A2 have passed the t -test).

Table 3.3. Parameter estimates including statistics obtained for Model A in Case A1 fitting the measured outlet molar fractions of methanol, oxygen and formaldehyde.

Parameter	Estimation	t -value* ($t_{ref} = 1.67$)
A_1 [(mol/m ³) ^{0.25} s ⁻¹]	$2.12 \cdot 10^8$	14.55
A_2 [s ⁻¹]	$5.03 \cdot 10^1$	39.08
E_{a1} [J/mol]	$9.01 \cdot 10^4$	10.56
E_{a2} [J/mol]	0.00	–
Lack of Fit Test** ($\chi_{ref}^2 = 75.62$)		
χ_{sample}^2	535.06	

*a t -value lower than the reference indicates that the information given by the experiments may not be sufficient to estimate the parameter precisely

**a χ_{sample}^2 larger than the χ_{ref}^2 tends to indicate a bad fit

Table 3.4. Parameter estimates including statistics obtained for Model A in Case A2 fitting the measured outlet molar fractions of methanol, formaldehyde and carbon dioxide.

Parameter	Estimation	t -value* ($t_{ref} = 1.67$)
A_1 [(mol/m ³) ^{0.25} s ⁻¹]	$7.92 \cdot 10^7$	14.71
A_2 [s ⁻¹]	$1.99 \cdot 10^1$	21.96
E_{a1} [J/mol]	$8.51 \cdot 10^4$	10.61
E_{a2} [J/mol]	0.00	–
Lack of Fit Test** ($\chi_{ref}^2 = 75.62$)		
χ_{sample}^2	124.62	

*a t -value lower than the reference indicates that the information given by the experiments may not be sufficient to estimate the parameter precisely

**a χ_{sample}^2 larger than the χ_{ref}^2 tends to indicate a bad fit

As one can see from the tables, the weighted residuals (quantified by χ_{sample}^2), in A1 are much higher with respect to A2, showing the limitations intrinsically linked to Model A in predicting the molar fraction of oxygen present at the outlet. This weakness has clear consequences in the prediction of the other two species considered (i.e. methanol and formaldehyde), resulting in a very unsatisfactory fitting. Notice that the χ_{sample}^2 obtained in these two cases are directly comparable because the same number of measures has been used in the fitting (i.e. 3 output variables measured in 20 experiments).

Also for the three-equation model: Model B; derived from Model A adding the third reaction of hydrogen oxidation (see Section 3.1.2), two parameter estimates have been computed for Cases B1 and B2:

- Case B1: the first estimate for Model B is obtained fitting only the outlet molar fractions of methanol, oxygen and formaldehyde is reported in Table 3.5;

- Case B2: the second estimate for Model B is evaluated fitting the outlet molar fractions of all the species considered by the model is reported in Table 3.6.

Table 3.5. Parameter estimates including statistics obtained for Model B in Case B1 fitting the measured outlet molar fractions of methanol, oxygen and formaldehyde.

Parameter	Estimation	t -value* ($t_{ref}=1.67$)
A_1 [(mol/m ³) ^{0.25} s ⁻¹]	$1.98 \cdot 10^8$	14.18
A_2 [s ⁻¹]	$1.43 \cdot 10^1$	8.24
A_3 [(mol/m ³) ^{-0.5} s ⁻¹]	$5.07 \cdot 10^2$	13.49
E_{a1} [J/mol]	$8.98 \cdot 10^4$	10.32
E_{a2} [J/mol]	0.00	–
E_{a3} [J/mol]	0.00	–
Lack of Fit Test** ($\chi_{ref}^2 = 74.46$)		
χ_{sample}^2	137.32	

*a t -value lower than the reference indicates that the information given by the experiments may not be sufficient to estimate the parameter precisely

**a χ_{sample}^2 larger than the χ_{ref}^2 tends to indicate a bad fit

Table 3.6. Parameter estimates including statistics obtained for Model B in Case B2 fitting the measured outlet molar fractions of methanol, oxygen, water, formaldehyde, hydrogen and carbon dioxide (i.e. all the species considered by the model).

Parameter	Estimation	t -value* ($t_{ref}=1.67$)
A_1 [(mol/m ³) ^{0.25} s ⁻¹]	$6.79 \cdot 10^7$	16.39
A_2 [s ⁻¹]	$1.07 \cdot 10^1$	16.63
A_3 [(mol/m ³) ^{-0.5} s ⁻¹]	$6.23 \cdot 10^2$	44.28
E_{a1} [J/mol]	$8.33 \cdot 10^4$	11.68
E_{a2} [J/mol]	0.00	–
E_{a3} [J/mol]	0.00	–
Lack of Fit Test** ($\chi_{ref}^2 = 142.14$)		
χ_{sample}^2	284.07	

*a t -value lower than the reference indicates that the information given by the experiments may not be sufficient to estimate the parameter precisely

**a χ_{sample}^2 larger than the χ_{ref}^2 tends to indicate a bad fit

Also in these two cases all the experiments performed on C1 have been taken into account. It can be noticed from the tables that, analogously to the estimates obtained in Cases A1 and A2, the activation energy of both the second and third reactions E_{a2} and E_{a3} have hit the lower bound zero in both Cases B1 and B2 making physically unacceptable also these estimates. The pre-exponential factors A_1 , A_2 , A_3 and the activation energy of the first reaction E_{a1} have all passed the t -test.

Since a different number of measurements has been fitted in Cases B1 and B2, the final values for the weighted residuals are not directly comparable, however, the χ_{sample}^2 is comparable between Cases B1 and A1 because the same measured variables have been fitted. As one can see from both Table 3.3 and Table 3.5, the weighted residuals obtained with Model B are much lower than in Model A, showing the importance of the third reaction for predicting the outlet molar fraction of oxygen.

The residuals obtained in the parameter estimation study presented in this section are further analysed in Section 3.2.1.3 to highlight the strengths and the weaknesses of the two considered models. The unphysical results obtained in all the cases considered here might be a consequence of the fact that the fitted responses are not influenced by a variation of the parameters which have been estimated equal to zero (i.e. E_{a2} in Model A and E_{a2}, E_{a3} in Model B). Further analysis, required to detect structural weaknesses in Model A and Model B, is carried out in Section 3.2.1.2 performing a sensitivity analysis.

3.2.1.2 Sensitivity analysis

In Section 3.2.1.1, the parameter estimates referring to the parameter estimation problems defined in Table 3.2 have been presented and discussed. The estimates obtained in all the cases analysed cannot be considered acceptable, in fact:

- null activation energy E_{a2} for the second reaction (i.e. the reaction describing the decomposition of formaldehyde), has been computed in Cases A1 and A2 fitting the experimental data with Model A;
- null activation energies E_{a2} and E_{a3} for the second and third reaction (i.e. the reactions describing the decomposition of formaldehyde and the oxidation of hydrogen respectively), have been computed in both Case B1 and Case B2 fitting the experimental data with Model B.

The unrealistic computed parameters might be a consequence of the very low sensitivity of the responses with respect to the parameters themselves. In this section, a structural check on Model A and B is proposed. This is executed through a sensitivity analysis evaluating the partial derivatives of the predicted responses \hat{y}_i ($i = 1, \dots, N_m$) with respect to the parameters θ_j ($j = 1, \dots, N_\theta$):

$$\left. \frac{\partial \hat{y}_i}{\partial \theta_j} \right|_{\hat{\theta}} \quad \forall i = 1, \dots, N_m \quad \wedge \quad j = 1, \dots, N_\theta \quad (3.8)$$

The sensitivities are evaluated only for the output variables (i.e. outlet molar fractions) fitted in the specific parameter estimation problem. Notice that the values computed for the sensitivities depend on the experimental conditions as well as on the computed value for the model parameters $\hat{\theta}$.

Two sensitivity analysis are presented in this section:

- the first sensitivity check is performed simulating an experiment with Model A adopting the values computed in Case A2 for its parameters (see Table 3.4);
- the second sensitivity check is performed simulating the same experiment with Model B adopting the values computed in Case B2 for its parameters (see Table 3.6).

The experimental conditions adopted in the sensitivity analysis are:

- inlet pressure $P^{IN} = 160000$ Pa;
- operating temperature $T = 783$ K;
- inlet volumetric flowrate in STC $F_{STC}^{IN} = 26.6$ ml/min;
- inlet composition $[y_{CH_3OH}^{IN}, y_{O_2}^{IN}, y_{H_2O}^{IN}] = [0.0982, 0.0414, 0.0744]$;

The sensitivities of the responses in Model A evaluated for methanol, formaldehyde and carbon dioxide (i.e. the species fitted in Case A2) are shown in Figure 3.2a. It can be appreciated from the bars in the plot that all the responses considered in Model A are influenced by a variation of the model parameters (i.e. sensitivity is never zero). The parameters related to the second reaction (i.e. A_2 and E_{a2}) have a lower influence on the model responses with respect the parameters involved in the first reaction, but anyway, their variation influences the model predictions for the outlet molar fractions, in particular for formaldehyde and carbon dioxide. The sensitivities of the responses in Model B have been calculated for methanol, oxygen, water, formaldehyde, hydrogen and carbon dioxide (i.e. all the species fitted in Case B2). These are shown in Figure 3.2b. It can be noticed that also in this case all the responses considered in Model B are influenced by a variation of the model parameters. The parameters related to the second and third reaction (i.e. A_2 , A_3 , E_{a2} and E_{a3}) influence the prediction of all the outlet molar fractions for the species considered.

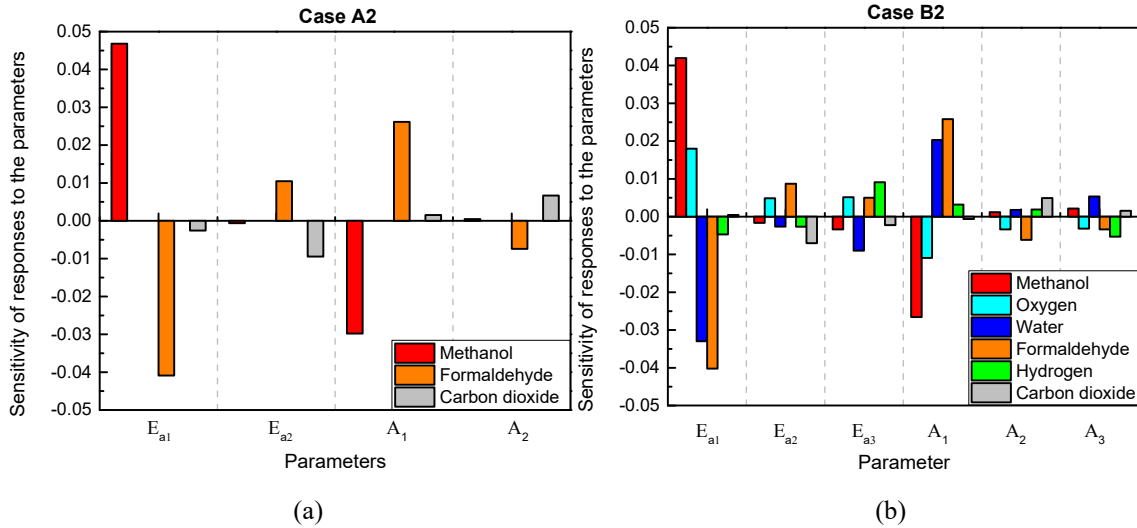


Figure 3.2. Sensitivities of the fitted model responses with respect to the model parameters: (a) Case A2; (b) Case B2.

For both the parameter estimates obtained in Case A2 for Model A and in Case B2 for Model B, the model prediction for the outlet variables involved in the fittings are sensitive to the activation energies of all the reactions included in the models. The physically unacceptable parameter estimates for E_{a2} in Model A, and E_{a2} and E_{a3} in Model B might be a consequence of the attempt of fitting experimental data with structurally inexact models (i.e. models involving a wrong or incomplete set of equations). A structurally inexact model that does not reflect precisely the physical process, might behave in meaningless ways when used to fit experimental data collected in a vast range of experimental conditions.

3.2.1.3 Model comparison on goodness of fit

This section is dedicated to a posterior analysis carried out using the detailed results on the residuals associated to every single measurement in all the cases analysed in Section 3.2.1.1. Parity plots are presented here to assess the quality of fitting achieved in cases A1, A2, B1 and B2. Parity plots are two-dimensional graphs identified by two axes: 1) measured value for the output variables; 2) predicted value of the output variables. In the cases presented here, the outlet molar fractions of the species used to perform the fitting are shown as scattered points in the parity plot in order to assess the goodness of fit observing their dispersion with respect to the diagonal.

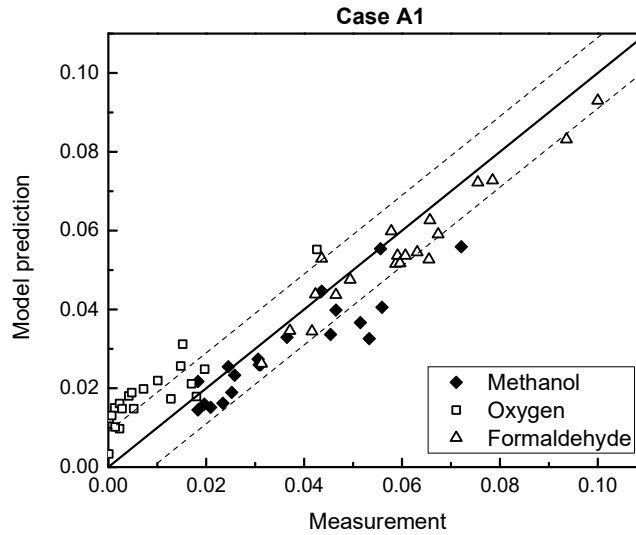


Figure 3.3. Parity plot showing the dispersion of the species included in the parameter estimation problem defined in Case A1: methanol (solid diamonds), oxygen (empty squares), formaldehyde (empty triangles). Dotted lines represent the error range of 3 SDVs ($SDV=3 \cdot 10^{-3}$).

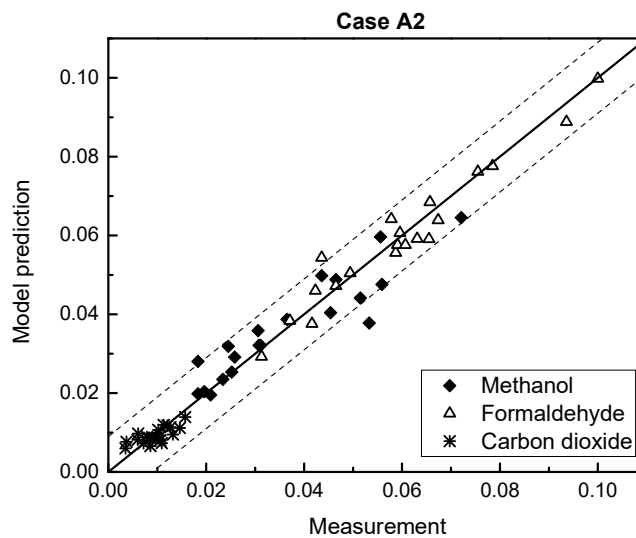


Figure 3.4. Parity plot showing the dispersion of the species included in the parameter estimation problem defined in Case A2: methanol (solid diamonds), formaldehyde (empty triangles) and carbon dioxide (asterisks). Dotted lines represent the error range of 3 SDVs ($SDV=3 \cdot 10^{-3}$).

The outlet molar fractions of methanol, oxygen and formaldehyde have been used to identify the two-equation model (Model A) in Case A1. It has been already pointed out that high residuals have been obtained because the two-equation model is not capable of representing the low amounts of oxygen present at the outlet. The fitting performance obtained in Case A1 is shown in Figure 3.3. It can be noticed that Model A always overestimates the outlet molar fraction of oxygen $y_{O_2}^{OUT}$ affecting also the prediction of the other two species involved in the fitting: 1) methanol and 2) formaldehyde. The conversion of methanol is globally underestimated.

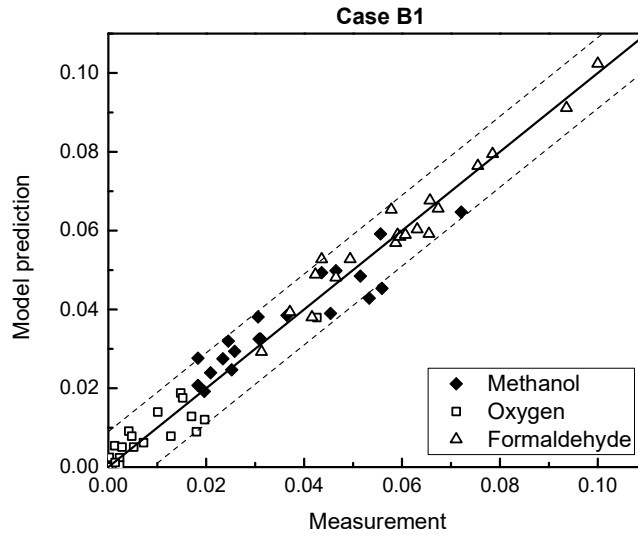


Figure 3.5. Parity plot showing the dispersion of the species included in the parameter estimation problem defined in Case B1: methanol (solid diamonds), oxygen (empty squares), formaldehyde (empty triangles). Dotted lines represent the error range of 3 SDVs ($SDV=3 \cdot 10^{-3}$).

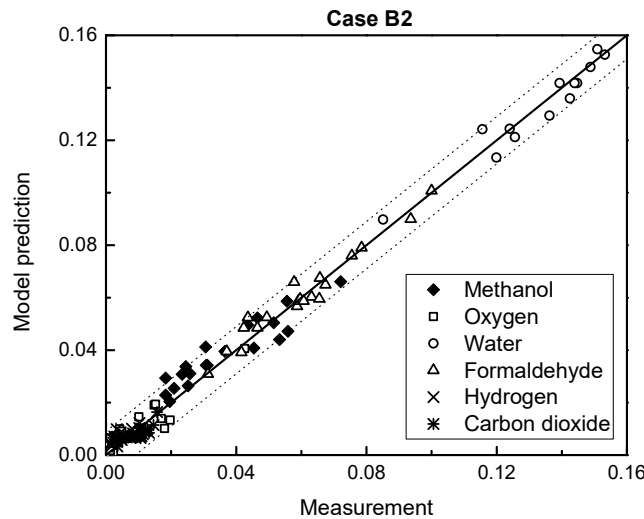


Figure 3.6. Parity plot showing the dispersion of the species included in the parameter estimation problem defined in Case B2: methanol (solid diamonds), oxygen (empty squares), water (empty circles), formaldehyde (empty triangles), hydrogen (crosses), carbon dioxide (asterisks). Dotted lines represent the error range of 3 SDVs ($SDV=3 \cdot 10^{-3}$).

More equilibrated is the dispersion of the residuals obtained in Case A2 in which the outlet molar fraction of carbon dioxide was fitted instead of the fraction of oxygen. In this case, the two-equation model performs well indeed almost all the points lay in the error range defined at 3 SDVs ($SDV=3 \cdot 10^{-3}$). The better fitting is obtained recognising the limit of Model A in describing the oxygen, removing this species from the parameter estimation problem.

Considering the residuals obtained in Case B1 fitting methanol, oxygen and formaldehyde (the same species fitted in Case A1) shown in Figure 3.5, it can be noticed that the prediction of the outlet molar fraction of oxygen improves significantly adding the third reaction. The global prediction achieved by Model B fitting is satisfactory since, as one can see from the figure, almost all the points lay in the error range.

In Case B2, the output molar fractions of all the species considered by the model have been fitted by the three-equation model. The dispersion of the residuals can be observed in Figure 3.6. It can be noticed that Model B is capable of realising limited residuals even when used to fit all the measured species considered by the model itself (i.e. methanol, oxygen, water, formaldehyde, hydrogen and carbon dioxide).

A quantitative comparison of the fitting achieved in the four cases is also proposed here comparing the average weighted residual obtained in each case. The χ_{avg}^2 is evaluated as the sum of the squared weighted residuals obtained, divided by the number of measurements included in the PE problem:

$$\chi_{avg}^2 = \frac{\chi_{sample}^2}{N_{exp}N_m} \quad (3.9)$$

It can be noticed from Table 3.7 that the highest average residuals are obtained in Case A1 in which Model A was used to fit the measured outlet molar fractions of methanol, oxygen and formaldehyde. The lowest average residual is achieved by the same model still fitting methanol and formaldehyde but including the carbon dioxide and removing the oxygen. The result obtained in this analysis still remarks the impossibility of describing the low amounts of oxygen at the outlet with the two-reaction model (i.e. Andreasen's [7]). Considering the average residuals obtained in both Case B1 and Case B2 with Model B, it can be noticed that the χ_{avg}^2 is not much higher than in A2. It should be also pointed out the fact that in B2, twice as many measurements as in A2 have been fitted obtaining comparable average residuals. This is considered as a proof of the better descriptive capability offered by the three-reaction model (i.e. Galvanin's [5]) which is capable of representing satisfactorily all the species involved.

It has been proved that Model B give the most complete description of the reaction mechanism, however, the fact that a null activation energy for both the second and the third reaction have been computed during the parameter estimation (see Section 3.2.1.1), make the identified model still unacceptable.

Table 3.7. Total and average weighted residuals achieved in the analysed cases: A1, A2, B1 and B2.

PE problem	Model	Number of measures fitted	χ^2_{sample}	χ^2_{avg}
Case A1	A	60	535.06	8.91
Case A2	A	60	124.62	2.08
Case B1	B	60	137.32	2.28
Case B2	B	120	284.07	2.36

3.2.2 *Parameter estimation with reduced set of experiments*

In Section 3.2.1 four different parameter estimation problems have been defined and solved comparing two different models: 1) Model A involving a reaction for the partial oxidation of methanol and a reaction for the decomposition of formaldehyde and 2) Model B involving the same reactions considered in Model A adding a third reaction for the oxidation of hydrogen. The three-equation model (Model B) has demonstrated to give a more complete picture of the physical phenomenon achieving low residuals for all the species involved (i.e. methanol, oxygen, water, formaldehyde, hydrogen and carbon dioxide). However, the parameter estimates cannot be accepted because null values for the activation energies of the second and third reactions have been computed by the solver.

Since it has also been demonstrated, through a sensitivity analysis, the fact that Model B is identifiable (see Section 3.2.1.3), the unphysical estimates might be a consequence of the incomplete or wrong structure of the model. The attempt of using a wrong model to fit data in experimental conditions that it is not supposed to describe may results in physically meaningless parameter estimates.

Additional parameter estimation problems have been performed with Model B considering all the measured species, but a reduced number of experiments. The initial guess used for this study was obtained from a first estimation (not presented in this work), computed fitting experiments 6-20. By removing experiments 1-5 from the PE problem, physically acceptable parameter estimates have been obtained (i.e. activation energies higher than zero for all the reactions). This first estimate has been used as starting point for further estimations adding gradually experiments 1-5.

Including experiments 4 and 5 does not affect much the values of the final estimates which are still physically acceptable. However, if just one among experiments 1-3 is added to the parameter estimation problem, at least one of the activation energies drops to zero and, in general, all the activation energies lower significantly (affecting also the pre-exponential factors because of the

parameter correlation). Being the first three experiments performed at low temperature, this result is interpreted as a limitation of Model B in the description of the physical phenomenon in that range of experimental conditions. An additional case (B3) is defined as:

- Case B3: the parameter estimation problem is solved fitting all the species measured in experiments 4-20 (i.e. the most numerous set of experiments fitted giving acceptable estimates) with the three-equation model (Model B).

Table 3.8. Parameter estimates including statistics obtained for Model B in Case B3 fitting the measured outlet molar fractions of all the species considering experiments 4-20.

Parameter	Estimation	<i>t</i> -value* ($t_{ref}=1.67$)
A_1 [(mol/m ³) ^{0.25} s ⁻¹]	$5.33 \cdot 10^{11}$	158.90
A_2 [s ⁻¹]	$1.03 \cdot 10^7$	13.41
A_3 [(mol/m ³) ^{-0.5} s ⁻¹]	$1.07 \cdot 10^4$	36.19
E_{a1} [J/mol]	$1.42 \cdot 10^5$	7.39
E_{a2} [J/mol]	$9.02 \cdot 10^4$	1.88
E_{a3} [J/mol]	$1.83 \cdot 10^4$	0.43*
Lack of Fit Test** ($\chi_{ref}^2 = 119.87$)		
χ_{sample}^2	204.21	

*a *t*-value lower than the reference indicates that the information given by the experiments may not be sufficient to estimate the parameter precisely

**a χ_{sample}^2 larger than the χ_{ref}^2 tends to indicate a bad fit

The physically meaningful parameter estimates obtained in Case B3 are presented in Table 3.8. It can be noticed from the table that fitting a reduced set of experiments, positive acceptable values are obtained for all the parameters. Also notice that these results are very different from the ones obtained in Case B2 (see Table 3.6). The only value that has not passed the *t*-test is E_{a3} (i.e. the activation energy of the hydrogen oxidation reaction). The quality of the fitting achieved in Case B3 is assessed in Section 3.2.2.1.

3.2.2.1 Assessment of fitting

A parity plot is proposed in Figure 3.7 showing the dispersion of the residuals associated to the measurements involved in Case B3 (see Table 3.8). It can be observed that also in this case, despite the completely different values estimated for the parameters with respect to Case B2, a good fitting is achieved for all the species.

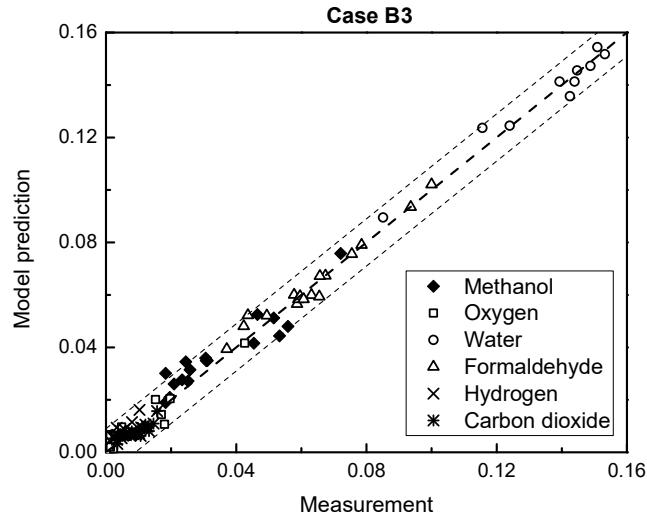


Figure 3.7. Parity plot showing the dispersion of the species included in the parameter estimation problem defined in Case B3. Only measurements and predictions of experiments 4-20 are plotted. Dotted lines represent the error range of 3 SDVs ($SDV=3 \cdot 10^{-3}$).

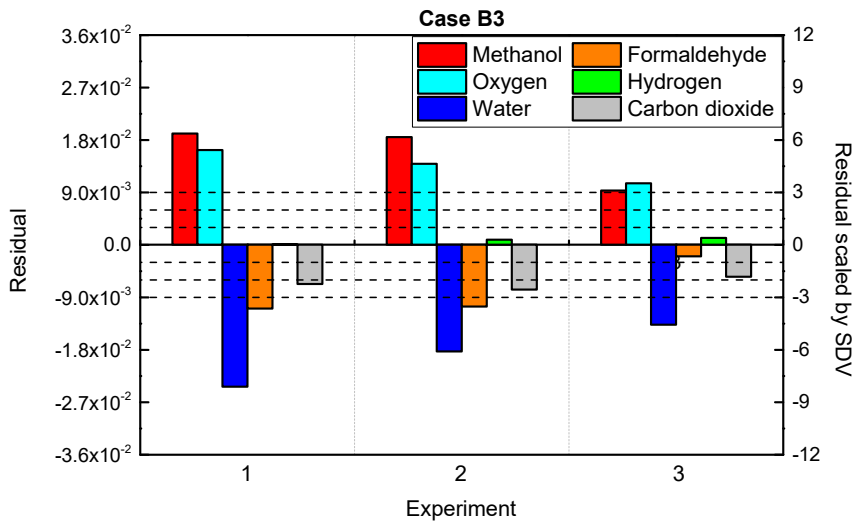


Figure 3.8. Difference between predicted and measured values for the outlet molar fractions associated to experiments 1-3 simulated in validation of Model B identified in Case B3. Right hand axis indicates the ratio between the residual and the $SDV 3 \cdot 10^{-3}$.

In order to show the poor compatibility of the model identified in Case B3 with the measurements collected in experiments 1-3, the computed parameters have been used to simulate these excluded trials calculating the associated absolute residuals. The residuals computed from the simulation of the first three experiments are shown in Figure 3.8. It can be observed that the most critical species causing the unphysical parameter estimates obtained in Case B2 are methanol, oxygen and water, whose associated residuals exceeds the threshold of 3 standard deviations in all the experiments. High residuals are also obtained for formaldehyde in experiments 1 and 2.

The distribution of the residuals shows that Model B, identified in case B3, overestimates the outlet molar fractions of methanol and oxygen at low temperature. It also underestimates the outlet molar fractions of water, formaldehyde and carbon dioxide. Thus, the explanation of the unphysical parameter estimates presented in Section 3.2.1.1 is that parallel reactions of methanol conversion, non-negligible at low temperatures are actually not considered by the candidate models.

3.2.3 Definition of a reference model

The aim here pursued is the selection of a kinetic model out of the ones identified in the previous sections of this Chapter for the catalytic oxidation of methanol to formaldehyde. The model identified with the experimental data collected on C1, will be used as reference for further analysis on the reactivity of the catalysts present in the other setups considered in this work.

Five parameter estimates have been presented in Sections 3.2.1 and 3.2.2 comparing the fitting capabilities of the candidate models (Model A and Model B); identifying their strengths and weaknesses. In Table 3.9 the considered parameter estimation problems are shown including the last case (B3) obtained with a reduced set of experiments.

Table 3.9. Summary of the analysed cases: model used for the fitting, experiments considered and measured species included in the parameter estimation problem.

PE problem	Model	Exp.	$y_{CH_3OH}^{OUT}$	$y_{O_2}^{OUT}$	$y_{H_2O}^{OUT}$	$y_{CH_2O}^{OUT}$	$y_{H_2}^{OUT}$	$y_{CO_2}^{OUT}$
Case A1	A	1-20	Included	Included	-	Included	-	-
Case A2	A	1-20	Included	-	-	Included	-	Included
Case B1	B	1-20	Included	Included	-	Included	-	-
Case B2	B	1-20	Included	Included	Included	Included	Included	Included
Case B3	B	4-20	Included	Included	Included	Included	Included	Included

Table 3.10. Total and average weighted residuals obtained in the analysed cases: A1, A2, B1, B2 and B3.

PE problem	Model	Number of measures fitted	χ_{sample}^2	χ_{avg}^2
Case A1	A	60	535.06	8.91
Case A2	A	60	124.62	2.08
Case B1	B	60	137.32	2.28
Case B2	B	120	284.07	2.36
Case B3	B	102	204.21	2.00

In Table 3.10 the average residuals obtained in all the cases considered are shown together for a comparison. It can be noticed that Model B identified in Case B3 not only is the only one for which physically acceptable estimates have been obtained, but it is also the model realising the lowest average residual χ_{avg}^2 . The average squared residuals obtained are even lower than in cases A1, A2 and B1 in which a much more limited number of measurements has been fitted.

The reference model for the partial oxidation of methanol is therefore defined as the three-reaction model B identified with the reduced set of experiments in Case B3 whose reactions, kinetics and parameters are summarised in Table 3.11.

Table 3.11. Chemical reactions included in the reference kinetic model for the partial oxidation of methanol on silver catalyst: stoichiometries, kinetics and kinetic parameters. Pre-exponential factors are expressed in various units; Activation energies are expressed in J/mol.

ID	Stoichiometry	Rate	Pre-exponential factor	Activation energy
1	$\text{CH}_3\text{OH} + \frac{1}{4}\text{O}_2 \leftrightarrow \text{CH}_2\text{O} + \frac{1}{2}\text{H}_2 + \frac{1}{2}\text{H}_2\text{O}$	$r_1 = A_1 e^{-\frac{E_{a1}}{R_g T}} \frac{C_{\text{CH}_3\text{OH}} C_{\text{O}_2}^{0.25}}{C_{\text{H}_2\text{O}}}$	$5.33 \cdot 10^{11}$	$1.42 \cdot 10^5$
2	$\text{CH}_2\text{O} + \frac{1}{2}\text{O}_2 \leftrightarrow \text{H}_2 + \text{CO}_2$	$r_2 = A_2 e^{-\frac{E_{a2}}{R_g T}} \frac{C_{\text{CH}_2\text{O}} C_{\text{O}_2}^{0.5}}{C_{\text{H}_2}^{0.5}}$	$1.03 \cdot 10^7$	$9.02 \cdot 10^4$
3	$\text{H}_2 + \frac{1}{2}\text{O}_2 \rightarrow \text{H}_2\text{O}$	$r_3 = A_3 e^{-\frac{E_{a3}}{R_g T}} C_{\text{H}_2} C_{\text{O}_2}^{0.5}$	$1.07 \cdot 10^4$	$1.83 \cdot 10^4$

It is convenient to point out the fact that this reference model has been obtained fitting the experimental data collected in experiments 4-20 performed on the wide-channel reactor C1. These experiments have been carried out adopting the following experimental conditions (see also Table 2.3):

- temperatures varying in the range between 764 – 826 K;
- inlet volumetric flowrate in STC always around 26 ml/min;
- inlet molar ratios methanol/oxygen in the range 1.11 – 3.82;
- inlet molar fraction of water laying in the range 0.02 – 0.021.

Since it has been demonstrated that the model is structurally inexact (see Section 3.2.2.1), one should be very careful and critical in extrapolating predictions outside this investigated range of experimental conditions.

3.3 Summary of results

In this chapter, two candidate models proposed on literature have been used for fitting the experimental data collected on the wide-channel microreactor C1 in 2008. Both models describe methanol oxidation as a two-step reaction system:

- the first step involves the conversion of methanol into formaldehyde;
- the second step describes the decomposition of formaldehyde into carbon dioxide.

The second model also includes a third reaction accounting for the oxidation of hydrogen into water. It has been demonstrated the necessity of including the third reaction in the simplified mechanism for achieving good model predictions for all the measured species (i.e. methanol, oxygen, water, formaldehyde, hydrogen and carbon dioxide).

The inexact structure of the two-step mechanism has also been detected. The inclusion of the experiments performed at lowest temperature dramatically affects the parameter estimation leading to the computation of physically unacceptable parameters. The problem has been overcome retaining the three-reaction model (i.e. Model B), recognising its low reliability in the low temperature region of the experimental design space and removing the critical experiments from the parameter estimation. The residuals associated to the removed experiments suggest the presence of parallel reactions of methanol oxidation non-negligible at low temperature.

A reference model has been defined adopting the three-reaction model and the most reliable parameter estimation (see Table 3.11). This model, identified with the experimental data collected on C1 is used as reference for further analysis, presented in Chapter 4, on the reactivity of the catalysts present in the latest setups.

Chapter 4: Catalyst reactivity and information

The assessment of catalyst reactivity carried out in Section 2.3.2 showed that reactor C1 was the one loaded with the less reactive catalyst among the setups considered in this work. The faster conversion of the reactants achieved in setups C2, R1, R2 and R3 may be due to the fact that the catalysts used have been synthesized separately in different batches. They might therefore present a different structure, with a different number of active sites or perhaps a different chemical composition impacting also the turnover frequency (i.e. the number of reactions occurring on an active site per unit of time).

In this Chapter, the reference model defined in Section 3.2.3 for C1 is used to assess the presence of compatible experimental results in the latest data sets collected in 2013 and 2015. This is done applying an MBDM-PE technique (see Section 1.2.3), estimating two new parameters to scale the pre-exponential factors of the first and second reaction (i.e. A_1 and A_2), to quantify the different reactivity of the catalyst present in C2, R1, R2 and R3.

The information obtained on the reactivity of the catalysts is then further analysed to plot the trace of the Fisher information matrix in the experimental design space to assess the role played by the catalyst reactivity on the information content of a trial.

4.1 Quantification of catalyst reactivity

In this section, the model defined in Chapter 3 (see Section 3.2.3) is employed as reference for understanding which of the experimental results obtained in C2, R1, R2 and R3 are compatible with those collected on C1.

The experiments performed are characterised by a faster conversion of the reactants with respect to the experiments executed on C1. The different reactivity of the catalyst is quantified evaluating two new parameters: κ_1 and κ_2 ; to scale the pre-exponential factors of the reactions that are expected to occur on the catalyst surface (i.e. the reaction accounting for the partial oxidation of methanol and the reaction accounting for the decomposition of formaldehyde to carbon dioxide). The set of equations describing the reaction kinetics has been modified as follows:

$$r_1 = \kappa_1 \cdot A_1 e^{-\frac{E_{a1}}{R_g T}} \frac{C_{CH_3OH} C_{O_2}^{0.25}}{C_{H_2O}^{0.5}} \quad (4.10)$$

$$r_2 = \kappa_2 \cdot A_2 e^{-\frac{E_{a2}}{R_g T}} \frac{C_{CH_2O} C_{O_2}^{0.5}}{C_{H_2}^{0.5}} \quad (4.11)$$

$$r_3 = A_3 e^{-\frac{E_{a3}}{R_g T}} C_{H_2} C_{O_2}^{0.5} \quad (4.12)$$

In (4.10-12) the kinetic parameters A_1 , A_2 , A_3 , E_{a1} , E_{a2} and E_{a3} have been fixed to the values estimated for C1 (see Table 3.11), and κ_1 and κ_2 are the parameters requiring estimation (i.e. $\boldsymbol{\theta} = [\kappa_1, \kappa_2]^T$). The pre-exponential factor of a catalytic reaction summarises the number of active sites present on the catalyst surface, thus, the estimation of these parameters will give a picture of the catalyst reactivity with respect to the one of C1. However, it is not reasonable to fit all the available experimental data because of two reasons:

- the measurements collected on C2, R1, R2 and R3 have been proved to be affected by significant systematic errors (see Section 2.3.1);
- repeated experiments executed on R3 have given completely different results (see Section 2.3.1.5), possibly because of the degradation of the catalyst that has resulted in an increment of the activation energy for the catalytic reactions.

The Gaussian filter in the form (1.34), described in Section 1.2.3.1, involving two arrays of binary variables $\boldsymbol{\alpha}$ and $\boldsymbol{\beta}$, is employed in this work for estimating the parameters κ_1 and κ_2 as well as identifying the experimental results that are not compatible with the reference model.

4.1.1 Application of the filter

This section is dedicated to presenting the results obtained from the application of the Gaussian filter (1.34) to the microreactors C2, R1, R2 and R3. The filtering process is performed fitting the experimental data with the reference model identified in Chapter 3 (see Section 3.2.3), to assess which results obtained in the latest setups are compatible with those collected in 2008 on C1 (i.e. the experimental results fitted to identify the reference model). The maximisation of the objective function defined by the Gaussian filter is carried out through the estimation of the following quantities:

- a set of additional continuous parameters (i.e. κ_1 and κ_2), appearing in (4.10-11);
- two sets of binary variables α_i ($i = 1, \dots, N_{exp}$) and β_j ($j = 1, \dots, N_m$) whose value can be either 0 or 1. The binary variables behave like switchers including or excluding respectively experiments and measured species from the parameter estimation problem (see Section 1.2.3.1 for further details).

The other kinetic parameters identifying the reference model (i.e. $A_1, A_2, A_3, E_{a1}, E_{a2}$ and E_{a3}), are considered fixed and equal to the values presented in Table 3.11. The values for σ_{ij} have been assumed equal to $3 \cdot 10^{-3}$ for all the measurements².

The values evaluated for the binary variables α_i ($i = 1, \dots, N_{exp}$) and β_j ($j = 1, \dots, N_m$) will tell respectively which are the experiments and the species the reference model is not able to describe even assuming the presence of a catalyst with a different level of reactivity (quantified by the continuous parameters κ_1 and κ_2 that are estimated together with α and β during the solution of the problem). In particular, a null value computed for the i -th element of vector α (i.e. α_i) may be interpreted in three different ways:

- the reference model is structurally inexact and is not able to explain the results obtained in the i -th experiment (associated to α_i), because the trial has been performed outside the reliability range of the model in the experimental design space;

² The Gaussian filter becomes more selective for increasing SDV (see Section 1.2.3.1). Adopting $\sigma_{ij} = 3 \cdot 10^{-3}$ for all the measurements in (1.32), the residual should be lower than $9.4 \cdot 10^{-3} \cong 3\sigma$ in order to give a positive contribution to the objective function and not be rejected by the filter. Adopting $\sigma_{ij} = 3 \cdot 10^{-3}$ for all the measurements, but considering the filter in the form (1.34), the average residual associated to an experiment should be lower than $9.4 \cdot 10^{-3}$ for the experiment to be retained; the average residual associated to a measured species should be lower than $9.4 \cdot 10^{-3}$ for the species to be accepted.

- it is not sufficient (or correct) to assume the presence of a catalyst with a different level of reactivity to explain the results of the i -th experiment. The incompatible results obtained in the i -th trial might be a consequence of an increment in the activation energy (i.e. the experiment has been performed with a degraded catalyst), which has been fixed during the filtering process;
- the outlet molar fractions measured in the i -th experiment might violate heavily the mass balance because of high, underestimated measurement errors and the conservative model is not able to fit the odd results associated to the experiment.

Table 4.1. Results given by the application of the Gaussian filter for each setup. Excluded experiments and species are presented together with the evaluated parameters κ_1 and κ_2 .

Setup	Experiments excluded	Measurements excluded	κ_1	κ_2
C1 wide-channel (2008)	N/A	N/A	1.00	1.00
C2 wide-channel (2013)	none	none	2.83	1.78
R1 serpentine (2015)	4, 8, 12, 13	none	7.46	5.98
R2 serpentine (2015)	none	none	8.82	4.85
R3 serpentine (2015)	4, 5, 6, 7, 8	water	8.42	3.18

Results obtained from the application of the Gaussian filter to all the sets of data, are presented in Table 4.1. Concerning the result of the analysis performed on C2, neither experiments nor output variables have been excluded. The reference model is capable of representing the behaviour of the catalyst present in the setup simply evaluating two constants to account for the different reactivity. Notice that since the experiments performed on C2 have been carried out investigating the same temperature (i.e. 783 K), it is not possible to detect a different value of the activation energies with respect to the values estimated for the reference model. The values evaluated for parameters κ_1 and κ_2 (i.e. 2.83 and 1.78), quantify the kinetic constants of the first two reactions, at temperature $T = 783$ K, in C2 with respect to C1. It is not possible, however, to understand if the difference is a consequence of a different pre-exponential factor or a different activation energy.

The results obtained after the application of the filter to R2 are analogous. Also for this setup all the experiments and all the measured species have been fitted successfully by the reference model evaluating the two constants κ_1 and κ_2 . Also in the case of R2, the experiments available have all been carried out at the same temperature (i.e. 783 K). It is therefore impossible to understand whether

the different kinetic constants for the first and second reactions at $T = 783$ K are a consequence of a different pre-exponential factor rather than a different activation energy.

In R1, no particular weaknesses in the prediction of specific measured variables have been highlighted. However, as one can see from the table, it is not possible to fit the results obtained in experiments 4, 8, 12 and 13. The temperatures investigated in these four experiments (i.e. 733 K, 765 K, 850 K and 900 K), lay outside or very close to the extrema of the range of temperatures investigated in experiments 4-20 performed on C1 (whose results have been fitted to identify the reference model). Being the reference model structurally inexact (see Section 3.2.2.1), one cannot expect it to give good predictions outside the range of the experimental conditions fitted for its identification. This can explain the exclusion of experiments 4, 8, 12 and 13 carried out in R1.

Regarding the results obtained for R3, experiments 4-8 have been excluded by the solver. The temperatures at which these experiments have been carried out are respectively: 783 K, 813 K, 843 K, 883 K and 933 K; thus, except for experiments 4 and 5, the excluded trials lay outside the reliability range of the reference model. The fact that the results of experiments 4-8 are incompatible with the results of experiments 1-3 performed on R3 had been already highlighted in Section 2.3.1.5. The explanation for the rejection of these experimental results (beside the fact that the reference model is structurally inexact), may be the fact that the filtering has been performed fixing the activation energies. The impossibility of fitting the measurements collected in experiments 4-8 simply acting on the pre-exponential factors A_1 and A_2 is interpreted as an increment of the activation energy associated to the catalytic reactions because of the deactivation of the active sites. It is therefore meaningless to consider these experiments, carried out with a degraded catalyst, for quantifying the reactivity. Also notice the fact that in the experiments accepted by the Gaussian filter the prediction of water has resulted unsatisfactory. It has therefore been excluded for estimating the two parameters κ_1 and κ_2 .

Since it can be reasonably assumed that the first reaction occurs only on the catalyst surface (i.e. the same reaction in the gas phase occurs at a negligible rate), the constant κ_1 quantifies numerically the reactivity of the catalyst present in each setup with respect to the catalyst loaded in C1. It can be noticed from Table 4.1 that the values computed for κ_1 related to the data sets collected in 2015 are very similar. This result was expected since the catalysts loaded in R1, R2 and R3 were synthesised together in the same batch.

Catalysts characterised by κ_1 higher than 1 (i.e. more reactive than the catalyst loaded in C1), have been detected by the filter in C2, R1, R2 and R3:

- the serpentine reactors R1, R2 and R3 employed in 2015 were loaded with a catalyst about 8 times more reactive than the one used in C1;
- in 2013, the wide-channel reactor C2 was loaded with a catalyst almost 3 times as much reactive as the one used in C1.

In the next subsections, the quality of the fitting achieved by the Gaussian filter is assessed for all the data sets presenting also the residuals associated to the measurements removed by the filter. After the application of the filter to each setup, the identified parameters have been used to simulate the trials. The residuals associated to all the data are presented in bar charts separating the measurements accepted by the filter (i.e. the data included and fitted in the PE problem), and the measurements rejected. The residuals associated to the excluded measures are proposed to highlight the good result obtained applying the Gaussian filter in identifying the incompatible experimental data.

4.1.1.1 C2 wide-channel reactor

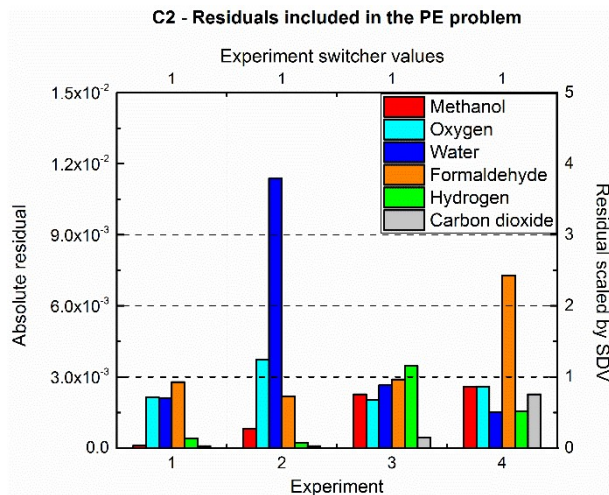


Figure 4.1. Residuals minimised after the application of the Gaussian filter to the experimental results collected on C2 with the reference model. Experiment switchers indicate which experiments have been included in the PE problem (1) and which have been removed (0).

The descriptive capability offered by the reference model for the experiments carried out on C2 has been assessed positively by the filter: neither experiments nor measured species have been removed from the parameter estimation problem. The residuals obtained are presented in Figure 4.1. It can be noticed from the bar chart that the estimation of two distinct parameters (i.e. κ_1 and κ_2), to account for the different catalyst behavior results in a satisfactory fitting. In fact, only four residuals exceed the range of one SDV. The only measurement whose associated residual exceeds the error range of 3

SDVs is the outlet molar fraction of water in experiment 2. However, the global prediction of the species, considering all the experiments, is acceptable.

4.1.1.2 R1 serpentine reactor

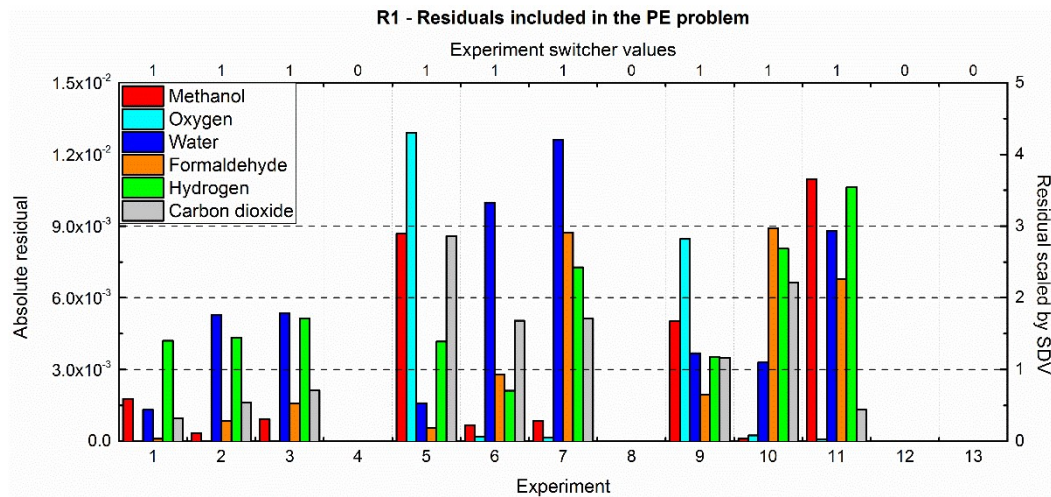


Figure 4.2. Residuals minimised after the application of the Gaussian filter to the experimental results collected on R1 with the reference model. Experiment switchers indicate which experiments have been included in the PE problem (1) and which have been removed (0). Only the residuals associated to measurements fitted in the PE problem are shown.

The application of the Gaussian filter to the experimental results collected on the serpentine reactor R1 has led to the removal of experiments 4, 8, 12 and 13. The residuals associated to the experiments 1-3, 5-7, 9-11 (i.e. the experiments retained by the filter), are presented in Figure 4.2. Considering the accepted experiments, all the species have been fitted. Higher residuals with respect to the cases considered for the wide-channel reactor are obtained. The only critical measurements, whose associated absolute residual exceeds the error range of 3 SDVs are:

- outlet molar fraction of oxygen in experiment 5;
- outlet molar fraction of water in experiment 6;
- outlet molar fraction of water in experiment 7;
- outlet molar fractions of methanol and hydrogen in experiment 11.

Since the filtering is performed at constant activation energies, this might limit the fitting potentially obtainable with the three-reactions model. However, the residuals obtained in the accepted experiments globally lay in the error range of 3 SDVs.

In Figure 4.3 the absolute differences between the model predictions and the measured values for the measurements that have been discarded by the filter are reported. The impossibility of fitting the experimental data collected in experiments 4, 8, 12 and 13 has been detected by the Gaussian filter which has removed them from the parameter estimation problem. The global absolute residuals associated to these experiments far exceeds the error range, making their fitting with the reference model meaningless for the quantification of the catalyst reactivity.

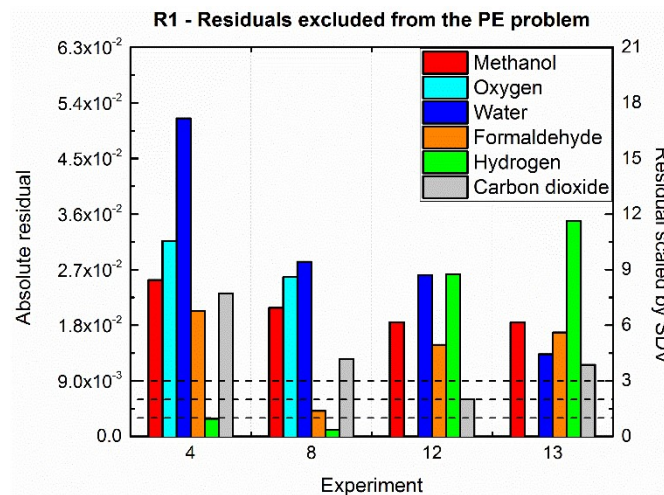


Figure 4.3. Absolute differences between model predictions and measurements employing the model identified applying the Gaussian filter to R1. Only residuals associated to measurements that have been rejected by the filter are shown.

4.1.1.3 R2 serpentine reactor

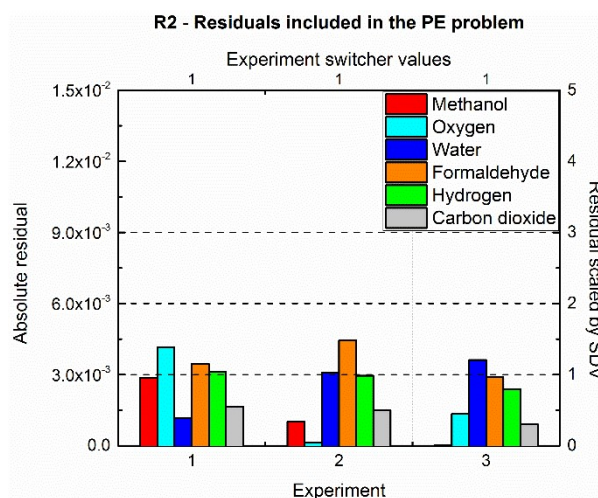


Figure 4.4. Residuals minimised after the application of the Gaussian filter to R2 with the reference model. Experiment switchers indicate which experiments have been included in the PE problem (1) and which have been removed (0).

The application of the Gaussian filter to R2 has not produced the rejection of any measurement. The fitting achieved by the reference model is statistically satisfactory. The residuals for all the output variables and all the experiments are shown in Figure 4.4. The estimation of κ_1 and κ_2 permits the achievement of a good fitting: the residuals associated to all the measured species in all the experiments lay in the range of 2 SDVs.

4.1.1.4 R3 serpentine reactor

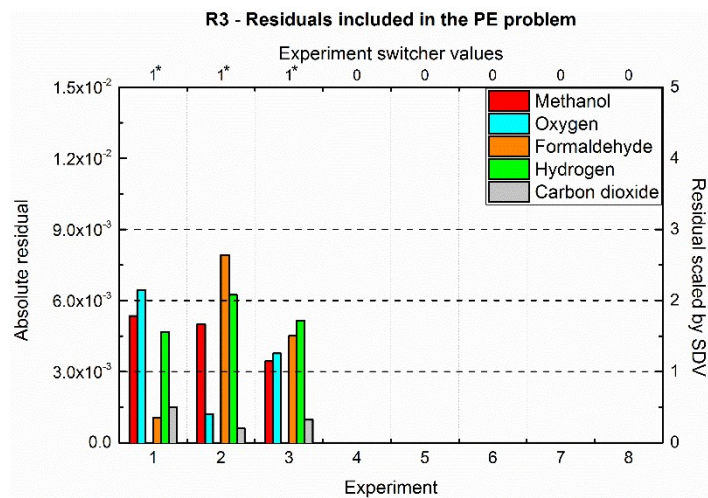


Figure 4.5. Residuals included in the PE problem after the application of the Gaussian filter to R3 with the reference model. Experiment switchers indicate which experiments have been included in the PE problem (1) and which have been removed (0). Experiment switchers marked with an asterisk indicate that water has not been included in the PE. Only the residuals associated to measurements fitted in the PE problem are shown.

The application of the Gaussian filter to the experimental data collected on R3 has resulted in the most severe removal of information. The measured values for methanol, oxygen, formaldehyde, hydrogen and carbon dioxide in experiments 1-3 have been fitted successfully by the reference model. Residuals associated to the fitted measurements are shown in Figure 4.5 where one can see that, despite the fact that water has been rejected by the filter, the model performs well for the other species, but predicting only the outcome of the first 3 experiments. Also in this case, the model identified has been employed to simulate the rejected experiments. The absolute differences between model predictions and measurements are plotted in Figure 4.6, where the residuals associated to the output variables rejected by the filter are reported. The residuals associated to the removed experiments clearly show the impossibility of fitting the experimental data of experiments 4-8 with the reference model evaluating κ_1 and κ_2 .

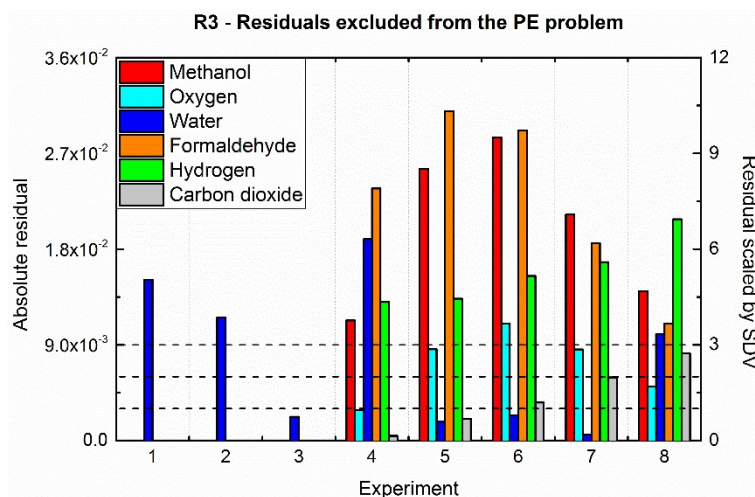


Figure 4.6. Absolute differences between model predictions and measurements adopting the model identified applying the Gaussian filter to R3. Only residuals associated to measurements that have been rejected by the filter are shown.

4.1.2 Summary of results

In Section 4.1.1 a Gaussian filter based on the likelihood function has been employed for the quantification of the reactivity of the catalysts loaded in the microreactors used to collect the latest data sets (i.e. C2, R1, R2 and R3). The numerical evaluation of the catalyst reactivity has been carried out fitting the experimental data of each setup with a reference model (see Section 3.2.3), estimating two parameters κ_1 and κ_2 scaling the pre-exponential factors of the first and second reaction respectively (i.e. the reactions expected to occur on the catalyst surface). The application of the Gaussian filter has facilitated the removal of the experimental results that cannot be explained by the reference model assuming a different number of active sites. The following anomalies have been detected:

- data collected in experiments performed outside the model reliability range in the experimental design space;
- experiments affected by inconsistent results (i.e. outlet molar fractions violating the mass balances), as consequence of high measurement errors;
- experimental data collected using a degraded catalyst (i.e. experimental data that can be explained only with an increment in the activation energy of the catalytic reaction).

The value estimated for parameters κ_1 and κ_2 characteristic of each setup, after the application of the Gaussian filter are summarised in Table 4.2. Notice that the values reported for κ_1 and κ_2 in C1 are both equal to 1 because the reference model is based on the catalyst that was present in that setup. The

final kinetic parameters of the three-reaction kinetic model (i.e. $\kappa_1 A_1$, $\kappa_2 A_2$, A_3 , E_{a1} , E_{a2} and E_{a3}), estimated for each of the considered catalysts, are proposed in Table 4.3.

Table 4.2. Value evaluated for parameters κ_1 and κ_2 in each setup. Also the parameters referring to the catalyst present in C1, assumed as reference, are reported.

Setup	κ_1	κ_2
C1 wide-channel (2008)	1.00	1.00
C2 wide-channel (2013)	2.83	1.78
R1 serpentine (2015)	7.46	5.98
R2 serpentine (2015)	8.82	4.85
R3 serpentine (2015)	8.42	3.18

Table 4.3. Parameters of the three-reaction model evaluated for the catalyst present in each setup.

Model parameter	C1 (2008)	C2 (2013)	R1 (2015)	R2 (2015)	R3 (2015)
$\kappa_1 A_1$ [(mol/m ³) ^{0.25} s ⁻¹]	$5.33 \cdot 10^{11}$	$1.51 \cdot 10^{12}$	$3.98 \cdot 10^{12}$	$4.70 \cdot 10^{12}$	$4.49 \cdot 10^{12}$
$\kappa_2 A_2$ [s ⁻¹]	$1.03 \cdot 10^7$	$1.83 \cdot 10^7$	$6.16 \cdot 10^7$	$5.00 \cdot 10^7$	$3.28 \cdot 10^7$
A_3 [(mol/m ³) ^{-0.5} s ⁻¹]	$1.07 \cdot 10^4$	$1.07 \cdot 10^4$	$1.07 \cdot 10^4$	$1.07 \cdot 10^4$	$1.07 \cdot 10^4$
E_{a1} [J/mol]	$1.42 \cdot 10^5$	$1.42 \cdot 10^5$	$1.42 \cdot 10^5$	$1.42 \cdot 10^5$	$1.42 \cdot 10^5$
E_{a2} [J/mol]	$9.02 \cdot 10^4$	$9.02 \cdot 10^4$	$9.02 \cdot 10^4$	$9.02 \cdot 10^4$	$9.02 \cdot 10^4$
E_{a3} [J/mol]	$1.83 \cdot 10^4$	$1.83 \cdot 10^4$	$1.83 \cdot 10^4$	$1.83 \cdot 10^4$	$1.83 \cdot 10^4$

In Figure 4.7a, the distribution of the species fitted to identify the reference model is proposed in a parity plot to compare experimental data against model predictions. Beside, in Figure 4.7b, the distribution of the species associated to all the measurements fitted for the identification of the five sets of kinetic parameters (i.e. the model parameters referring to C1, C2, R1, R2 and R3), is proposed. The plots are meant to show the quality of fitting achieved with the three-reaction model after the application of the filter in all the data sets considered in this work demonstrating that the contrasting results in the sets of data can be explained with a different catalyst reactivity.

The pre-exponential factor of a reaction occurring on the catalyst surface synthesizes the number of active sites and their global turnover frequency. Since it can be reasonably assumed that the first reaction occurs at a negligible rate in the gas phase (i.e. the reaction takes place only on the catalyst surface), the value estimated for κ_1 quantifies the reactivity of the catalyst present in each setup referred to C1. The assumption is also confirmed by the fact that very similar values have been

computed for κ_1 in R1, R2 and R3. The serpentine reactors, used in 2015, have in fact been loaded with catalysts synthesized in the same batch and are expected to behave similarly.

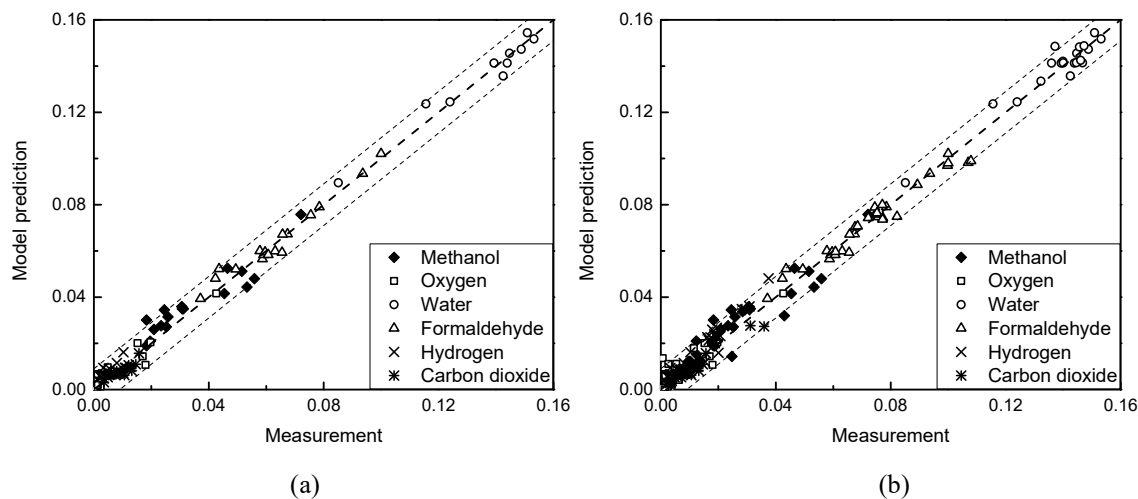


Figure 4.7. Parity plots showing the residuals associated to the measurements fitted with the three-reaction model for the identification of the sets of kinetic parameters in: (a) C1 (i.e. the reference model); (b) C1 and C2, R1, R2 and R3 after the application of the MBDM-PE technique. Only measurements included in the parameter estimation problems are shown.

4.2 Reactivity and information

The analysis presented in Section 4.1 has demonstrated the fact that catalysts with different levels of reactivity have been used in 2008 (performing the experiments using the wide-channel reactor C1), in 2013 (carrying out the trials on the wide-channel reactor C2), and in 2015 (when the serpentine reactors R1, R2 and R3 have been employed for the investigation).

The numerical quantification of the catalyst present in each reactor has been summarised in five sets of kinetic parameters for the three-reaction model, presented in Table 4.3. In this section, the models identified are employed for further analysis to assess how the different reactivity of the catalyst impacts the information content of the experiment. The investigation presented here is carried out evaluating the trace of the Fisher information matrix $\text{Tr}(\mathbf{H})$ (see Section 1.2.2.1 for further details), in a convenient subspace of the experimental design space for each of the five sets of kinetic parameters identified.

The experimental design space is limited to 4 dimensions represented by the following variables:

- operating temperature T ;
- residence time τ , defined using the inlet volumetric flowrate in standard conditions F_{STC}^{IN} ;
- inlet molar ratio methanol/oxygen $y_{CH_3OH}^{IN}/y_{O_2}^{IN}$;
- inlet molar fraction of water $y_{H_2O}^{IN}$.

The remaining input variables considered by the model have been fixed for the purpose of the analysis presented here:

- geometry of the reactor;
- operating pressure $P=160000$ Pa (pressure drops are not considered);
- inlet molar fraction of oxygen $y_{O_2}^{IN}=0.044$.

Notice that once it has been decided and fixed, the choice of the geometry (i.e. the length of the catalyst film and the cross-sectional area of the reactor), does not affect the result of the analysis since a variation of the residence time can be interpreted as a variation either in the geometry or in the flowrate:

$$\tau = \frac{L_c A}{F_{STC}^{IN}} \quad (4.13)$$

The residence time τ is a function of the catalyst film length L_c , the cross-sectional area A and the flowrate F_{STC}^{IN} , thus its variation can be interpreted as a variation of any of these quantities. Since all the possible experimental conditions cannot be represented graphically in only two dimensions it has been chosen to limit the analysis of the information to 6 cases presented in Table 4.4. In each case, the trace of the information matrix is evaluated in a 2-dimensional subspace of the 4-dimensional experimental design space, varying only 2 inputs in a range of possible experimental conditions, but fixing the remaining 2 variables:

- Case 1: Evaluation of the information at fixed inlet composition varying the operating temperature T and the residence time τ ;
- Case 2: Evaluation of the information at fixed residence time τ and fixed inlet molar fraction of water $y_{H_2O}^{IN}$ varying the operating temperature T and the inlet molar ratio methanol/oxygen $y_{CH_3OH}^{IN}/y_{O_2}^{IN}$;

- Case 3: Evaluation of the information at fixed residence time τ and fixed inlet molar ratio methanol/oxygen $y_{CH_3OH}^{IN}/y_{O_2}^{IN}$ varying the operating temperature T and the inlet molar fraction of water $y_{H_2O}^{IN}$;
- Case 4: Evaluation of the information at fixed temperature T and fixed inlet molar fraction of water $y_{H_2O}^{IN}$ varying the residence time τ and the inlet molar ratio methanol/oxygen $y_{CH_3OH}^{IN}/y_{O_2}^{IN}$;
- Case 5: Evaluation of the information at fixed temperature T and inlet molar ratio methanol/oxygen $y_{CH_3OH}^{IN}/y_{O_2}^{IN}$ varying the residence time τ and the inlet molar fraction of water $y_{H_2O}^{IN}$;
- Case 6: Evaluation of the information at fixed temperature T and residence time τ varying the inlet molar ratio methanol/oxygen $y_{CH_3OH}^{IN}/y_{O_2}^{IN}$ and the inlet molar fraction of water $y_{H_2O}^{IN}$;

Table 4.4. Values and range of variation assumed for the input variables in the 6 cases considered for the analysis of the information.

Case ID	T [K]	τ [ms]	$y_{CH_3OH}^{IN}/y_{O_2}^{IN}$	$y_{H_2O}^{IN}$
Case 1	764 – 834	1.5 – 12	2.25	0.074
Case 2	764 – 834	4.5	1.1 – 2.9	0.074
Case 3	764 – 834	4.5	2.25	0.02 – 0.20
Case 4	783	1.5 – 12	1.1 – 2.9	0.074
Case 5	783	1.5 – 12	2.25	0.02 – 0.20
Case 6	783	4.5	1.1 – 2.9	0.02 – 0.20

The trace of the Fisher information matrix $\text{Tr}(\mathbf{H})$ has been evaluated from equation (1.31) in the 6 cases for each of the five sets of kinetic parameters identified, assuming σ_{ij} equal to $3 \cdot 10^{-3}$ for all the measured output variables considered (i.e. $y_{CH_3OH}^{OUT}$, $y_{O_2}^{OUT}$, $y_{H_2O}^{OUT}$, $y_{CH_2O}^{OUT}$, $y_{H_2}^{OUT}$, $y_{CO_2}^{OUT}$).

The reactivity of the catalysts present in the different microreactors is quantified by κ_1 whose value, characteristic of each setup, is presented in Table 4.2. As one can see from the table, C1 was the reactor loaded with the less reactive catalyst, while R2 was the reactor loaded with the most reactive one. In order to emphasise the effect played by the reactivity on the information carried by an experiment, in the next subsections it is chosen to consider only these two setups adopting the following notation:

- CLR: denotes a C1-type catalyst with low reactivity;
- CHR: denotes a R2-type catalyst with high reactivity.

4.2.1 Case 1: Temperature vs. Residence time

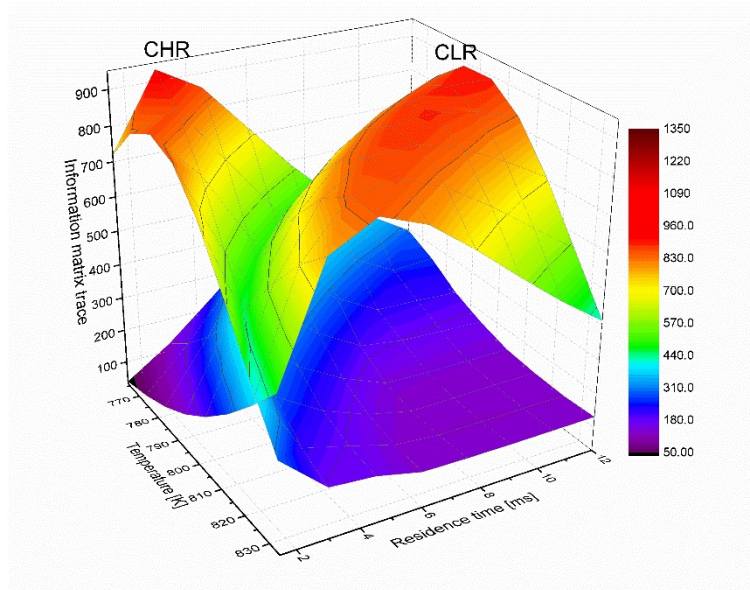


Figure 4.8. Information matrix trace distribution in the 2-dimensional experimental design subspace identified by the operating temperature T and residence time τ (Case 1), referring to the sets of kinetic parameters identified for a CLR and a CHR.

The effect of a variation in both temperature T and residence time τ on the information carried by an experiment is presented in Figure 4.8. The maximum value of information obtained in the considered subset of experimental conditions is similar, but it is interesting to notice that the peaks are located in completely different positions of the design space. It is therefore an aspect of key importance to consider the reactivity of the catalyst for the proper choice of the experimental conditions so as to extract valuable information from a trial. A CLR should be studied allowing more time for the reaction and adopting higher operating temperatures with respect to the study of a CHR. Furthermore, performing experiments over a CHR adopting the optimal conditions identified for a CLR (and vice versa) reduces dramatically the value of the information obtainable. The fact that the surfaces cross in the experimental design space show the presence of an indifference curve in which one should consider to start the investigation when no previous knowledge on the level of reactivity is available. This is a region of robust design where a certain minimum level of information can be obtained, whichever is the reactivity (see Section 4.3 for further details).

4.2.2 Case 2: Temperature vs. Inlet molar ratio methanol/oxygen

The effect of a variation in both temperature T and the inlet methanol/oxygen molar ratio $y_{CH_3OH}^{IN}/y_{O_2}^{IN}$ on the Fisher information is shown in Figure 4.9. Still in this case, the analysis highlights the importance of choosing the range of operating temperatures for the experiments taking into account the reactivity of the catalyst. For a certain residence time, higher temperature should be adopted in CLR with respect to CHR. The choice of the inlet molar ratio between methanol and oxygen should always tend to rich mixtures, regardless of the reactivity.

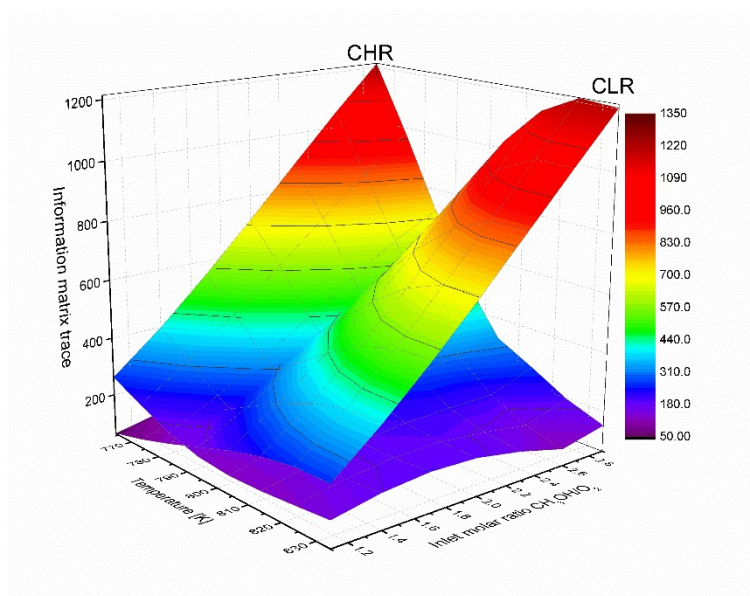


Figure 4.9. Information matrix trace distribution in the 2-dimensional experimental design subspace identified by the operating temperature T and inlet molar ratio methanol oxygen $y_{CH_3OH}^{IN}/y_{O_2}^{IN}$ (Case 2), referring to the sets of kinetic parameters identified for a CLR and a CHR.

4.2.3 Case 3: Temperature vs. Inlet molar fraction of water

The effect of a variation in both temperature T and the inlet molar fraction of water $y_{H_2O}^{IN}$ on the information content of an experiment is presented in Figure 4.10. Still the trend of the information shows that for a fixed residence time the optimal temperature is higher for CLR with respect to CHR. The effect played on the information by the inlet molar fraction of water is not uniform in the design space, in fact:

- if the experiment is carried out using a CLR at low temperature, increasing the inlet molar fraction of water produces a decrement of the information;

- if the experiment is carried out still using a CLR, but adopting high temperature, the information reaches a maximum for a specific inlet molar fraction of water;
- if the experiment is executed using a CHR, increasing the inlet molar fraction of water has a good impact on the information, regardless of the temperature adopted.

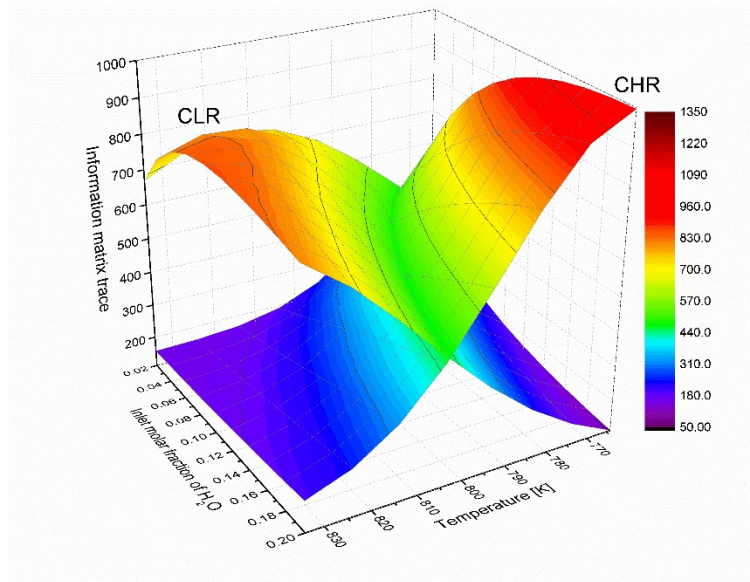


Figure 4.10. Information matrix trace distribution in the 2-dimensional experimental design subspace identified by the operating temperature T and inlet molar fraction of water $y_{H_2O}^N$ (Case 3), referring to the sets of kinetic parameters identified for a CLR and a CHR.

These effects can be explained by the fact that the first reaction (representing the partial oxidation of methanol), providing the reagents for the following two reactions, is inhibited by water. It is therefore possible to change the global velocity of the reaction varying the inlet molar fraction of water. Since the Fisher information is a function of sensitivities (see Section 1.2.2.1 for further details), and sensitivities are function of the experimental conditions, it is possible to state that:

- if a specific set of experimental conditions (for a specific catalyst), makes the reactions too slow for reaching the stage of highest sensitivity (e.g. CLRs studied at low temperature), decreasing the amount of water at the inlet has a positive effect on the information, increasing the rates;
- on the other hand, if the set of experimental conditions makes the reactions too fast (e.g. CHRs studied at high temperature), reaching the quasi-equilibrium stage before the outlet, increasing properly the amount of water can have a good impact on the information, reducing the rates.

4.2.4 Case 4: Residence time vs. Inlet molar ratio methanol/oxygen

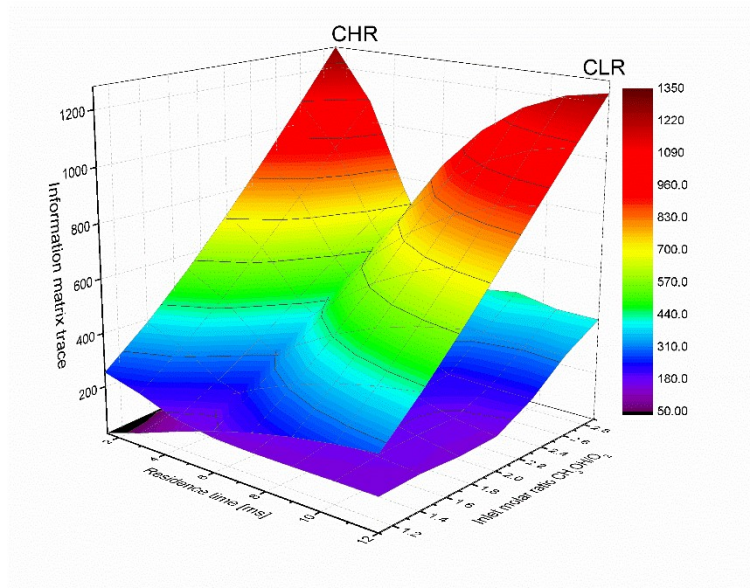


Figure 4.11. Information matrix trace distribution in the 2-dimensional experimental design subspace identified by the residence time τ and inlet molar ratio methanol/oxygen $y_{CH_3OH}^{IN}/y_{O_2}^{IN}$ (Case 4), referring to the sets of kinetic parameters identified for a CLR and a CHR.

The effect of a variation in both residence time τ and the inlet methanol/oxygen molar ratio $y_{CH_3OH}^{IN}/y_{O_2}^{IN}$ on the information is shown in Figure 4.11. The trend of the distributions of information reminds the one obtained in Case 2 (see Section 4.2.2), in which the effect of a variation in both temperature and inlet methanol/oxygen ratio was considered. Still the analysis suggests the use of rich mixtures with high inlet molar ratios methanol/oxygen to increase the obtainable information regardless of the catalyst reactivity. In this case, temperature is fixed, but varying residence time produces similar trends. Short residence time should be chosen in the case of CHRs, while higher residence time should be adopted for CLR.

4.2.5 Case 5: Residence time vs. Inlet molar fraction of water

The effect of a variation in both residence time τ and the inlet molar fraction of water $y_{H_2O}^{IN}$ on the information carried by an experiment is proposed in Figure 4.12. As in Case 4 (see Section 4.2.4), the impact of the residence time on the information reminds the impact given by temperature. For a fixed value of temperature, high residence time should be preferred for CLR and short residence time should be investigated for CHR.

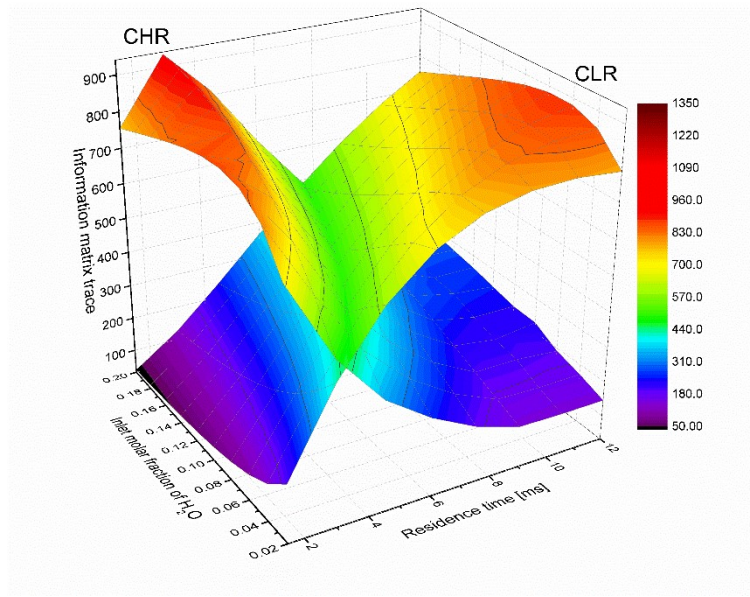


Figure 4.12. Information matrix trace distribution in the 2-dimensional experimental design subspace identified by the residence time τ and inlet molar fraction of water $y_{H_2O}^{IN}$ (Case 5), referring to the sets of kinetic parameters identified for a CLR and a CHR.

The effect given by the quantity of water present at the inlet is still non-uniform, but similar to Case 3 (see Section 4.2.3), where the impact of the inlet molar fraction of water was compared with the impact of the temperature on the information. As one can see in Figure 4.12, the information obtainable can be sensibly increased adding the proper amount of water which depends clearly on the reactivity of the catalyst as well as on the other experimental conditions. For instance, an experiment performed at the temperature considered in this case ($T = 783$ K), on a CHR, setting a residence time $\tau = 3$ ms with an inlet molar fraction of water $y_{H_2O}^{IN} = 0.02$, carries information equals to 629; an experiment performed in the same conditions, but adopting an inlet molar fraction of water around 0.16 carries information equals to 938 (49% higher).

4.2.6 Case 6: Inlet molar ratio methanol/oxygen vs. Inlet molar fraction of water

The effect of a variation in both the inlet methanol/oxygen molar ratio $y_{CH_3OH}^{IN}/y_{O_2}^{IN}$ and the inlet molar fraction of water $y_{H_2O}^{IN}$ on the information carried by an experiment are presented in Figure 4.13. Also in this case it can be observed the convenience of using rich mixtures with high methanol/oxygen ratios to increase the information content of the experiment. Concerning the impact given by the water, the trend shown by the CLR and the CHR is completely opposite.

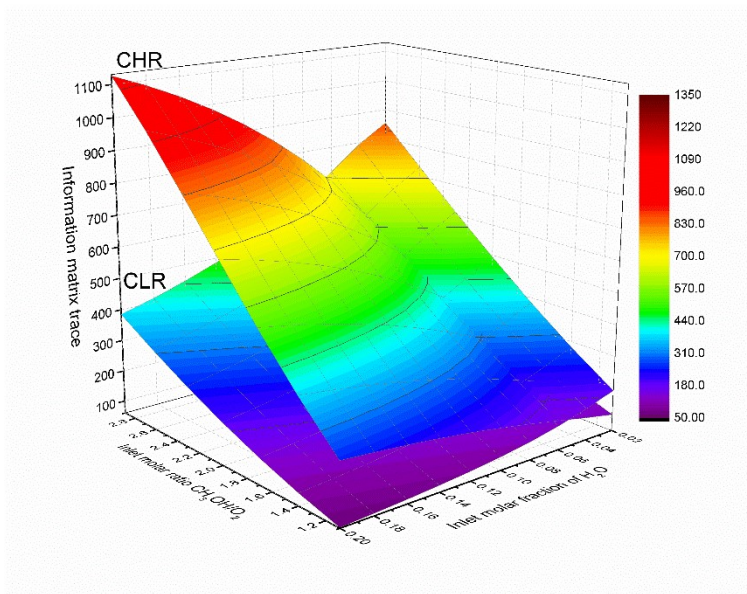


Figure 4.13. Information matrix trace distribution in the 2-dimensional experimental design subspace identified by the inlet methanol/oxygen molar ratio $y_{CH_3OH}^{IN}/y_{O_2}^{IN}$ and inlet molar fraction of water $y_{H_2O}^{IN}$ (Case 6), referring to the sets of kinetic parameters identified for a CLR and a CHR.

The reason is that in Case 6 temperature and residence time were fixed to 783 K and 4.5 ms respectively and according to the surfaces shown in Figure 4.8 (referring to a fixed inlet composition with methanol/oxygen ratio equals to 2.25 and water molar fraction equals to 0.074), this is a region of too high temperature and too long residence time for a CHR while it is a region of too low temperature and too short residence time for a CLR. In other words, in case of CHRs, the reactions in this region of the design space should be slowed down adding water while in case of CLR reactions should be promoted, lowering the inlet fraction of water.

4.3 Robust design of experiments

The distribution of the information in the experimental design space shows the importance of taking into account the uncertainty on the reactivity when planning the investigation of the kinetic mechanism associated to the catalyst. In this section, additional comments on the results obtained from this analysis are proposed.

As one can see in Figure 4.8, the location of the information “wave” is completely different for a CLR (represented by the C1-type catalyst), and a CHR (represented by the R2-type catalyst). For increasing reactivity, the peak of information shifts in the experimental design subspace identified by temperature and residence time:

- the crest of information for CLR is located in the region of the experimental design space characterised by high temperature and long residence time;
- the peak of information for CHR is situated in the region of the experimental design space characterised by low temperature and short residence time.

The surfaces shown in Figure 4.8 refer to a specific inlet composition (i.e. $[y_{CH_3OH}^{IN}, y_{O_2}^{IN}, y_{H_2O}^{IN}] = [0.098, 0.044, 0.074]$). The fact that the surfaces plotted in Figure 4.8 intersect each other highlights the presence of an indifference curve in the experimental design subspace. Carrying out experiments in the conditions identified by the intersection leads to the collection of the same amount of information either with a CLR or with a CHR. If it is assumed that all the possible qualities of silver catalyst have a reactivity within those of setups C1 and R2, then the information crest will always lay between the two peaks shown in Figure 4.8.

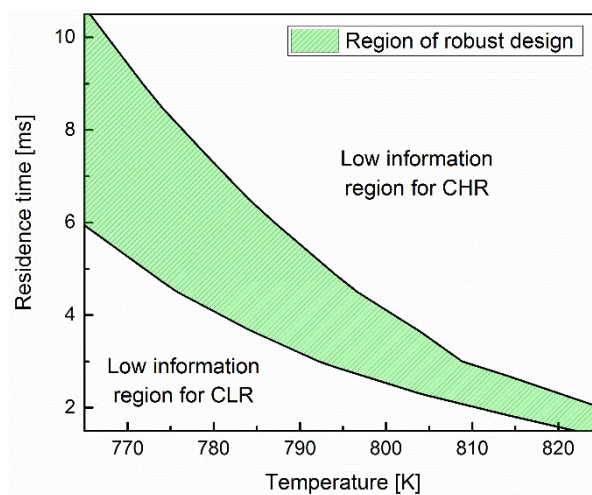


Figure 4.14. Experimental conditions of robust design in the experimental design subspace identified by: 1) temperature; 2) residence time; the green-coloured area identifies the experimental conditions at $Tr(\mathbf{H}) \geq 350$ for any catalyst with reactivity between those of setups C1 and R2, and for the inlet composition considered in the analysis.

If no previous knowledge on the catalyst is available and the reactivity is completely unknown, adopting experimental conditions close to the intersection represents the best compromise for collecting preliminary information to characterise the catalyst behaviour. In order to represent the robust design region (i.e. the most informative experimental conditions considering the parameter uncertainty [10]), the contours for $Tr(\mathbf{H}) = 350$ have been extracted from both the information surfaces referring to setups C1 and R2 and plotted in Figure 4.14. The green-coloured area represented in figure, laying between the two contours, highlights the robust design region (in the

experimental design subspace identified by temperature and residence time), for which the condition $\text{Tr}(\mathbf{H}) \geq 350$ is always respected if:

- the catalyst analysed has a reactivity within the range identified by setups C1 and R2;
- the experiment is carried out at the inlet composition adopted for the analysis (Section 4.2).

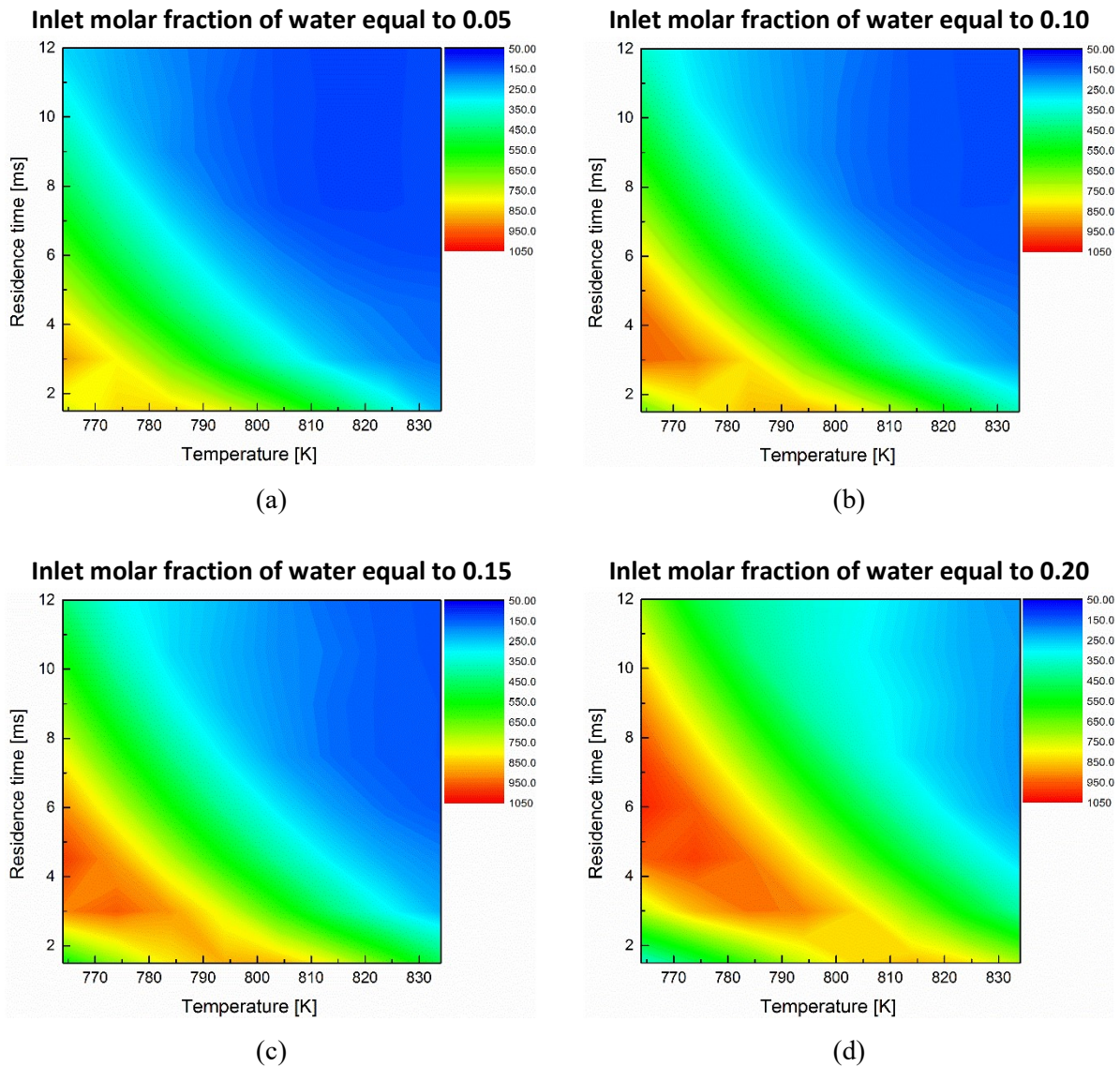


Figure 4.15. Trace of the Fisher information matrix represented for a CHR in the experimental design subspace identified by: 1) temperature; 2) residence time; for fixed inlet molar fractions of methanol and oxygen at different inlet molar fraction of water $y_{H_2O}^{IN}$: (a) 0.05; (b) 0.10; (c) 0.15; (d) 0.20.

Adopting different inlet compositions has an impact on the location of the robust design region. For example, analysing the results obtained in Case 6 (Section 4.2.6), it appears that by acting on the inlet

fraction of water it is possible to shift the information waves shown in Figure 4.8. Increasing the fraction of water, the effect is to move the information surfaces towards the region of higher temperature. The shift of the information wave in the experimental design subspace identified by temperature and residence time can be appreciated in Figure 4.15, where the coloured contours represent the information for a CHR at four different inlet fractions of water. This shift also causes the robust design region, shown in Figure 4.14, to move in the same direction.

4.4 Summary of results

In this chapter, the three-reaction model identified for C1 has been used as reference for quantifying the reactivity of the catalysts present in C2, R1, R2 and R3. The numerical quantification of the catalyst reactivity has been carried out applying a Gaussian filter in the form (1.34) for removing irrelevant experiments from the parameter estimation problem (see Section 4.1 for further details).

A good fitting is achieved with the three-reaction model in all the setups proving the fact that the contrasting experimental data were consequence of a different reactivity of the catalysts used (see Section 4.1.2 for further details). Catalysts characterised by a reactivity higher than that of C1 have been detected in all the setups. The serpentine reactor R2 was the one loaded with the most reactive catalyst.

The sets of kinetic parameters identified for the catalysts loaded in C1 and R2 (respectively the less and the most reactive catalyst analysed), have been employed for further analysis to assess the impact played by the catalyst reactivity on the information content of a trial. The analysis demonstrated the importance of taking into account the reactivity for a proper choice of the experimental conditions. In order to obtain valuable information for the estimation of the kinetic parameters of the three-reaction model, the following aspects have to be considered:

- the inlet molar ratio between methanol and oxygen always have to tend to rich mixtures, regardless of the reactivity;
- for a fixed value of temperature and inlet composition, longer residence time must be set in a CLR with respect to a CHR.

The reactivity of the catalyst analysed may be so high that the peak of information is achieved for too low values of temperature, outside the model reliability range in the experimental design space (see Section 3.2.2.1 for further details). Experiments carried out at such low temperature are not significant

for the estimation of the kinetic parameters, however, it is possible to shift the peak of information in the region of high reliability increasing the inlet molar fraction of water (see Figure 4.15).

The presence of a robust design region in the experimental design space has also been highlighted (see Figure 4.14). This region identifies the most informative experimental conditions for characterising the catalyst behaviour when the reactivity is completely unknown.

Conclusions

Throughout this Thesis, five sets of data for the partial oxidation of methanol to formaldehyde on silver catalyst have been intensively analysed for the purpose of the identification of simplified kinetic models. These data sets were collected in different years, performing steady-state experiments on microreactors with different geometries and different catalyst film lengths. The catalysts loaded in the reactors were synthesised in different batches and were not expected to behave necessarily in the same way. The reactors employed for the investigation of the phenomenon are:

- wide-channel reactor C1;
- wide-channel reactor C2;
- serpentine reactors R1, R2 and R3.

The available sets of experimental data have been employed for preliminary analysis on the quality of data, detecting the presence of significant experimental errors in the experiments carried out on C2, R1, R2 and R3 (see Section 2.3.1.6 for further details). Furthermore, experiments repeated at the same conditions in R3 gave very different results, possibly because of the degradation of the catalyst in that reactor. The experimental data collected on C1 have instead been proved to be both consistent and affected by low measurement errors. Measurements collected on C1 have been then used for defining a parameter estimation problem aimed at identifying a deterministic phenomenological model.

Two candidate kinetic models proposed in the literature [5,9] have been used for fitting the experimental data collected on C1. Both models describe methanol oxidation as a two-step reaction system. The second model also includes a third reaction accounting for the oxidation of hydrogen into water. In both models the kinetics are described by Arrhenius-type equations.

It has been demonstrated the necessity of including the third reaction in the simplified mechanism for achieving good model predictions. The poor descriptive capability of the two-step mechanism in the low temperature region of the experimental design space has also been detected. The distribution of

the residuals associated to the critical experimental conditions suggest the presence of parallel reactions of methanol oxidation, non-negligible at low temperature.

The three-reaction model identified for C1 has been used as reference for quantifying the reactivity of the catalysts present in C2, R1, R2 and R3. The numerical quantification of the catalyst reactivity has been carried out applying a novel model-based data mining technique (MBDM-PE, see Section 1.2.3 for further details), for removing the most unlikely or irrelevant experiments from the parameter estimation problem: *i*) experiments affected by high measurement errors; *ii*) experiments carried out on a degraded catalyst; *iii*) experiments performed outside the model reliability range in the experimental design space. Catalysts characterised by a reactivity higher than C1 have been detected in all the setups. The serpentine reactor R2 is the microreactor loaded with the most reactive catalyst.

It has been chosen to consider the sets of kinetic parameters identified for C1 and R2 (respectively the less and the most reactive catalyst analysed), for assessing the impact played by the catalyst reactivity on the information content of a trial. The trace of the Fisher information matrix [12], chosen as suitable metric of information, has been plotted in a convenient subspace of the experimental design space for:

- a C1-type catalyst with low reactivity (CLR);
- a R2-type catalyst with high reactivity (CHR).

The analysis demonstrated the importance of taking into account the catalyst reactivity for a proper choice of the experimental conditions. The study also highlighted the presence of a robust design region for preliminary investigation when the catalyst reactivity is still unknown. The following aspects have been detected:

- the choice of the inlet molar ratio between methanol and oxygen should always tend to rich mixtures, regardless of the reactivity;
- for a fixed residence time, higher temperature should be investigated in CLR with respect to CHR.
- for a certain value of the operating temperature, longer residence time should be set in CLR with respect to CHR.
- a variation of the inlet molar fraction of water causes the information surface to shift in the experimental design subspace defined by temperature and residence time (see Figure 4.15);
- the surfaces of information associated to a CLR and to a CHR intersect each other in the experimental design space, proving the existence of an indifference curve (see Figure 4.8).

It may happen that the catalyst reactivity is so high that the peak of information is achieved at too low temperature, outside the region of model reliability (see Section 3.2.2.1 for further details). Despite the high theoretical information associated to these experimental conditions, experiments carried out outside the region of model reliability are not significant for the estimation of the kinetic parameters. However, it is possible to shift the peak of information towards the region of higher temperature, where the model is reliable, increasing the inlet molar fraction of water (see Figure 4.15).

The indifference curve identifies the region of robust design of experiments, where the experimentalist should run preliminary trials when no previous knowledge on catalyst reactivity is available (see Figure 4.14). Once the reactivity of the catalyst is quantified, more informative experimental conditions should be investigated applying known MBD_{oE} methods for PP [2-5].

References

1. Turns, S.R., *An Introduction to Combustion: Concepts and Applications*. 2012: McGraw-Hill.
2. Box, G.E.P. and H.L. Lucas, *Design of Experiments in Non-Linear Situations*. *Biometrika*, 1959. 46(1/2): p. 77-90.
3. Espie, D. and S. Macchietto, *The optimal design of dynamic experiments*. *AIChE Journal*, 1989. 35(2): p. 223-229.
4. Galvanin, F., S. Macchietto, and F. Bezzo, *Model-Based Design of Parallel Experiments*. *Industrial & Engineering Chemistry Research*, 2007. 46(3): p. 871-882.
5. Galvanin, F., et al., *Optimal design of experiments for the identification of kinetic models of methanol oxidation over silver catalyst*. *Chemistry Today*, 2015. 33(3).
6. Bartholomew, C.H., *Mechanisms of catalyst deactivation*. *Applied Catalysis A: General*, 2001. 212(1-2): p. 17-60.
7. Andreasen, A., et al., *Simplified kinetic models of methanol oxidation on silver*. *Applied Catalysis A: General*, 2005. 289(2): p. 267-273.
8. Bard, Y., *Nonlinear Parameter Estimation*. 1974: Academic Press.
9. Fisher, R.A., *The design of experiments*. 1966: Hafner Pub. Co.
10. Han, L., Z. Zhou, and G.M. Bollas, *Model-based analysis of chemical-looping combustion experiments. Part II: Optimal design of CH₄-NiO reduction experiments*. *AIChE Journal*, 2016. 62(7): p. 2432-2446.
11. Reuss, G., et al., *Formaldehyde*, in *Ullmann's Encyclopedia of Industrial Chemistry*. 2000, Wiley-VCH Verlag GmbH & Co. KGaA.
12. Andreasen, A., et al., *A microkinetic model of the methanol oxidation over silver*. *Surface Science*, 2003. 544(1): p. 5-23.
13. Box, G.E.P. and W.J. Hill, *Discrimination among Mechanistic Models*. *Technometrics*, 1967. 9(1): p. 57-71.

14. Hunter, W.G. and A.M. Reiner, *Designs for Discriminating between Two Rival Models*. Technometrics, 1965. 7(3): p. 307-323.
15. Schubert, H., U. Tegtmeier, and R. Schlögl, *On the mechanism of the selective oxidation of methanol over elemental silver*. Catalysis Letters, 1994. 28(2): p. 383-395.
16. Cao, E. and A. Gavriilidis, *Oxidative dehydrogenation of methanol in a microstructured reactor*. Catalysis today, 2005. 110: p. 154-163.
17. McNair, H.M. and J.M. Miller, *Basic Concepts and Terms*, in *Basic Gas Chromatography*. 2008, John Wiley & Sons, Inc. p. 29-52.
18. Schlichting, H., *Boundary-layer theory*. 1979: McGraw-Hill.
19. Yaws, C.L. and J.A. Gomes, *Chapter 2 - Viscosity of Gas – Inorganic Compounds*, in *Transport Properties of Chemicals and Hydrocarbons*. 2009, William Andrew Publishing: Boston. p. 93-100.

Acknowledgements

Dr. Federico Galvanin

for his wise guidance and his careful supervision during my Master's Thesis writing

Prof. Fabrizio Bezzo

for his constant support and for the splendid opportunity he offered to me

Prof. Asterios Gavriilidis and his research group

for having welcomed me in UCL's Chemical Engineering Department

Dr. Enhong Cao

for the experimental data that made possible the achievement of the results presented in this Thesis

Model identification through A-optimality criterion

An example for the application of a MBD_oE technique is presented here applied to a virtual system in gPROMS Model Builder environment. The design of experiments is embedded in a wider framework synthesized in Figure I.I to show the conventional procedure adopted for parameter estimation. The A-optimal approach is assumed in this example (i.e. the trace of the posterior covariance matrix \mathbf{V}_θ associated to the estimates is adopted as objective function to be minimised). An initial guess θ^0 for the parameters is assumed to be available; using the initial guess, a design of a single dynamic experiment is performed acting on the input variable profiles and on the sampling times in order to minimise the trace of the posterior covariance matrix. The designed experiment is simulated using a given set of true parameters θ^* adding a normally distributed noise to obtain virtual experimental results that are then used to improve the first estimation of the parameters. The quality of the estimates is assessed through statistical analysis and unsatisfactory results are amended performing a new experiment to gather additional information.

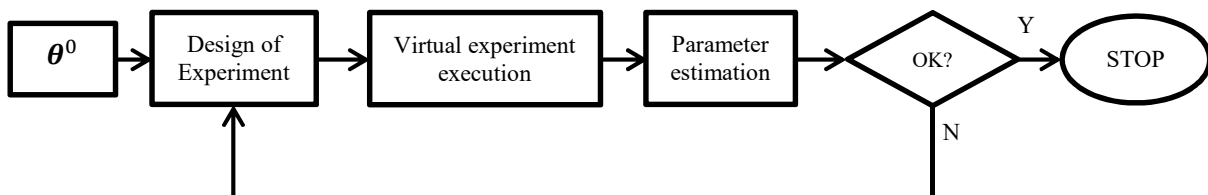


Figure I.I. Information fluxes for model based design of experiments embedded in a parameter estimation problem.

The model used is a baker's yeast growth model obtained from literature [4] described by the following set of equations:

$$\frac{dx_1}{dt} = (r - u_1 - \theta_4)x_1 \quad (\text{I.I})$$

$$\frac{dx_2}{dt} = -\frac{rx_1}{\theta_3} + u_1(u_2 - x_2) \quad (\text{I.II})$$

$$r = \frac{\theta_1 x_2}{\theta_2 + x_2} \quad (\text{I.III})$$

Where $x_1(t)$ is the biomass concentration (g/L), $x_2(t)$ is the substrate concentration (g/L), $u_1(t)$ is the dilution factor (range $0.05 - 0.20 \text{ h}^{-1}$), $u_2(t)$ is the substrate concentration in the feed (range $5 - 35 \text{ g/L}$) and $\theta = [\theta_1, \theta_2, \theta_3, \theta_4]$ is a set of four non-measurable parameters. Both $x_1(t)$ and $x_2(t)$ can be measured directly. Since experiments are performed in silico, and virtual experimental data are generated adding normally distributed noise to the true model prediction, a set of true values for parameters is assumed:

$$\theta^* = [0.310, 0.180, 0.550, 0.050]$$

Initial guesses for the first design are given:

$$\theta^0 = [0.357, 0.153, 0.633, 0.043]$$

The duration of the experiment is optimised within a range going from 5 h to 40 h. Control variables $u_1(t)$ and $u_2(t)$ are parametrised by piecewise-constant profiles switching over 5 time intervals (this parametrisation leads to a limited degree of freedom optimisation problem). The initial biomass concentration $x_1(0)$ is optimised within a range going from 1 to 10 g/L while the initial substrate concentration $x_2(0)$ is assumed to be fixed at 0.01 g/L and cannot be manipulated. The experiment is designed assuming a budget of 10 independent sampling times for each of the state variables x_1 and x_2 . The minimum time between two sampling points is set to 0.5 h. A total of 35 variables are optimised in the experiment (i.e. 1 initial condition, 10×2 sampling times for the measured variables x_1 and x_2 , 4 switching times and 5×2 levels for the control variables u_1 and u_2). Control variables profiles for the dilution factor u_1 and the substrate concentration u_2 computed performing a first design are shown in Figure 2. Optimised initial biomass concentration $x_1(0)$ is equal to 1.043 g/L. The total computed duration of the experiment is equal to 31.0 h.

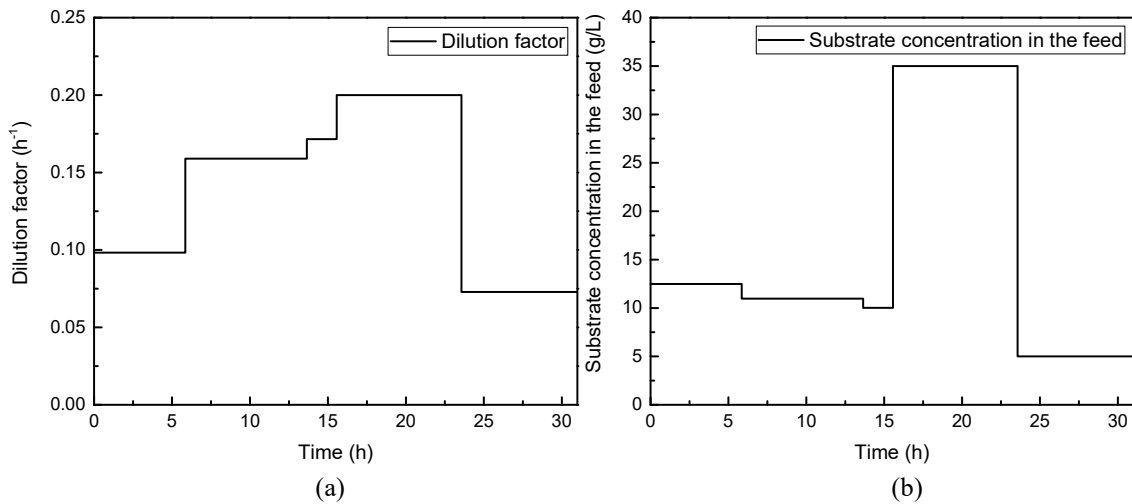


Figure I.II. Optimal input profiles obtained from first design with A-optimal for the dilution factor, u_1 (a) and the substrate concentration in the feed, u_2 (b).

The designed experiment is performed *in silico* generating the true profiles of the state variables. Virtual measurements are obtained adding a normally distributed noise with zero mean, $V_{x_1} = 0.1$ and $V_{x_2} = 0.5$. The synthetic experimental points for the two state variables x_1 and x_2 are shown in Figure 3 together with the true profiles. The values obtained for the mock measurements are used to solve a parameter estimation problem through the maximisation of the likelihood function. The parameter estimates obtained $\hat{\theta}$, presented in Table 1, have not been estimated with satisfactory accuracy.

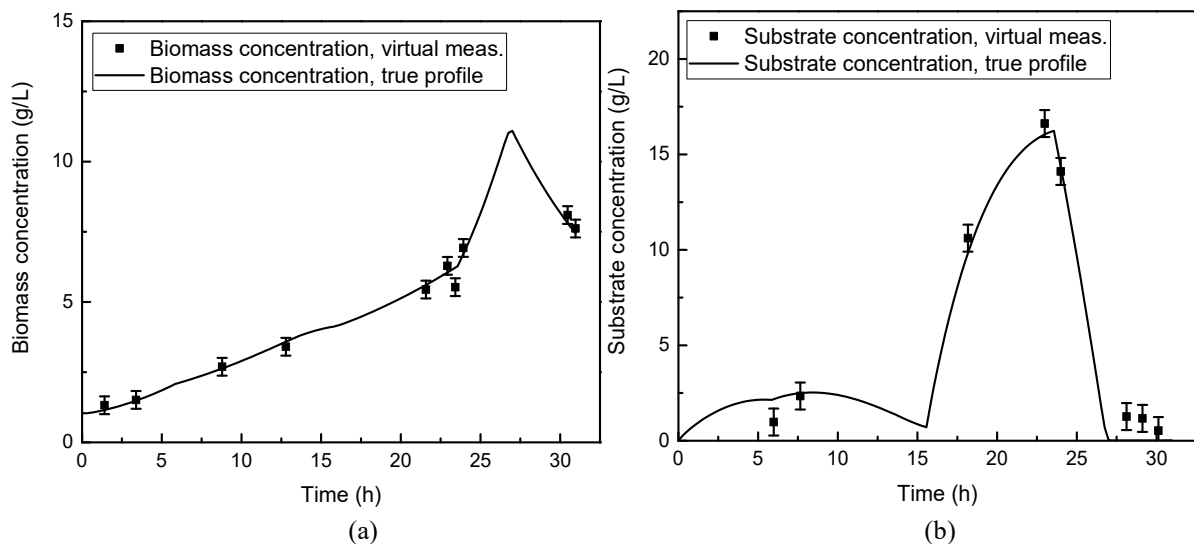


Figure I.III. Synthetic experimental data obtained “*in silico*” for biomass concentration, x_1 (a) and substrate concentration, x_2 (b). Lines represent the profile of measured variables in the “*true*” system.

Table I.I. Parameter estimations after first design with A-optimal criterion.

Parameter	Estimation	t -value* ($t_{ref}=1.74$)
θ_1	0.299	8.724
θ_2	0.212	0.857*
θ_3	0.522	5.153
θ_4	0.038	1.157*
Lack of Fit Test** ($\chi_{ref}^2 = 26.30$)		
χ_{sample}^2	18.74	

*a t -value lower than the reference indicates that the information given by the experiments may not be sufficient to estimate the parameter precisely

**a χ_{sample}^2 larger than the χ_{ref}^2 tends to indicate a bad fit

The new estimate is used to perform a second design optimising the same variables and adopting the same assumptions and boundaries used before. The second designed experiment is simulated and used for generating other synthetic measurements. The new data points together with the ones obtained in the first experiment are fitted to solve a second parameter estimation problem. The second estimate, presented in Table 2, now satisfies the desired statistical requirements. Also the χ^2 -test is satisfied demonstrating the goodness of fit. Since all the statistical tests give positive results, the problem of model identification can be considered solved.

Table I.II. Parameter estimations after second design with A-optimal criterion.

Parameter	Estimation	t -value* ($t_{ref}=1.69$)
θ_1	0.311	24.976
θ_2	0.199	2.490
θ_3	0.555	14.357
θ_4	0.051	5.878
Lack of Fit Test** ($\chi_{ref}^2 = 51.00$)		
χ_{sample}^2	39.68	

*a t -value lower than the reference indicates that the information given by the experiments may not be sufficient to estimate the parameter precisely

**a χ_{sample}^2 larger than the χ_{ref}^2 tends to indicate a bad fit

Appendix II

Available experimental data

Detailed experimental results for the experiments used in this work for the purpose of model identification for the partial oxidation of methanol to formaldehyde over silver catalyst. The data sets have been collected on 5 different micro-reactor devices and are here proposed in 5 tables divided by setup. A more detailed description of the experimental apparatus can be found in Section 2.2 or in previous literature works [16].

C1 – wide-channel reactor – 2008											
N° exp	T [K]	Site	P [Pa]	F_{STC} [$\frac{ml}{min}$]	y_{CH_3OH}	y_{O_2}	y_{H_2O}	y_{CH_2O}	y_{H_2}	y_{CO_2}	y_{CO}
1	725	Inlet	159200	26.5	0.0982	0.0436	0.0744	0	0	0	N/A
		Outlet	N/A	27.2	0.0556	0.0148	0.1199	0.0313	0.002	0.0086	N/A
2	744	Inlet	160600	26.5	0.0982	0.0436	0.0744	0	0	0	N/A
		Outlet	N/A	27.2	0.0436	0.0101	0.1256	0.0416	0.0023	0.0109	N/A
3	765	Inlet	162000	26.5	0.0982	0.0436	0.0744	0	0	0	N/A
		Outlet	N/A	27.7	0.0365	0.0042	0.1362	0.0465	0.0035	0.0106	N/A
4	784	Inlet	163400	26.5	0.0982	0.0436	0.0744	0	0	0	N/A
		Outlet	N/A	27.8	0.0258	0.0013	0.1425	0.0587	0.0052	0.009	N/A
5	805	Inlet	164700	26.5	0.0982	0.0436	0.0744	0	0	0	N/A
		Outlet	N/A	27.9	0.0183	0.0002	0.1447	0.0674	0.0056	0.0079	N/A
6	764	Inlet	162000	26.6	0.1483	0.0606	0.1123	0	0	0	N/A
		Outlet	N/A	28.1	0.0721	0.0197	0.1722	0.0578	0.0026	0.0102	N/A
7	785	Inlet	163400	26.6	0.1483	0.0606	0.1123	0	0	0	N/A
		Outlet	N/A	28.5	0.0465	0.0072	0.1916	0.0785	0.0045	0.0127	N/A
8	804	Inlet	164700	26.6	0.1483	0.0606	0.1123	0	0	0	N/A
		Outlet	N/A	28.8	0.0306	0.0023	0.1993	0.0936	0.008	0.0121	N/A
9	826	Inlet	164700	26.6	0.1483	0.0606	0.1123	0	0	0	N/A
		Outlet	N/A	29.0	0.0234	0.0007	0.2026	0.1	0.0103	0.0113	N/A
10	783	Inlet	163400	26.4	0.1029	0.0269	0.078	0	0	0	N/A
		Outlet	N/A	27.2	0.0533	0.0001	0.124	0.0436	0.0033	0.0035	N/A
11	783	Inlet	163400	26.5	0.1038	0.0443	0.0786	0	0	0	N/A
		Outlet	N/A	27.8	0.0308	0.0028	0.1439	0.0591	0.0032	0.0093	N/A
12	783	Inlet	163400	26.5	0.1063	0.0504	0.0805	0	0	0	N/A
		Outlet	N/A	28.0	0.0245	0.0048	0.1488	0.0631	0.0034	0.0132	N/A

13	783	Inlet	163400	26.5	0.1042	0.0659	0.079	0	0	0	N/A
		Outlet	N/A	28.1	0.0183	0.0152	0.1532	0.0655	0.0048	0.0146	N/A
14	783	Inlet	163400	26.5	0.1064	0.0962	0.0806	0	0	0	N/A
		Outlet	N/A	28.1	0.0252	0.0426	0.1573	0.0596	0.0034	0.0157	N/A
15	783	Inlet	163400	25.8	0.1395	0.0462	0.079	0	0	0	N/A
		Outlet	N/A	27.2	0.0515	0.0023	0.1509	0.0755	0.0108	0.0061	N/A
16	783	Inlet	163400	27.1	0.0684	0.0428	0.0775	0	0	0	N/A
		Outlet	N/A	28.4	0.0196	0.017	0.1156	0.0371	0.0012	0.0072	N/A
17	783	Inlet	163400	26.4	0.1035	0.0427	0.0184	0	0	0	N/A
		Outlet	N/A	28.0	0.0209	0.0014	0.0851	0.0657	0.0083	0.0106	N/A
18	783	Inlet	163400	26.5	0.1038	0.0443	0.0786	0	0	0	N/A
		Outlet	N/A	27.8	0.0311	0.0052	0.1393	0.0607	0.0055	0.0084	N/A
19	783	Inlet	163400	26.5	0.1038	0.0443	0.143	0	0	0	N/A
		Outlet	N/A	27.6	0.0454	0.0128	0.1901	0.0494	0.0027	0.006	N/A
20	783	Inlet	163400	26.5	0.1057	0.043	0.2114	0	0	0	N/A
		Outlet	N/A	27.4	0.0559	0.018	0.248	0.0423	0.0021	0.0037	N/A

C2 – wide-channel reactor – 2013											
N° exp	T [K]	Site	P [Pa]	F_{STC} [$\frac{ml}{min}$]	y_{CH_3OH}	y_{O_2}	y_{H_2O}	y_{CH_2O}	y_{H_2}	y_{CO_2}	y_{CO}
1	783	Inlet	163400	58.8	0.0996	0.0441	0.0754	0.0000	0.0000	0.0000	0.0000
		Outlet	N/A	61.4	0.0188	0.0063	0.1399	0.0676	0.0119	0.0060	0.0001
2	783	Inlet	163400	29.6	0.0990	0.0442	0.0750	0.0000	0.0000	0.0000	0.0000
		Outlet	N/A	31.9	0.0135	0.0037	0.1372	0.0722	0.0117	0.0072	0.0002
3	783	Inlet	163400	20.5	0.0986	0.0442	0.0746	0.0000	0.0000	0.0000	0.0000
		Outlet	N/A	21.4	0.0100	0.0020	0.1456	0.0772	0.0154	0.0078	0.0003
4	783	Inlet	163400	13.7	0.0991	0.0441	0.0750	0.0000	0.0000	0.0000	0.0000
		Outlet	N/A	14.3	0.0096	0.0026	0.1473	0.0822	0.0138	0.0096	0.0003

R1 – serpentine reactor – 2015											
N° exp	T [K]	Site	P [Pa]	F_{STC} [$\frac{ml}{min}$]	y_{CH_3OH}	y_{O_2}	y_{H_2O}	y_{CH_2O}	y_{H_2}	y_{CO_2}	y_{CO}
1	783	Inlet	260000	73.1	0.0994	0.0415	0.0753	0.0000	0.0000	0.0000	0.0000
		Outlet	160000	76.8	0.0124	0.0000	0.1401	0.0749	0.0179	0.0078	0.0004
2	783	Inlet	220000	41.7	0.0997	0.0414	0.0755	0.0000	0.0000	0.0000	0.0000
		Outlet	160000	44.0	0.0094	0.0000	0.1468	0.0750	0.0188	0.0071	0.0004
3	783	Inlet	200000	29.1	0.0996	0.0414	0.0755	0.0000	0.0000	0.0000	0.0000
		Outlet	160000	30.3	0.0101	0.0000	0.1360	0.0748	0.0187	0.0065	0.0005
4	733	Inlet	220000	50.9	0.1468	0.0975	0.2293	0.0000	0.0000	0.0000	0.0000
		Outlet	160000	53.5	0.0339	0.0101	0.3568	0.0447	0.0133	0.0391	0.0008
5	765	Inlet	226000	50.9	0.1468	0.0975	0.2293	0.0000	0.0000	0.0000	0.0000
		Outlet	160000	53.6	0.0123	0.0006	0.3401	0.0893	0.0201	0.0359	0.0012
6	796	Inlet	235000	50.9	0.1468	0.0975	0.2293	0.0000	0.0000	0.0000	0.0000
		Outlet	160000	53.7	0.0049	0.0002	0.3467	0.0998	0.0188	0.0293	0.0013
7	826	Inlet	240000	50.9	0.1468	0.0975	0.2293	0.0000	0.0000	0.0000	0.0000
		Outlet	160000	53.8	0.0016	0.0001	0.3417	0.1070	0.0195	0.0309	0.0011
8	765	Inlet	280000	93.9	0.1469	0.0980	0.2296	0.0000	0.0000	0.0000	0.0000
		Outlet	160000	99.8	0.0171	0.0063	0.3467	0.0865	0.0174	0.0306	0.0011
9	796	Inlet	286000	93.9	0.1469	0.0980	0.2296	0.0000	0.0000	0.0000	0.0000
		Outlet	160000	100.0	0.0054	0.0026	0.3481	0.1000	0.0181	0.0312	0.0012
10	826	Inlet	295000	93.9	0.1469	0.0980	0.2296	0.0000	0.0000	0.0000	0.0000
		Outlet	160000	100.5	0.0015	0.0016	0.3507	0.1079	0.0179	0.0282	0.0011

11	800	Inlet	240000	54.6	0.2590	0.1064	0.2122	0.0000	0.0000	0.0000	0.0000
		Outlet	160000	59.7	0.0430	0.0001	0.3449	0.1686	0.0375	0.0187	0.0014
12	850	Inlet	245000	54.6	0.2590	0.1064	0.2122	0.0000	0.0000	0.0000	0.0000
		Outlet	160000	59.8	0.0260	0.0000	0.3183	0.2089	0.0458	0.0143	0.0016
13	900	Inlet	252000	54.6	0.2590	0.1064	0.2122	0.0000	0.0000	0.0000	0.0000
		Outlet	160000	60.6	0.0187	0.0000	0.3226	0.2116	0.0523	0.0127	0.0015

R2 – serpentine reactor – 2015											
N° exp	T [K]	Site	P [Pa]	F_{STC} [$\frac{ml}{min}$]	y_{CH_3OH}	y_{O_2}	y_{H_2O}	y_{CH_2O}	y_{H_2}	y_{CO_2}	y_{CO}
1	783	Inlet	290000	73.1	0.0994	0.0415	0.0753	0.0000	0.0000	0.0000	0.0000
		Outlet	160000	76.4	0.0124	0.0016	0.1323	0.0771	0.0193	0.0070	0.0002
2	783	Inlet	240000	41.7	0.0997	0.0414	0.0755	0.0000	0.0000	0.0000	0.0000
		Outlet	160000	44.0	0.0094	0.0005	0.1446	0.0745	0.0197	0.0084	0.0002
3	783	Inlet	220000	29.1	0.0996	0.0414	0.0755	0.0000	0.0000	0.0000	0.0000
		Outlet	160000	30.9	0.0070	0.0014	0.1461	0.0771	0.0207	0.0081	0.0003

R3 – serpentine reactor – 2015											
N° exp	T [K]	Site	P [Pa]	F_{STC} [$\frac{ml}{min}$]	y_{CH_3OH}	y_{O_2}	y_{H_2O}	y_{CH_2O}	y_{H_2}	y_{CO_2}	y_{CO}
1	783	Inlet	290000	73.1	0.0994	0.0415	0.0753	0.0000	0.0000	0.0000	0.0000
		Outlet	160000	76.4	0.0284	0.0115	0.1292	0.0607	0.0167	0.0033	0.0001
2	783	Inlet	240000	41.7	0.0997	0.0414	0.0755	0.0000	0.0000	0.0000	0.0000
		Outlet	160000	43.7	0.0247	0.0074	0.1234	0.0752	0.0175	0.0038	0.0001
3	783	Inlet	220000	29.1	0.0996	0.0414	0.0755	0.0000	0.0000	0.0000	0.0000
		Outlet	160000	30.7	0.0193	0.0053	0.1447	0.0685	0.0161	0.0032	0.0001
4	783	Inlet	240000	41.7	0.0997	0.0414	0.0755	0.0000	0.0000	0.0000	0.0000
		Outlet	160000	43.5	0.0326	0.0140	0.1446	0.0470	0.0096	0.0024	0.0000
5	813	Inlet	250000	41.7	0.0997	0.0414	0.0755	0.0000	0.0000	0.0000	0.0000
		Outlet	160000	43.6	0.0313	0.0131	0.1376	0.0529	0.0145	0.0023	0.0000
6	843	Inlet	260000	41.7	0.0997	0.0414	0.0755	0.0000	0.0000	0.0000	0.0000
		Outlet	160000	43.8	0.0291	0.0127	0.1369	0.0578	0.0149	0.0024	0.0000
7	883	Inlet	270000	41.7	0.0997	0.0414	0.0755	0.0000	0.0000	0.0000	0.0000
		Outlet	160000	43.8	0.0213	0.0089	0.1400	0.0664	0.0163	0.0024	0.0000
8	933	Inlet	280000	41.7	0.0997	0.0414	0.0755	0.0000	0.0000	0.0000	0.0000
		Outlet	160000	44.0	0.0140	0.0051	0.1469	0.0710	0.0171	0.0029	0.0002

Pressure correction for serpentine reactors

Since in the serpentine reactors R1, R2 and R3 pressure cannot be considered uniform in the main channel, a linear pressure profile is assumed in the models implemented in gPROMS between the pressures at the extrema of the catalyst film. These values of pressure have been evaluated through a correlation explained in this Appendix. This schematic representation of the microchannel presented in Figure 3.1 is also proposed here in Figure III.I as support for the explanation of the pressure correction adopted throughout this thesis for the serpentine reactors. The microchannel is divided into 4 sections, each characterised by specific uniform geometrical parameters:

- Inlet channel from coordinate z_{IN} to z_{MC} ;
- Main channel from coordinate z_{MC} to z_R ;
- Retainer from coordinate z_R to z_{OC} ;
- Outlet channel from coordinate z_{OC} to z_{OUT} .

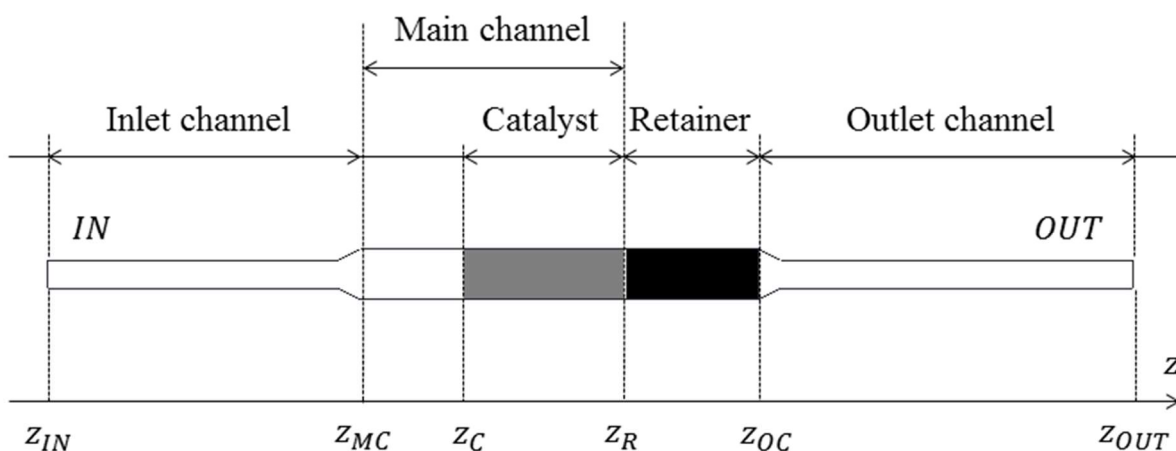


Figure III.I. Schematic representation of the serpentine reactor's channel. The grey-coloured area represents the catalyst film region; black-coloured area represents the retainer. Drawing is not in scale.

The coordinate z_C laying in the range between z_{MC} and z_R denotes the beginning of the zone occupied by the catalyst, thus, $z_R - z_C$ represents the length of the catalyst film L_C . The geometry characteristic of each of the sections is presented in Table III.I.

Table III.I. Serpentine reactor, geometry of the microchannel.

Section	Geometry	Cross-section [mm ²]	Wetted perimeter [mm]	Hydraulic diameter [mm]	Length [mm]
Inlet channel	Single rectangular channel	$6.00 \cdot 10^{-2}$	1.24	$1.94 \cdot 10^{-1}$	52.0
Main channel	Single rectangular channel	$1.08 \cdot 10^{-1}$	2.04	$2.12 \cdot 10^{-1}$	79.3
Retainer	11 rectangular parallel channels	$5.28 \cdot 10^{-2}$	3.52	$6.00 \cdot 10^{-2}$	1.1
Outlet channel	Single rectangular channel	$6.00 \cdot 10^{-2}$	1.24	$1.94 \cdot 10^{-1}$	63.1

The pressure profile along the reactor has been evaluated adopting a correlation derived from Poiseuille's law valid in laminar flow and corrected for microchannels [18]:

$$dP = \frac{12\mu v}{d_h^2} dz \quad (\text{III.I})$$

where μ is the dynamic viscosity, v is the axial velocity in the channel and d_h is the hydraulic diameter of the channel. The correlation has been integrated in each section assuming an ideal behaviour for the gas mixture to evaluate the variation of velocity with pressure and constant molarity (i.e. total molar flowrate \dot{n}_{tot} uniform along the reactor) obtaining the following set of equations:

$$P(z_{MC}) = \sqrt{P^2(z_{IN}) - \frac{24\mu\dot{n}_{tot}R_gT}{d_{h,IC}^2}(z_{MC} - z_{IN})} \quad (\text{III.II})$$

$$P(z_R) = \sqrt{P^2(z_{MC}) - \frac{24\mu\dot{n}_{tot}R_gT}{d_{h,MC}^2}(z_R - z_{MC})} \quad (\text{III.III})$$

$$P(z_{OC}) = \sqrt{P^2(z_R) - \frac{24\mu\dot{n}_{tot}R_gT}{d_{h,R}^2}(z_{OC} - z_R)} \quad (\text{III.IV})$$

$$P(z_{OUT}) = \sqrt{P^2(z_{OC}) - \frac{24\mu\dot{n}_{tot}R_gT}{d_{h,OC}^2}(z_{OUT} - z_{OC})} \quad (\text{III.V})$$

Where R_g is the ideal gas constant, T is the operating temperature and $d_{h,IC}$, $d_{h,MC}$, $d_{h,R}$ and $d_{h,OC}$ are the hydraulic diameters in the inlet channel, main channel, retainer and outlet channel respectively. The system of equations has been solved evaluating the four unknowns:

- viscosity μ ;
- the pressure at the beginning of the main channel $P(z_{MC})$;
- the pressure at the end of the main channel (beginning of the retainer), $P(z_R)$;
- the pressure at the end of the retainer (beginning of the outer channel), $P(z_{OC})$;

Boundary conditions $P(z_{OUT}) = P^{OUT}$ and $P(z_{IN}) = P^{IN}$ have been set for the solution of the problem where P^{OUT} and P^{IN} are the values measured for the pressure at outlet and inlet respectively that are reported in the data sets for all the experiments performed on the serpentine reactors (See Appendix II). Viscosity μ , in all the experiments performed in R1, R2 and R3 has been evaluated in the range $10^{-4} \div 10^{-5}$ Pa · s (the values agree with the viscosity tabulated in literature for helium at 800 K, i.e. $4.1 \cdot 10^{-5}$ Pa · s [19]).

Since in equation (III.III) the second term the under square root is an order of magnitude lower than the pressure $P(z_{MC})$ appearing in the first term, the pressure profile along the main channel is well approximated by a line. The pressure at the beginning and of the catalyst film region $P(z_C)$ has been evaluated assuming that a linear pressure profile is realised between the values at the extrema $P(z_{MC})$ and $P(z_R)$ in the main channel, i.e.:

$$P(z_C) = \frac{P(z_{MC}) - P(z_R)}{z_R - z_{MC}}(z_R - z_C) + P(z_R) \quad (\text{III.VI})$$